Titre: Title:	Properties of Lightning Strike Protection Coatings
Auteur: Author:	Martin Gagné
Date:	2016
Type:	Mémoire ou thèse / Dissertation or Thesis
Référence: Citation:	Gagné, M. (2016). Properties of Lightning Strike Protection Coatings [Mémoire de maîtrise, École Polytechnique de Montréal]. PolyPublie. https://publications.polymtl.ca/2118/

UNIVERSITÉ DE MONTRÉAL

PROPERTIES OF LIGHTNING STRIKE PROTECTION COATINGS

MARTIN GAGNÉ

DÉPARTEMENT DE GÉNIE PHYSIQUE

ÉCOLE POLYTECHNIQUE DE MONTRÉAL

MÉMOIRE PRÉSENTÉ EN VUE DE L'OBTENTION

DU DIPLÔME DE MAÎTRISE ÈS SCIENCES APPLIQUÉES

(GÉNIE PHYSIQUE)

AVRIL 2016

UNIVERSITÉ DE MONTRÉAL

ÉCOLE POLYTECHNIQUE DE MONTRÉAL

Ce mémoire intitulé :

PROPERTIES OF LIGHTNING STRIKE PROTECTION COATINGS

présenté par : GAGNÉ Martin

en vue de l'obtention du diplôme de : Maîtrise ès Sciences Appliquées

a été dûment accepté par le jury d'examen constitué de :

M. YELON Arthur, Ph. D., président

Mme KLEMBERG-SAPIEHA Jolanta-Ewa, Doctorat, membre et directrice de recherche

M. MARTINU Ludvik, Ph. D., membre

DEDICATION

I wish to dedicate this thesis to my family, who believe in me even when I do not.

ACKNOWLEDGEMENTS

I would like to give thanks to the Consortium for Research and Innovation in Aerospace in Quebec (CRIAQ), Bombardier Aerospace, Bell Helicopter and 3M Canada for financing and helping for this project and thesis. Particular, or special, appreciation goes to Alexandra Desautels, Judith Roberge and the technical staff from Bell Helicopter, and Mario Simard from Bombardier Aerospace and Daniel Therriault the project leader. I thank the CRIAQ COMP-502 composite team member Dr. Thomas Schmitt for his given useful technical advice with the characterization of the coated samples, as well as other members such as Xavier Cauchy and Rajesh Ponnada for their help and collaboration.

I also want to acknowledge the help of the LM^2 technicians for help with mechanical tests, Isabella Nowlan and Martin Cardonne, and the LM^2 students who worked on this project but could still find time to help me with various ideas and their aid, such as Rouhollah Dermanaki Farahani.

Thanks to Professor Frederic Sirois and Masters Student Kevin McMeekin in the electrical engineering department for help with electrical equipment and concepts.

I would also like to thank the personnel at FCSEL for various aid, help and advice throughout my thesis, the technicians Francis Turcot and Sébastien Chénard, and the students Julien Schmitt, Simon Loquai, Michael Laberge, William Trottier-Lapointe and Thomas Poirié. Also special thanks to Jiri Kohout, Ph.D., who fabricated the aluminum samples for us.

Last but not least I want to thank my director Jolanta Ewa Klemberg-Sapieha, who motivated me to push my limits and excel at what I do.

RÉSUMÉ

Les matériaux composites sont de plus en plus utilisés dans plusieurs domaines. Dans le cas des compagnies aéronautiques, ces matériaux sont introduits dans leurs avions pour réduire le poids et ainsi réduire les coûts de carburants. Ces avions sont donc plus légers mais la perte de conductivité électrique rend l'avion vulnérable à la foudre ; celle-ci peut frapper les avions commerciaux en moyenne une fois par an. La protection contre la foudre devient donc très importante. Les mailles de cuivre actuelles offrent une bonne protection mais elles augmentent le poids des composites. Dans le cadre du projet CRIAQ COMP-502, une équipe de partenaires industriels et de chercheurs académiques étudient de nouveaux revêtements conducteurs ayant les caractéristiques suivantes : bonne protection électromagnétique, résistance mécanique élevée, bonne protection contre l'environnement, bonne fabricabilité et des coûts modérés. Les objectifs principaux de ce mémoire, dans le cadre de ce projet, était de déterminer les caractéristiques principales (électriques et tribomécaniques) pour les revêtements conducteurs placés sur les panneaux composites. Leurs propriétés étaient également testées après des essais destructifs tels que des injections de courants et des essais environnementaux.

Bombardier Aerospace a fourni le substrat, un matériau composite constitué de fibres de carbone qui renforcent une matrice époxy, et le produit commercial actuel, un film surfacique (*surfacing film*) qui comprend une feuille de cuivre déployé (*expanded copper foil*) pour comparer avec les autres revêtements. Voici la liste des revêtements conducteurs fabriqués par les étudiants: des nanoparticules d'argent dans une matrice (PEDOT:PSS ou un mélange d'époxy et de PEDOT:PSS); des nanofibres de carbone couvertes d'argent et intégrées dans le film de surface; un revêtement d'étain par projection à froid (*cold spray*); du graphène oxydé et fonctionnalisé (*functionalized*) avec des nanofils d'argent et un dépôt d'argent autocatalytique (*electroless plating*). De plus, dans le cadre du projet et mémoire, des revêtements d'aluminium ont été pulvérisés à l'aide d'un magnétron.

Il y a trois principaux types de tests pour caractériser les revêtements conducteurs : électriques, mécaniques et environnementaux. Les tests électriques consistent à trouver la résistance-carré et la résistivité spécifique des revêtements conducteurs. Les tests mécaniques comprennent l'adhérence, le test d'éraflure, la dureté et le module de Young des revêtements. Les tests environnementaux comprennent des cycles thermiques et embrun salin (*salt spray*). Ces

caractéristiques de base sont étudiées en premier, mais d'autres tests combinent les catégories ensemble, comme des tests électriques avant, pendant et après les tests environnementaux ainsi que les effets des injections de courants électriques sur les propriétés mécaniques de l'échantillon.

Les propriétés électriques des revêtements conducteurs ont été améliorées et sont très proches de celles des mailles de cuivres métalliques ou dans un ordre de grandeur similaire. Les propriétés mécaniques sont également bonnes pour la plupart de ces revêtements ; elles montrent une bonne adhérence et dureté. Elles ne montrent aucune perte significative des propriétés de flexion après des injections de courant. Les tests environnementaux sont plus mitigés : certains revêtements conducteurs perdent leur conductivité sur leurs surfaces, d'autres avaient une légère augmentation de leur résistivité et quelques-uns n'étaient pas affectés. D'autres tests comme l'analyse thermogravimétrique, ou l'analyse des tests d'éraflure par microscope électronique à balayage ainsi que des observations par microscope optique sont inclus pour l'analyse supplémentaire des résultats des revêtements conducteurs.

Les revêtements conducteurs ont été caractérisés et testés dans le cadre du projet CRIAQ. Des tests de coup de foudre sont nécessaires pour recueillir de plus amples informations sur ces revêtements. L'application principale de ces revêtements est la protection contre la foudre pour les avions, mais ils peuvent aussi être utilisés pour la protection contre la foudre sur le sol et pour la protection électromagnétique.

ABSTRACT

Composite materials are being increasingly used by many industries. In the case of aerospace companies, those materials are installed on their aircraft to save weight, and thus, fuel costs. These aircraft are lighter, but the loss of electrical conductivity makes aircraft vulnerable to lightning strikes, which hit commercial aircrafts on average once per year. This makes lightning strike protection very important, and while current metallic expanded copper foils offer good protection, they increase the weight of composites. Therefore, under the CRIAQ COMP-502 project, a team of industrial partners and academic researchers are investigating new conductive coatings with the following characteristics: High electromagnetic protection, high mechanical resistance, good environmental protection, manufacturability and moderate cost. The main objectives of this thesis, as part of this project, was to determine the main characteristics, such as electrical and tribomechanical properties, of conductive coatings on composite panels. Their properties were also to be tested after destructive tests such as current injection and environmental testing.

Bombardier Aerospace provided the substrate, a composite of carbon fiber reinforced epoxy matrix, and the current commercial product, a surfacing film that includes an expanded copper foil used to compare with the other coatings. The conductive coatings fabricated by the students are: silver nanoparticles inside a binding matrix (PEDOT:PSS or a mix of Epoxy and PEDOT:PSS), silvered carbon nanofibers embedded in the surfacing film, cold sprayed tin, graphene oxide functionalized with silver nanowires, and electroless plated silver. Additionally as part of the project and thesis, magnetron sputtered aluminum coated samples were fabricated.

There are three main types of tests to characterize the conductive coatings: electrical, mechanical and environmental. Electrical tests consist of finding the sheet resistance and specific resistivity of conductive coatings. Mechanical tests include adhesion, scratch, hardness and Young's modulus of the coatings. The environmental tests are temperature cycling and salt spray cycling. These basic characteristics were investigated first, but further tests also combine the categories, such as electrical tests before, during and after environmental tests, and the effects on the sample's mechanical properties after high electrical current injections.

The electrical properties of the conductive coatings have improved and are very close to that of current expanded metallic foil or within an order of magnitude. The mechanical properties of

most of these coatings are also good. They exhibit good adhesion, hardness, and no significant loss of flexion properties after current injections. The environmental tests are more mitigated, with some conductive coatings losing their surface conductivity, others having a small increase in specific resistivity, and some were simply unaffected. Tests such as thermogravimetric analysis, scanning electron microscope analysis of scratch tests, and optical microscope observations are included to provide additional analysis of the results of the conductive coatings.

The conductive coatings were characterized and tested as part of the CRIAQ project. Lightning strike tests are required to gather further information on these conductive coatings. The main application for these coatings is for lightning strike protection of aircraft, but they can also be used for ground based lightning strike protection and general electromagnetic shielding.

TABLE OF CONTENTS

LIST OF TABLES

LIST OF FIGURES

LIST OF SYMBOLS AND ABBREVIATIONS

The list of symbols and abbreviations presents the symbols and abbreviations used in the thesis or dissertation in alphabetical order, along with their meanings:

A	Ampere
AFN	Advanced Fiber Nonwovens
ARP	Aerospace Recommended Practices
BP	Buckypaper
CC/CS	Conductive Coating/Composite Structure
CF	Correction Factor
CFRP	Carbon Fiber Resin Polymer
CNFP	Carbon Nanofiber Papers
CNT	Carbon Nanotube
CRIAQ	Consortium for Research and Innovation in Aerospace in Quebec
CP-CNFP	Composite Panel Carbon Nanofiber Papers
EMI	Electromagnetic Interference
EPT	Electrical Percolation Threshold
ECF	Expanded Copper Foil
FAA	Federal Aviation Agency
FHC	Filled-Hole Compression
FHT	Filled-Hole Tension
FLG	Few-Layer Graphene
FRP	Fiber Reinforced Polymer
HiPIMS	High Power Impulse Magnetron Sputtering
HS	Harness Satin

LSP	Lightning Strike Protection
LWD	Long Width Diamond
MGP	Multi-Graphene Platelets
MWCNT	Multi-Walled Carbon Nanotube
Pd	Penetration Depth
PEDTOS:PSS	Poly(3,4-Ethylenedioxythiophene) Polystyrene Sulfonate
PSF	Pound per Square Feet
PSI	Pound per Square Inch
RD	Residual Depth
RF	Radio Frequency
SAE	Society of Automotive Engineers
SEM	Scanning Electron Microscope
SF	Surfacing Film
SPS	Spark Plasma Sintering
SWCNT	Single-walled Carbon Nanotube
SWD	Short Width Diamond
TGA	Thermogravimetric Analysis
UNT	Unnotched Tension
UNC	Unnotched Compression

LIST OF APPENDICES

CHAPTER 1 INTRODUCTION

Commercial aircraft are struck by lightning once every 1,000-10,000 hours of flight, or about once a year [1], as shown in Figure 1.1. Electrical currents as high as 200,000 Amperes (A) travel through the least resistant parts of the aircraft, and if the aircraft is not well protected, severe consequences such as vaporization of critical aircraft parts can follow [2]. Aircraft were usually made of aluminum before composites were introduced around 40 years ago [3]. It provided the necessary electrical conductivity to keep the aircraft and its systems, such as onboard electronics or metallic control cables, safe [4]. The aircraft antenna is protected by a radome, which diverts the strike to the grounded section of the aircraft while allowing electromagnetic waves used for communications [5, 6].

Figure 1.1: Aircraft struck by a lightning strike [7].

Aircraft companies are investing in research to change from metal structures to composite structures with high mechanical properties to reduce overall weight of the aircraft, leading to fuel savings for environmental and monetary benefits [8]. Fiber reinforced polymer (FRP) composites, even those made of carbon fibers, are unable to carry the high currents and electromagnetic forces to prevent lightning damage on the aircraft. There is a need for lightning strike protection (LSP) to prevent damage such as embrittlement, delamination of composite fiber/matrix and/or structural failure [2]. The LSP system must be able to carry high currents and electromagnetic interference (EMI) forces generated by a lightning strike. It lets the current flow through the protected aircraft without causing damage and to exit towards the ground. Damage occurs where the current is densest, usually at the entrance or exit of a lightning strike. The current commercial product for LSP is a copper or aluminum expanded metallic foil adhered to the surface of the composite panels. Other materials, such as nickel [6] and phosphorus bronze [9], were used but the additional weight negated the weight savings from using composite materials.

1.1 LSP Principles

Lightning commonly strikes an aircraft when it passes through a storm cloud or during landing/takeoff moments [10]. There are a few types of lightning strikes, such as cloud to ground, cloud to cloud, ground to cloud, which is also called a return stroke, and intracloud, which is within the cloud itself and occurs more commonly on aircraft than ground strikes do [5, 11]. Lighting usually strikes the aircraft's nose, wing tip or another extremity, and the current will take the shortest and most conductive path possible to exit at another extremity, completing the 'electrical circuit' [2]. Due to the aircraft moving during a lightning strike, the lightning discharge will be 'swept' along the aircraft for a short distance. Lightning current flows through an attachment point which is called the hang on. The entry and exit points of a strike will have the largest density of energy/current of the lightning strike. Very high energy densities can result in material vaporization, while this energy spike can be more quickly diffused in high conductivity materials. A lightning strike's type and magnitude of damage depends on its energy level, the LSP surface materials, the underlying composite type and layup (the fiber orientations and stacking order), as well as paint thickness [8]. Therefore the LSP's main goal is to keep the lightning current on the exterior and quickly exit the aircraft by providing an electrically conductive path on the exterior structure [2].

1.2 Regulations and Standards

Preventing catastrophic structural damage, hazardous electrical shocks and loss of flight control are the main objectives for developing LSP. Metallic frame aircraft can do this [5] but non-metallic components have more difficulty minimizing the effects of a direct lightning strike or a high amperage current [12]. There are government agencies, military standards as well as organizations such as Society of Automotive Engineers (SAE) and aircraft manufacturers who all have their own standards and internal requirements to address LSP [4].

The important LSP standards and regulations are described below. According to Federal Aviation Administration (FAA) regulations Advisory Circular AC 25–21, Section 25.581 “Lightning Protection of Structure”, an aircraft struck by lightning must be able to continue to fly and perform normal operations [12]. Current industry standards like the SAE Aerospace Recommended Practices (ARP) contain guidelines and tests to pass government regulations, as

there is no minimum electrical conductivity to pass the standards and regulations, though higher conductivity materials undergo less damage than more resistive [13]. This can be seen during lightning tests on panels where more conductive materials do not have damage that penetrates the panel or is smaller in area [13]. Simulated lightning waveforms and aircraft zones demonstrate lightning strike phenomena according to the SAE ARP 5412 and 5414 standards. By using different protection layers in different zones it is possible to tailor the aircraft lightning protection to reduce the weight while still keeping the aircraft protected.

The six lightning strike zones, seen in Figure 1.2 for a commercial aircraft, determined by SAE ARP 5414 represent the probability of being struck by lightning and subjected by the various density currents. This is one of the steps required to show the aircraft is protected [14]. These zones, determined by laboratory lightning strike tests, are represented thus [5, 11]:

- Zone 1: High likelihood of initial lightning strike attaching itself to the frame at attachment point with first return strokes.
- Zone 1A: Low expectation of hang on.
- Zone 1B: High expectation of hang on.
- Zone 1C: First return stroke of reduced amplitude and low expectation of hang on.
- Zone 2: Likelihood of having subsequent swept strokes or re-strikes. Swept strokes occur as the aircraft traverses a lightning channel such that the strike 'sweeps' across the surface. Zone 2A: Low expectation of hang on.
- Zone 2B: High expectation of hang on.
- Zone 3: Supports large currents between areas of attachment points.

Standard SAE ARP 5412 shows four lightning flash current waveforms named A-D as seen in Figure 1.3 recommended to emulate lightning strikes and evaluate their effects. Each zone mentioned in standard SAE ARP 5414 is required to sustain certain of these current waveforms, such as an A component which can go up to 200,000 A [15]. Component A simulates the first return stroke, components B and C the long duration of currents following a strike due to the aircraft moving and return strokes causing long duration currents, while components D are the subsequent stroke. Zone 1 needs to be able to protect against waveform A while Zone 2 need only protect against component D, which is lower in current amplitude than A. A lightning generator was fabricated for the project for A-component strikes. Tests for lightning strikes are normally passed or failed only and depend on whether aircraft safety has been compromised or not by the damage resulting from the strike [5].

Materials used for LSP must be able to contain large currents in amplitude and density according to the SAE and AC standards. Zone 1 requires better protection as higher current densities must be able to pass through them, unlike Zone 2 and 3, which have a more dispersed current density. Some graphite/carbon fiber composites in Zone 2 do not require additional LSP [5]. Other standards are listed in Table 1.1 and deal with tangentially related safeguards such as the protection of fuel systems against ignition from lightning strikes and electronic equipment protection [16].

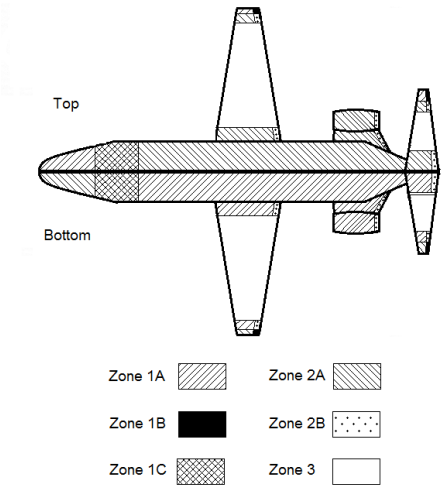

Figure 1.2: Lightning strike zones according to SAE ARP 5414 [14] [17].

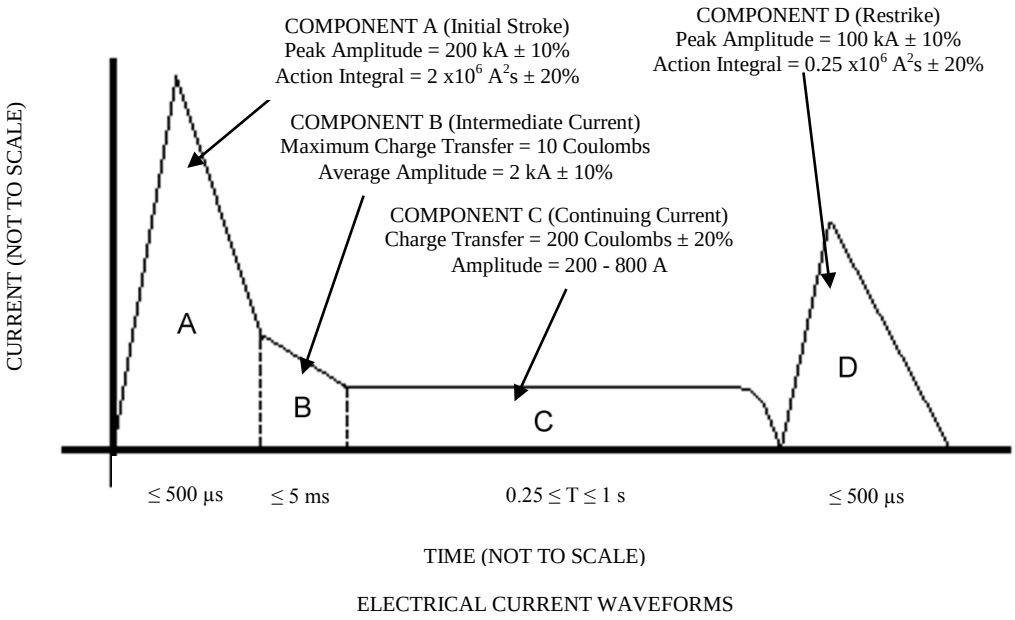

Figure 1.3: Lightning strike simulation according to SAE ARP 5412 [18].

1.3 Present LSP Coatings

LSP materials can be applied on the outer surface (coating) or embedded inside the composite structure (embedded conductive fibers inside the composite laminate, resin modifications with fillers to improve its electrical conductivity) [3].

Table 1.1 shows many of the currently available commercial products, most of which consist of metallic mesh or expanded foil bonded with modified resin bonded to the composite surface.

Table 1.1: Overview of select LSP products [17].

Type of LSP	**Example of configuration**	**Commercial product**	**Main characteristics**
Metallic mesh or foil bonded with resin	• Mesh materials (copper, aluminum, bronze, titanium) • Resin materials (epoxy, vinyl ester, modified epoxy) • Prepreg materials	Astrostrike by Astroseal Products Mfg. Corp. MicroGrid by Dexmet Corp. Strikegrid by Alcore Corp. HexWeb CR-PAA by Hexcel Corp.	High conductivity of metal Heavy surface material Problem with porosity
Metal or metalized fibers bonded with resin	• Fibers, woven or non-woven screens (carbon, graphite, glass, polyester, synthetic fibers) • Coatings (nickel, copper, silver, platinum)	Coated fibers by Metal Coated Fibers Metal hybrids by Electro Fiber Technologies Hexply by Hexcel	Lightweight Less efficient than mesh Flexible process (multicoating and multilayer is possible)
Polymer-based film or conductive adhesives	• Enhanced polymer with additives	Peel-and-stick by Integument Technologies Scotch-Weld by 3M	Lightweight Smooth finish Must be replaced if struck

1.4 Objectives

This thesis was completed as part of a Consortium for Research and Innovation in Aerospace in Quebec project: CRIAQ COMP-502. The main objective of the CRIAQ project was to develop a lightweight conductive coating for efficient lightning strike protection of composite structures of aircraft while featuring the desired characteristics: High electromagnetic protection, high mechanical resistance, good environmental protection, manufacturability and moderate costs.

Bombardier Aerospace (BA), Bell Textron Helicopter Canada (BTHC), and 3M have expressed their interests on the development of conductive films or coatings for composite structures. This multidisciplinary project required the collaboration between the industrial partners and the diversified academic research team from Polytechnique Montréal, Université du Québec a Montréal, and McGill University.

Within this project **the main objective of my thesis** was to determine the electrical and tribomechanical in order to evaluate the performance of surface conductive coating/composite structure systems (CC/CS) and to observe their environmental stability. In particular we study the conductive coatings (fabricated under the conditions described in Section 3.1) mechanical (hardness H, and Young's Modulus, E), tribological (coefficient of friction), and functional properties (specific resistivity) and their stability in harsh environment. The change in mechanical flexion modulus and flexural strength of the composite substrate after current injection was also studied to see the effectiveness of the conductive coating's protection of the substrate from electrical damage. These characteristics are compared with the baseline current expanded copper foil technology.

Different conductive coatings were prepared by students at different universities. Magnetron sputtered aluminum coatings were fabricated as part of this thesis. They are described in Section 3.1.

1.5 Sections Outline

After the introduction on lightning strike protection, important information on current LSP coatings and regulations is described in Chapter 1. The project and thesis objectives are then presented.

The background information of this thesis in Chapter 2 includes current and potential materials, methods and coatings from the literature for LSP. It details various materials like metallic materials, types of metal meshes, metal fibers, metal nanowires, carbon nanotubes, graphene, and synergy between the last two materials, most of which are used by the other students of the project. It describes the coating processes used by students such as magnetron sputtering, electroless plating, and thermal/cold spray. It explains important physical phenomena like electrical percolation threshold, which is an important concept for conductive coatings prepared by students working in this project.

The methodology in Chapter 3 describes the LSP conductive coatings, designs and fabrication methods by the students working in this project. Each coating uses a different fabrication method, described in some detail, but the magnetron sputtering deposition method is given in more detail and attention, as this was done as part of this thesis.

The various tests used to characterize the sample LSP conductive coating properties are explained and described in Chapter 3. This includes the electrical characterization done on the samples, including those done as part of multi-cycle thermal and salt spray tests and the mechanical characterization, which includes adhesion, scratch, indentation and three-point flexion tests. Other tests that were part of the thesis, such as Thermogravimetric Analysis (TGA), Scanning Electron Microscope (SEM) and tribological test are included in this section.

The experimental results are shown in Chapter 4, including electrical, mechanical, environmental and tribological properties. The mechanical properties include results of hardness and the Young's modulus of the coatings from indentation tests, the results of the scratch tests including SEM image and residual depth, and the changes in the flexural modulus and strength after larger electrical currents are injected. A comparison is provided between bulk materials, the baseline commercial product, and materials provided by the industrial partners, and LSP conductive coatings designed in this project.

Chapter 5 builds on Chapter 4 to present a thorough conclusion. Following that is a discussion of suggested improvements to the samples used and to the methodology of the tests, including notes on further tests that could be included in the project. Finally, additional applications of the project's results are covered.

CHAPTER 2 BACKGROUND

This background information review details many of the properties of materials, conductive coating designs and fabrication techniques used for LSP and more specifically those used in this project and thesis. Section 2.10 includes electrical properties for LSP coatings. Section 2.11 details the testing of certain mechanical properties of LSP composites. A more detailed literature review about LSP can be found in the literature review [17].

2.1 Properties of LSP Metallic Materials

Low electrically resistive materials are needed for LSP. Plastics used in aerospace composites have surface resistance near 10^{12} ohm/sq and are considered insulators [19]. A low volume resistivity and/or low volumetric mass density mean a low specific resistivity and thus a good choice for LSP. Some observations to note about metallic materials:

- Low volume resistivity and low prices make aluminum and copper the most used materials [3].
- Silver is the most conductive, but is heavy and expensive compared to copper and aluminum [20].
- Galvanic corrosion occurs between aluminum and carbon[3, 21].

Some highly conductive materials have severe drawbacks that prevent their use in LSP applications:

- Calcium, lithium, potassium and sodium have exothermic reactions in water and release hydrogen, which may ignite it in the atmosphere [22].
- Magnesium is flammable but could be used in alloy form currently used in the aerospace domain such as magnesium alloys to reduce weight in fuselage structures [23].
- Alloys traditionally have conductivity levels at about fifty percent of solid bulk metal foil materials [24].
- Beryllium is expensive and toxic but currently used in the aerospace domain such as in copper/beryllium alloys to improve component service life [25].

2.2 Metal Meshes

The main LSP processes and products for LSP can be found in the literature review on lightning strike protection of aircraft [17] and Table 1.1, which includes a short list of some companies that work on LSP. The current main protection against lightning strikes is a flat metal mesh (expanded metallic foil, which is used as a comparison baseline for all conductive coatings) of aluminum or copper over the composite outer structure [5]. Non-expanded metal foil is currently

not used due to delamination, its prevention of resin bonding, and the resin underneath the foil could vaporize causing a buildup of pressure that causes greater damage to the foil from the blow out pressure [5]. Figure 2.1a shows a woven mesh, which can be made of alloys, but the contact point between strands have higher resistance and non-uniform thickness but are nonetheless still being used for LSP [20, 24, 26]. Figure 2.1b shows a non-woven mesh (expanded metal foil) that can be expanded by pulling/stretching to alter its thickness and electrical resistance, a smoother surface, and reduce the volume and weight of resin to fill the mesh [27]. A non-woven (expanded metal foil) can be made of almost pure metal, and thus have the best electrical conductivity possible [24].

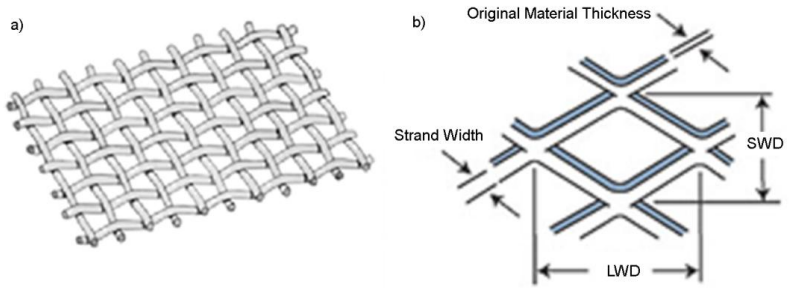

Figure 2.1: a) Woven mesh design [28, 29]. b) Typical metallic perforated mesh (expanded metal foil) [17, 30, 31] image courtesy of Dexmet Corporation.

Very thin meshes can be problematic by not providing enough electrical conductivity or by being at risk of vaporization from lightning strikes [32], although that might be desirable if it helps protect the underlying structure by acting as a sacrificial layer such as LS-1000® from Integument Technologies [33]. One advantage of non-woven meshes is that they do not unravel or have loose strands, which avoids complications during fabrication or installation of LSP on composite panels, the mesh staying homogenous and smooth around shapes and contours to provide constant conductivity to the aircraft surface [31]. Metal meshes are adhered to composite panels using resins, adhesives or surfacing films. Various methods exist such as piling separate products, pre-impregnation (pre-preg), and ply-integrated solution to ensure bonding [3]. Figure 2.2 shows a conceptual schematic of the metal mesh between two adhesive films. Isolation layers may need to be added if one of the plies is an aluminum mesh in addition to the surface adhesive to adhere the metal mesh to the underlying composite as well as protect it from outside elements.

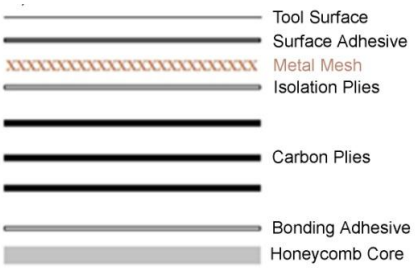

Figure 2.2: Typical layup showing position of metal mesh from StrikeGrid™ Continuous expanded aluminum foil brochure [15].

2.3 Metal Coated Fibers

Some of the other LSP products include metallic fibers, such as an interconnected network of nickel coated carbon fibers from Advanced Fiber Nonwovens (AFN) Group [34]. The use of nickel on the carbon fibers removes the need of an isolation layer to prevent galvanic corrosion. Tests were performed and were successfully passed by this coating with no structural damage or delamination of the protected panels, with most of the damage being on the surface just like an aluminum LSP panel [34]. Silver-coated carbon nanofibers use a similar concept for LSP as shown in Section 3.1.4.

2.4 Metallic Coating Processes

With metal being one of the most conductive materials available, it is also possible to coat this conductive material onto other materials such as mica [35], glass [36] or carbon [37] particles or structures. Possible methods include Physical Vapour Deposition (PVD) [38], Spark Plasma Sintering (SPS) [39, 40], or Flame Spray with aluminum [41]. Some of these methods are used in

Table 1.1 such as metalized fibers provided by commercial companies for LSP products. The following deposition method, magnetron sputtering, is used in this thesis and the other methods, electroless plating and cold spray, by students in the project as shown in Section 3.1.

2.4.1 Magnetron Sputtering

This method was used as part of this thesis as shown in Section 3.1.8. One of these metallization methods is physical vapor deposition. PVD involves formation of vapors from a solid source using thermal energy (evaporation) or momentum (sputtering). It is usually performed at low pressures to allow directional transport of gaseous species from the source to the substrate. PVD

may be used for the deposition of pure materials or compounds. Compounds are frequently deposited by reactive processes. Magnetron sputtering uses electromagnetic fields to ionize the gas. It can deposit a film of a few thousand Angstroms (less than one micron) [42] of condensed elemental, alloy and compound materials. Thicker deposits can be accomplished with multiple depositions. Décor Engineering uses this method with aluminum to protect the aircraft from EMI and lightning strikes by providing multiple layers of PVD [38]. In this thesis the relatively new method of high power impulse magnetron sputtering (HiPIMS), combining magnetron sputtering with pulsed power technology, is used to fabricate aluminum surface coatings. There are two parts of this process: the pre-treatment of the surface and the film growth process. The ionization of the sputtered atoms leads to the availability of ions for both pre-treatment and for well-adhered surface coatings. HiPIMS uses greater power densities during pulses compared to the normal mid-frequency pulsed magnetron sputtering. Two definitions of HIPIMS are: A technical definition, "HIPIMS is pulsed sputtering where the peak power exceeds the time-averaged power by typically two orders of magnitude" while a physical definition is " HIPIMS is pulsed sputtering where a very significant fraction of the sputtered atoms becomes ionized" [43].

2.4.2 Electroless Plating

This method was used as shown in Section 3.1.7. Spark plasma sintering (SPS) and electroless plating processes have also been considered, with multiwalled carbon nanotubes electrical and thermal properties tuned by SPS [40] and increasing the conductivity of carbon black and carbon nanotubes (CNT) particles with SPS temperature [39], for possible use in LSP. Electroless plating uses a chemical reduction produced by a catalyst to deposit metal on the substrate, with various methods detailed by the American Society for Metals (ASM) ASM Handbooks Online Volume 5 (Surface Engineering) to deposit copper, nickel, chromium and other metals [44]. Some metal fibers are coated by electroless plating which can provide LSP [45].

2.4.3 Thermal and Cold Spray

The cold spray method was used as shown in Section 3.1.5. Thermal spraying [46] can deposit metal using rods, wires or powders as sources on various substrates, and are classified by energy input source, such as flame and cold spray which reference the lower and higher temperature ranges of this method. A material is melted and atomized before it is sprayed in a gas stream of

high velocity, bonding on the surface via mechanical bonding as the particle freezes and interlocks on the substrate, as seen in Figure 2.3. Various metals could be used such as nickel, copper, aluminum, titanium and others [47-49].

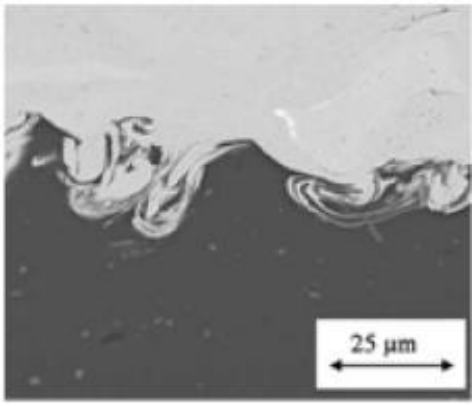

Figure 2.3: SEM image of copper (light area) coating on aluminum (dark area) [50].

Using cold spray has some difficulties, such as oxidation of the metal powders even at lower gas temperatures than regular thermal spraying, which leads to reduced conductivity. To bond with the substrate, the particle must have a certain critical velocity and be neither too big or energetic [51]. Coatings of 30 µm or less can sometimes be easily peeled off, and a proposed solution is to have a thin layer of plasma sprayed aluminum to act as bonding layer for the next cold sprayed particles to anchor and adhere onto a composite. Figure 2.4 shows the volume resistivity of cold spray aluminum coatings and the interlayer plasma sprayed coating. It shows that the gas temperature and process used in the coating process has an effect on the coating, with higher gas temperatures leading to higher volume resistivity.

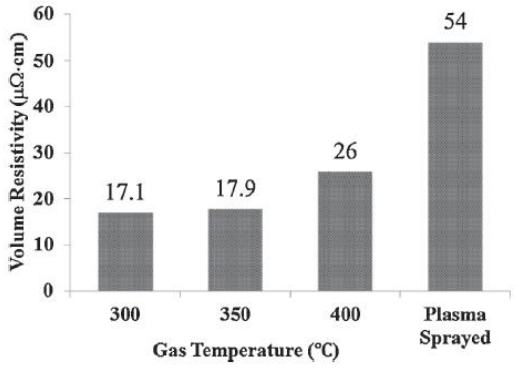

Figure 2.4: Volume resistivity of cold spray aluminum layers at different gas temperatures and of plasma sprayed aluminum [51].

2.5 Metallic Nanowires

Silver nanowires was used as shown in Section 3.1.6. Metallic nanowires have attracted scientific attention [52-62], such as copper nanowires with high electrical conductivity [62]. They have good mechanical and electrical properties to replace standard nanofillers [60]. Other materials include aluminum, silver, gold and nickel, and like CNTs they have high surface area and aspect ratios [63] but lower electrical conductivities than bulk conductivities (10^4 S/m [63] vs. 10^6 S/m [64]) making them poor stand-alone replacement for copper meshes [65]. They could be used to percolate adhesive films and matrix to fabricate conductive coatings such as one study that used copper nanowires at 0.24 vol.% [52] or used synergistically with carbon nanoparticles.

2.6 Carbon Nanotubes

Carbon nanotubes was used as shown in Section 3.1.4. CNTs are used in many applications due to their mechanical and electrical properties, including in composites for automotive and aircraft industries [66]. They are carbon sheets of hexagonal networks of carbon atoms and chemically similar to graphite, rolled into a hollow seamless cylinder [67]. The two types of CNTs, single-walled carbon nanotubes (SWCNTs) and multi-walled carbon nanotubes (MWCNTs) are walls of a single atom about 1-2 nm thick of graphene cylinders bonded together by weak van der Waals forces. CNTs high strength-to-weight ratios are achieved due to the covalent bonds between carbon atoms [67]. Axial electrical conductivity values for CNTs electrical conductivity can reach 2×10^7 S/m [39]. With high electrical and thermal conductivity and their high Young's modulus, CNTs added in a connected network increase the composite's electrical/thermal/mechanical properties. In particular a buckypaper (BP) which is a paper of intertwined carbon nanotubes can be formed and used for LSP [2]. As seen in the literature [68], CNTs have a high theoretical conductivity but experimentally this value is orders of magnitude lower, and their non-uniformity reduces their potential for LSP.

2.7 Graphene

Graphene sheets was used as shown in Section 3.1.6. A graphene sheet is a dense honeycomb crystalline monolayer of carbon atoms with a larger area per unit mass than CNTs. It is commonly fabricated by exfoliation [69]. Graphene can also come in multi-layer carbon plates called multi-graphene platelets (MGPs), but its electrical conductivity normal to its plane is

smaller than the parallel direction [70]. They have promising applications as nanofiller materials for their high aspect ratios, high conductivity, unique graphitized plane structure and low costs [71].

2.8 Synergy between Graphene and CNT

A similar synergy was used as shown in Section 3.1.6 with graphene oxide functionalized with silver nanowires. One way to increase conductivity with nanoparticles is to create a synergetic mix of CNT and graphene as shown in some studies [70, 71] where few-layer graphene (FLG), MGPs and MWCNTs were used as fillers. One of the mixing methods is shown in Figure 2.5 where FLGs and MWCNTs are placed in distilled water, dispersed with high shear mixing, sonicated, and then mixed and filtered into a paper with high air pressure and oven drying. Mechanical and electrical properties were improved much more than if only graphene sheets or CNTs were added alone [71]. It is thought the MWCNTs prevented stacking and aggregation of MGPs while connecting them together electrically.

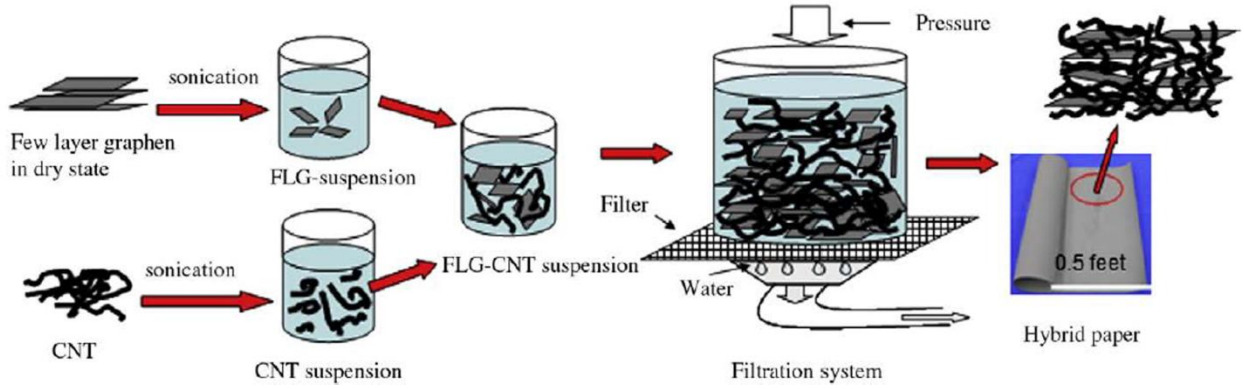

Figure 2.5: A hybrid of CNT and FLG mixing to creature a hybrid paper [17] [70].

2.9 LSP Nanoparticles and Percolation Networks

Three separate coatings designed by students were fabricated using the principle of the percolation network for electrical conductivity: silver nanoparticles in matrix in Section 3.1.3, silver-coated carbon nanofibers in Section 3.1.4, and graphene oxide with silver nanowires in Section 3.1.6. Adding micro or nano level scale conductive particles to a material does not automatically make it conductive overall. Factors such as the concentration, particles dimensions, aspect ratio and their size are different from the macroscale level, which affects interactions mechanisms. Volume and weight percentages, vol.% and wt.% respectively, are used to measure

the amounts of particles added to a material and thus used to measure the electrical percolation threshold (EPT). The EPT is at the critical concentration where a non-conductive material becomes conductive by creating a continuous network of connected particles together, such that adding more particles creates more electrical pathways and thus rapidly increases the material's conductivity. The right distribution, the location of particles in a volume, and the right dispersion, the distance between each particle, is necessary to form the EPT.

Many of the studies on EPT with electrical particles are on CNTs [52, 72-77]. The contact resistance between particles determines the overall resistance at the critical content value of the EPT [76, 78]. Figure 2.6 shows a threshold model for CNTs or metal nanowires, and the resistance variation at different concentrations. The percolation threshold occurs when the 3D network of particles is created throughout the sample, and a small increase in volume fraction changes result in a large volume resistivity decreases. Volume resistivity decreases rapidly due to the formation of the network before decreasing less rapidly. A poor distribution and good dispersion ensures a connected and conductive percolated network of particles [79].

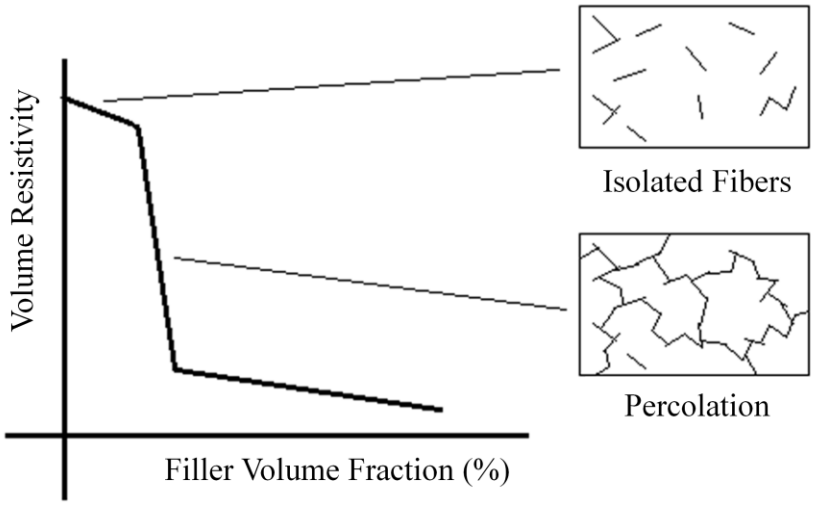

Figure 2.6: Volume resistivity vs. filler volume fraction [17] [79].

EPT values and the necessary dispersion/distribution requirements are affected by the particles used, which have three possible dimensions: 1-D particles like CNTs, 2-D like graphene sheets, and 3-D like silver nanoparticles. The particle dimension types affect their aspect ratio, ratio of interfacial volume to particle volume and their size [80]. The nanoscale level also reduces surface roughness and average separation between particles leading to higher dispersive forces between

particles [80]. Very low EPTs can be achieved with high aspect ratios [80] allowing the creation of conductive adhesives.

2.10 Electrical Tests of LSP Coatings

Although there is no minimum volume resistivity required by law or regulation mentioned earlier, it was found that the more conductive LSP coatings received less damage from lightning strike [13]. There are various types of electrical tests performed in literature to evaluate the performance of LSP of different materials, which are divided in two categories. The first tests characterize intrinsic properties of the materials such as volume and surface resistance including the four points probe method for volume resistivity measurements described in Section 3.3.1 on LSP surface coatings. The results of these first tests are used to check the effectiveness of coating methods and parameters, such as in cold spray. Different parameters can lead to different volume resistivity and thus different lightning strike protection effectiveness. Table 2.1 shows the volumetric mass density and electrical properties of materials used in the project and mentioned in this thesis. The second category is electrical tests using a lightning emulator, but these tests are part of another student's study as part of the project and are only partially completed at this time.

Table 2.1: Volumetric mass density, volume resistivity and specific resistivity for metallic and carbon materials [17].

Material	Volumetric Mass Density (g/cm^3)	Volume Resistivity ($\Omega \cdot cm$) $\cdot 10^{-6}$	Specific Resistivity ($\Omega \cdot g/cm^2$)$\cdot 10^{-5}$	Price*	Comment	Ref.
Metals						[64]
Aluminum	2.7	02.65	0.72	$	Galvanic corrosion with carbon	
Beryllium	1.8	4	0.72	$$$	Toxic	
Calcium	1.55	3.17	0.49	$	Exothermic reaction with water	
Chromium	7.19	13.00	9.35	$	Toxic	
Copper	8.96	01.68	1.51	$		
Lithium	0.53	9.35	0.50	$	Exothermic reaction with water	
Magnesium	1.7	4.44	0.76	$	Ignitable	
Potassium	0.85	7.19	0.61	$$$	Exothermic reaction with water	
Silver	10.49	01.59	1.67	$$		
Sodium	0.96	4.76	0.46	$$$	Exothermic reaction with water	
Tin	7.35	11.0	8.09	$$		
Zinc	7.13	5.92	4.22	$		
Carbon materials						
Theoretical Carbon Nanotube	1.4	1.30	0.18	$$$$	Applies to only one CNT	[68]
Carbon Nanotube	1.4	100	14.0	$$$$	Variations	[81] [68]
Single Graphene Sheet	0.3	1	0.03	$$$	2D only	[82] [83]
Graphite	2.25	1375.52	309	$		[64]

*:$: 19$/kg or less. $$: 20-199, $$$: 200-1999, $$$$: 2000-or more

2.11 Mechanical Testing of LSP Coatings

There are tests that can give the mechanical properties of composites such as tension, compression and three point flexion tests. The LSP coating itself should not have an effect on the properties of the composite substrate. After a lightning strike, the composite's mechanical performance could be degraded [13] due to damage on the composite fiber. The main reason for these mechanical tests then is to see if the LSP coating protects the underlying composite structure from lightning strike damage. Thus if the mechanical properties degrade after current is injected or lightning strikes from the ones found in pristine samples, it can be concluded that the lightning strike protection coating was ineffective or insufficient.

The literature [2] [4] [10] [84] describes mechanical measurements done on samples that were tested before and after large current injections that simulate lightning strikes. It is expected that high current lightning strikes would reduce the mechanical properties of a struck composite panel but one example below show that is not always the case. One such material test are the carbon nanofibers and nickel nanostrands paper placed on composite panels (CP) and then cut into strips for flexion test conducted after a 100,000 A strike. Testing showed that the high conductivity strips had no significant degradation of flexural strength or elasticity modulus but a significant decrease for the samples with more resistive strips with a 38% loss of flexural strength. Other LSP coatings have been tested, such as nickel-nanostrand veil, aligned buckypaper, random buckypaper, mixed buckypaper, and single-walled nanotubes at 100,000 A with reduction in ultimate compressive strength ranging from 30% to 75%. Tension and compression mechanical tests have also been performed at lower lightning strike currents (0, 10, 30 and 50 kA) as shown in Figure 2.7, which shows the residual strength for UNT and UNC specimens.

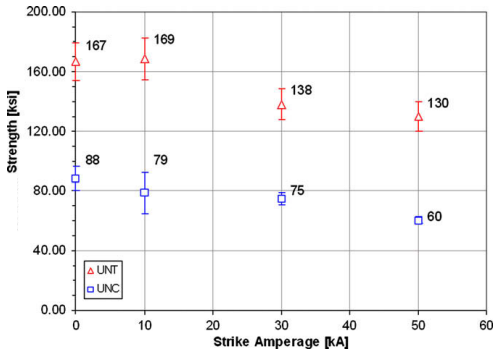

Figure 2.7: Tension and compression strength (in kilopound per square inch) vs. injected current for unnotched specimens in tension (UNT) and compression (UNC) [4].

There is a roughly linear decrease in strength for both tension and compression as the current intensity increases which is expected in the results for flexion tests performed for this thesis. However there is unintuitive behavior in mechanical results published by Boeing [84] where a linear increase of tension strength as lightning strike current is increased with a noticeable variation in the data for each current value. These results are also observed in Section 4.3.4.

CHAPTER 3 METHODOLOGY

The main part of this thesis is the study of electrical and mechanical properties of the LSP coatings provided as a baseline by the industrial partners and fabricated by other students detailed below. While it was not originally part of the objectives, the fabrication and study of magnetron sputtered aluminum coatings were added later and thus was not explored as thoroughly as possible. Each conductive coating's materials and fabrication methods are detailed in Section 3.1. SEM was also performed on samples to analyze the surface microstructure and to evaluate the scratch test results.

The electrical characterization of the samples is one of the most important tests to be done on the LSP coatings due to its importance regarding lightning strike protection. The important property used to compare the LSP coatings is the specific resistivity, which is the product of volume resistivity and volumetric mass density of the coating. As the main objective for the CRIAQ requires the new surface coating with the smallest weight and volume resistivity as possible, this means that the coating with the smallest specific resistivity will have the greater potential as LSP for aircraft. Thermogravimetric analysis was also performed on two silver inks used in one of the coatings to investigate the effects of silver concentration by weight on specific resistivity. Annealing of samples was limited to 200°C to prevent damage on the underlying composite substrate, with various times and temperatures used to see if the conductive coating could be optimized.

The mechanical tests such as adhesion/scratch, indentation, and flexion test, also give relevant properties of conductive coatings, particularly adhesion. The flexion tests were paired with two types of electrical tests: the current injections and the resistance changes during the test itself. Current injections in the flexion samples were done after the first tests, such that the second flexion test determined the change in mechanical properties due to the effectiveness of the LSP coating to handle large currents.

Environmental tests were performed on samples to determine mass and resistance changes before and after environmental test cycles. The environmental tests determined the feasibility of using the conductive coating without a protective surfacing film. However, the project assumed that a surfacing film would be placed over the conductive coating for protection and surface finishing.

3.1 LSP Conductive Coatings

The conductive coatings for LSP were provided by other students and by the industrial partners or fabricated as part of this thesis and summarized below. The composite and coatings provided by the industrial partners are considered the baseline by which to compare the prototype conductive coatings of other students. Table 3.1 below shows the conductive coatings prepared by the industrial partners and university students with the abbreviations and color code used for each, and a short description that is further expanded upon in the following sub-sections. The materials and fabrication methods were chosen to have conductive coatings with the lowest specific resistivity possible, as well as ease of manufacturing prototypes.

Table 3.1: List of all LSP conductive coatings.

Abbreviation	Color Code	Student Initials	LSP Coating Short Description
CFRP		-	Baseline Carbon Fiber and Epoxy Composite
ECF/SF		-	Baseline with Expanded Copper Foil and Surfacing Film
Nano Ag		RF	Silver Nanoparticles and Resin (PEDOT:PSS and or Epoxy)
Ag CNF		XC	Silver-Coated Carbon Fibers (with surfacing film underneath)
CS Sn		HC	Cold Sprayed Tin on Composite Substrate with Thicker Epoxy Layer
GO AgNW		JN	Graphene Oxide Layers and Silver Nanowires
EP Ag		RP	Silver Chemically Coated on Composite Substrate
MS Al		MG	Aluminum Deposited by Sputtering on Composite Substrate

3.1.1 Baseline Substrates-Composite (Carbon/Epoxy) with no LSP (CFRP)

The substrate for all samples is a carbon fiber resin polymer (CFRP), a carbon and epoxy composite without any lightning strike protection provided by Bombardier Aerospace Company. The material manufacturer is Cytec Industries Inc. with materials composed of Cycom 5276-1 resin / WT650 / 35 3k 8 Harness Satin (HS) weave fiber (BAMS 532-019 Class II. The layup, which is the fiber layout in the matrix that are perpendicular at 0° and 90° degrees, repeated once, and symmetrical from the middle of the composite thickness), is written as $(0/90)_{2s}$. No surfacing

film or expanded copper foil was installed. It was processed by Bombardier per internal reference standard BAPS 260-002 (curing at 177°C/350°F) with a finish of defect-free pinhole filling (a surface finish for the composite) per BAPS 138-013 Type I. The carbon fibers are conductive but not enough for purposes of LSP.

3.1.2 Baseline Substrates-Composite (Carbon/Epoxy) with Expanded Copper Foil within Surfacing Film Cytec SurfaceMaster 905C (ECF/SF)

The baseline LSP solution is a carbon/epoxy composite substrate with expanded copper foil and surfacing film (ECF/SF) protection: expanded copper foil (ECF) is placed inside the surfacing film (SF) of Cytec Surface Master 905, 0.017 g/cm^2 (0.035 pound per square feet (psf)) resin, 0.020 g/cm^2 (0.040 psf) mesh/foil (BAMS 553-001 Class 2, Type II Grade 7) provided by Bombardier Aerospace Company. These samples were provided pre-fabricated in two by two feet panels, the samples were cut into the required sample sizes.

3.1.3 Silver Nanoparticles in Matrix (Nano Ag)

The first LSP coating was fabricated by Rouhollah Farahani in the LM^2 lab at École Polytechnique. Silver ink (Ag-1 or Ag-2 based on reducing agent, monoethaloamine or diethanolamine respectively) was mixed with conductive PEDOT:PSS matrix, or with a 50/50 mixture of PEDOT:PSS and Epoxy matrix. The first method used to fabricate this coating on the CFRP was by casting directly on the sample with a masked adhesive tape on the side to prevent spilling. The second method was done with a spraying process that evaporated water using a heat gun as the coating was deposited on the surface. Additional annealing at 140°C was done in a closed oven with air at atmospheric pressure.

3.1.4 Silver-Coated Carbon Nanofibers (Ag CNF)

The next LSP surface coating fabricated was silver-coated carbon nanofibers mixed with surfacing film (Cytec SurfaceMaster 905) and cured on the composite substrate by Xavier Cauchy in the LM^2 lab at École Polytechnique. The silver-coated carbon nanofibers were fabricated by using Tollen's Reagent, a reducing agent, where the resulting silver particles then adhered to the nanofibers. The mixture was filtered and placed onto a surfacing film Cytec Surface Master 905 without expanded copper foil and placed on the carbon/epoxy composite for

curing. For the purposes of environmental and flexion tests, the conductive coating was placed on the surface of the surfacing film rather than underneath it in order to be able to measure the electrical resistance.

3.1.5 Cold Sprayed Tin (CS Sn)

This conductive coating consists of cold sprayed metal coating of pure metallic tin provided and fabricated by Hanqing Che from McGill University. Tin powder was accelerated at supersonic velocities onto substrate. The spray was layered by multiple passes over the panel, which was then cut into the required sizes for the various tests. The process of cold spray uses mechanical energy to deform the particles plastically onto the substrate and form bonds that make the conductive tin layer adhere to the composite substrate. Various cold sprayed tin conductive coatings were deposited with different gas temperatures, pressures and powder composition, such as tin/copper or tin/zinc. Other metal powders and combinations thereof were tried but only tin was able to adhere to the surface of the composite without destroying carbon fibers or bouncing off. The samples used for environmental and flexion tests were made only of tin coatings.

3.1.6 Graphene Oxide and Silver Nanowires in PEDOT:PSS Resin (GO AgNW)

Graphene oxide and silver nanowires were functionalized together and mixed with PEDOT:PSS resin, fabricated by Jeanne N'Diaye from Université du Québec a Montréal. Graphene oxide clumps were exfoliated into layered graphene, which were mixed and functionalized with silver nanowires to provide better electrical connections between graphene and nanowires. The aqueous solution was mixed with PEDOT:PSS to increase the adhesion of the coating on the substrate. This conductive coating was deposited on composite substrate by spin coating so that the coating could spread uniformly on the entire sample. The conductive coating was then heated at 90°C for 1 minute. The spin coating and heating steps were repeated 4 times.

3.1.7 Electroless Plated Silver (EP Ag)

The silver-coated composites were fabricated by Rajesh Ponnada in the LM^2 lab at École Polytechnique. The silver was chemically coated on the composite from Tollen's solution via electroless plating. The plating process was preceded by a short tin chloride sensitization process.

The sensitized composite was placed in the chemical bath containing Tollen's reagent and a reducing agent for 30 minutes before being removed, washed and annealed at 80°C, 100°C or 120°C for 3, 6 or 12 hours. The fabricated coating is very thin but very conductive.

3.1.8 Magnetron Sputtered Aluminum (MS Al)

The magnetron sputtered aluminum coatings were fabricated at the Functional Coating and Surface Engineering Laboratory (FCSEL). A target (or cathode) plate made of aluminum was bombarded by energetic ions (Ar+) in a glow discharge plasma, situated in front of the target. The bombardment process caused the removal of target aoms (Al) which then condensed on a substrate as a thin film. The aluminum-coated samples were fabricated using the following parameters starting with a pre-treatment by bombarding the composite with argon ions for 6 minutes. On the target, a Rubig power supply was used with High-Power Impulse Magnetron Sputtering (HiPIMS) discharge with a pulse length of 20 µs, a frequency of 10 kHz with an average target power of 250 W on pure aluminum. The pressure was 8 mTorr during deposition. A 13.56 MHz radio frequency (RF) power supply with RF power 80W and RF bias of ~200V was applied on the substrate. The deposition was performed with six periods of 30 minutes each with 30 minutes pause between each deposition period to prevent overheating the substrate. Other parameters were tried at first (3 hour long deposition and without surface pre-treatment with HiPIMS) but the longer deposition process heats the substrate and can cause damage in a ring area on the substrate. The deposition parameters were then changed to those described above.

3.2 Morphology/SEM/Optical Microscope

Cross-section surfaces as well as the top surfaces of the coatings were observed using a field emission scanning electron microscopy (FESEM JEOL, JSM-7600TFE [85]) and a scanning electron microscope (SEM JEOL, JSM840 [86]) which can also perform Energy-Dispersive X-ray Spectroscopy (EDX or EDS) at the CM^2 laboratory at École Polytechnique de Montreal. The former was used when high quality images were required while the latter was used for comparison and for its EDX capabilities for element chemical qualitative analysis. SEM images of scratch tests from Section 3.5.2 results were also obtained. Optical images for surface and cross-section were also obtained using a ZEISS AXIOSCOPE A1 in the FCSEL at École Polytechnique de Montreal.

3.3 Electrical Characterization

This section details the various test methods used to measure specific resistivity of the LSP coatings. The 4-point probe setup detailed below was the main test method used in this study. The other methods, the uniform current distribution in four-terminal sensing and the probes used during flexion tests, are also explained and detailed but do not play as important role for this thesis. The conductive coatings were all compared using the same method 4-point probe method. Oxidation was expected on some surfaces and was still measured since it could affect lightning strike simulation results. It was assumed for electrical calculations that the coatings are uniformly rectangular with no porosity or holes. While this is definitely not the case, it simplifies the calculations considerably. Such defects could affect the results by showing a higher specific resistivity than expected.

3.3.1 4-Point Probe on Coating

The volume resistivity of LSP coatings on composite coupons was measured using a four-point probe electrical apparatus at École Polytechnique de Montreal in the GCM lab. A current was injected with a Keithley 220 programmable current source from the outer probes onto the surface of the LSP conductive coating and the change in voltage was measured with the inner probes using Hewlett Packard 34401A multimeter. The probes were on springs to ensure a good connection with the conductive coating. The measurements were performed three times for each sample at different locations and their locations were aligned centered along its longest axis near the middle of the sample as seen in Figure 3.1.

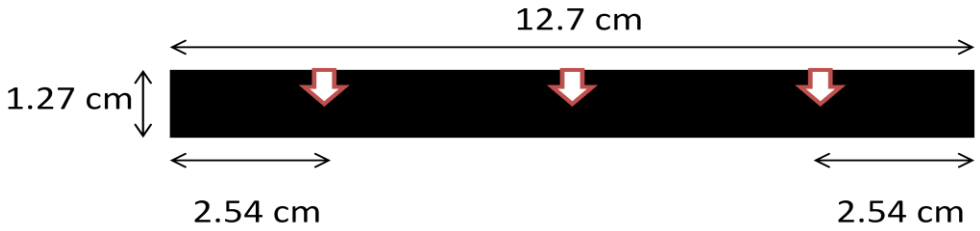

Figure 3.1: Three locations of electrical resistance measured for the 12.7 cm x 1.27 cm (5x0.5in) samples in the middle and 2.54 cm (1 in) from the sample ends.

Figure 3.2 shows the 4-point probe setup diagram. The coating's resistance $R = \frac{V}{I}$ was obtained from the injected current and voltage measurement and was multiplied by a correction factor (CF) to obtain the coating's sheet resistance $R_S = CF\frac{V}{I}$. This CF takes into account the coating

geometry and the measurement apparatus dimensions. It is noted that the coating dimensions varied which affected the CF. Since the thickness of the conductive coatings is always smaller than half of the distance between probes ($0.5 \leq t/s$), the current was assumed uniform throughout the thickness of the coating. The injected current lines cannot be assumed parallel to each other but are instead arranged in a series of curved lines from one current probe to the other and therefore, the current flow in the conductive coating is not parallel and uniform in current density and the CF corrects the measured voltage of the apparatus to account for this. Figure 3.3 shows correction factor approximation based on sample dimensions and its shape that was always rectangular. R_S is sheet resistance, V is voltage, I is current, ρ is volume resistivity, t is coating thickness, a is the sample length, d is the sample width, s is the distance between each probe, and CF is the correction factor, determined by the ratio of the sample width and distance between probes (d/s).

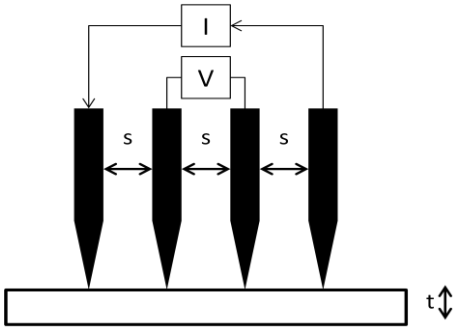

Figure 3.2: Diagram for electrical measurement of specific resistivity of 4-point probe method [87].

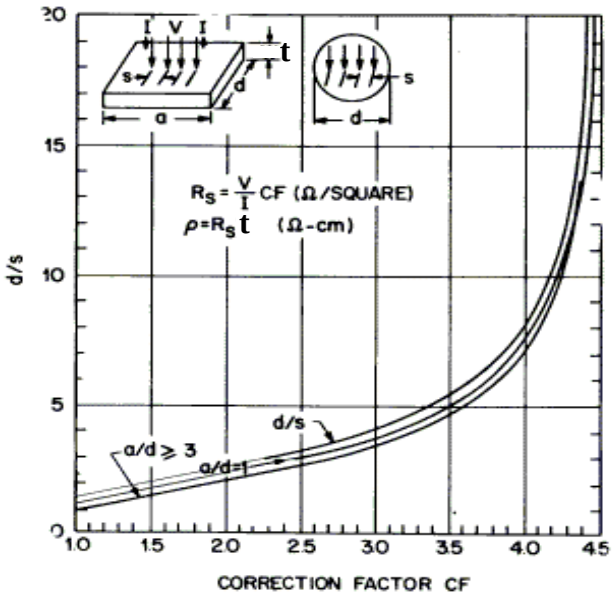

Figure 3.3: Correction factor based on geometry of the sample measured [88] [89].

Distances were measured with a ruler such as the distance between each probes in the 4-point probe apparatus are collinear and equal to s = 1 mm. The d/s ratio accounted for the non-linear current on the surface and determines which CF to use, as did the coating geometry. All coatings had rectangular geometry, where the ration of length over width (a/d) is greater than three. Therefore the line a/d ≥ 3 is used on Figure 3.3. In the case of disk-shaped samples, the d/s line would be used, and in the case of square samples, the a/d=1 line would be used. Using the ratio of d/s (about 13) for the vast majority of samples tested, the correction factor was therefore about 4.3-4.5. The three measured sheet resistances were averaged. The volume resistivity was obtained using $\rho = R_S \cdot t$. The specific resistivity was calculated by taking the coating's sample sheet resistance multiplied by its area density or its volume resistivity multiplied by its volumetric mass density.

3.3.2 Four-Terminal Sensing

The main difference between this method and the previous one (4-point probes) is that the current is assumed to be uniform and constant throughout the cross-section of the sample. A current from a Keithley 6221 DC and AC current source was sent through the sample's coating. Current enters and exits through large copper plates ensuring good contact between sample and current injection. The two outer spring probes in the middle measured the tension across two points in the sample. The probes were on springs to ensure a good connection with the conductive coating. Due to the distance between the copper plates and the voltage probes of the Keithley 2182A nanovoltmeter, the current was assumed constant, in parallel flow and uniform between voltage probes. The voltage tension that was created by the current was then measured across a known distance of 2.54 cm (1 inch) between voltage probes as seen in Figure 3.4. The coating's geometry (coating thickness and width) were used with the calculated resistance to determine the volume resistivity as per $\rho = \frac{R*d*t}{a}$ where d is the sample width, t is the sample thickness, and a is the length between the voltage probes. The volume resistivity was multiplied by the volumetric mass density to obtain the specific resistivity.

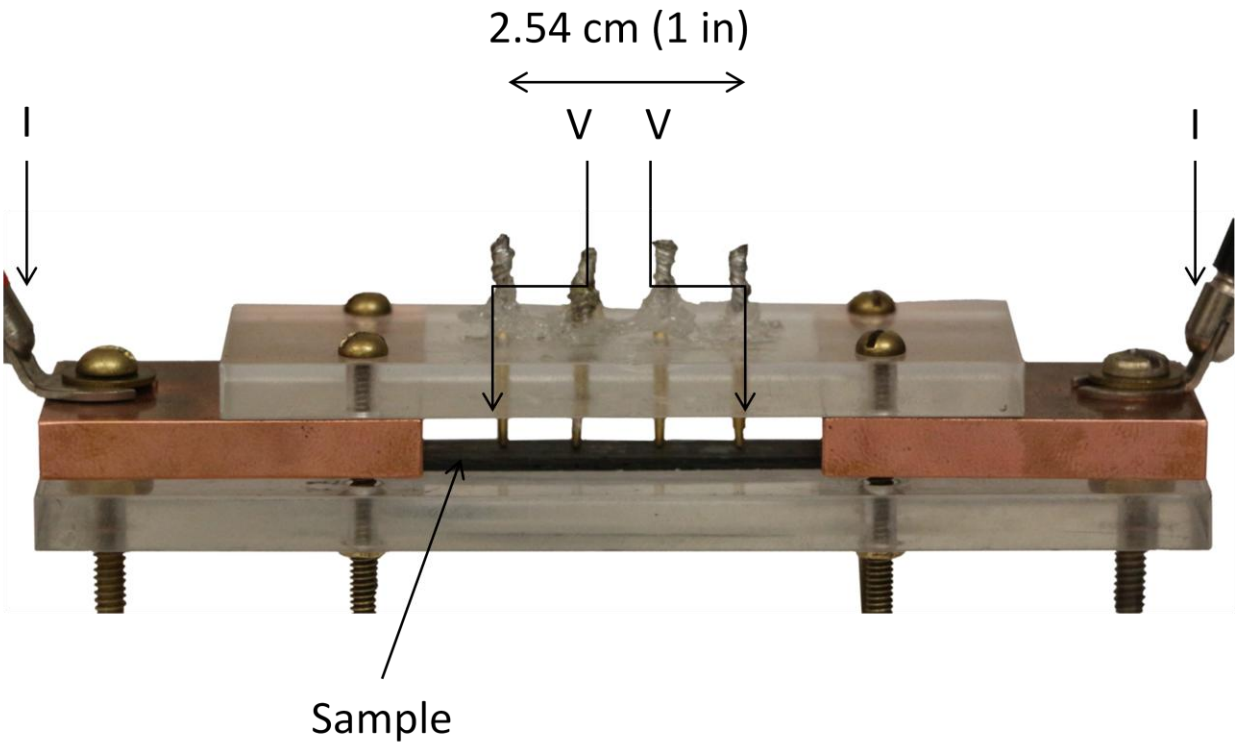

Figure 3.4: Four-terminal sensing by uniform current distribution.

3.3.3 Change in Resistance During Flexion Tests

During the flexion test (see Section 3.5.4 and 3.5.5 for more information), the electrical resistance of the conductive coatings was measured in real time. The acquisition rate was 1 Hz. The current was applied by a Keithley 6221 DC and AC current source and the voltage was displayed by a Keithley 2182A nanovoltmeter. A current of 100 mA was injected inside the conductive coating and the voltage was measured over time during the flexion test. The change in voltage is equivalent to the change in specific resistivity (due to ohm's law) and its percent change was calculated by comparing it at the start and end of the test. The specific resistivity was compared with the strain of the sample to highlight how this deformation affects resistance. The nanovoltmeter was measuring voltage relative to time independently of the flexion machine while the flexion machine was measuring strain relative to time, so the measurements are synchronized by using the break-off point as the synchronization point between specific resistivity and strain. Figure 3.5 shows the setup of this system. Injected current passes through outer alligator clips and voltage measured through the inner clips. The measured distance between voltage probes was 10.16 cm (4 inches).

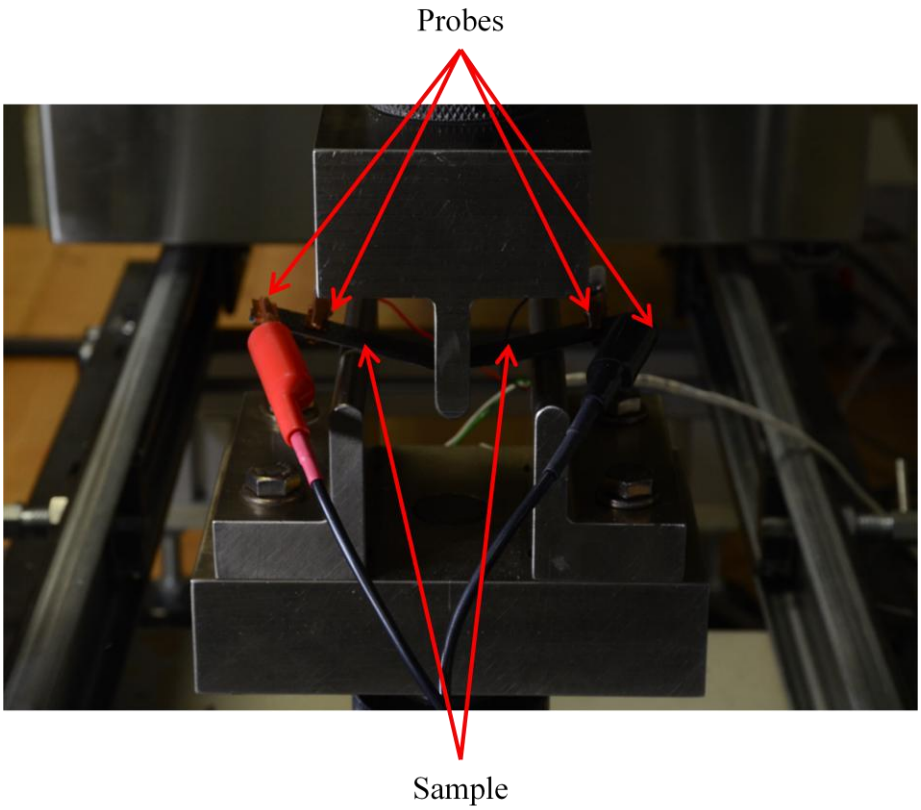

Figure 3.5: In progress electrical characterization of sample during 3-point flexion test.

3.3.4 4 Point Probe for Environmental Tests

This method used the same principles as in Section 3.3.1. It used the four probes (two outer probes for current, two inner probes for voltage) in the apparatus from 3.3.2 including the Fluke 5520A current source and the Keithley 2182A nanovoltmeter at Bell Helicopter Textron Canada at Mirabel. With the different sample size, a new CF was calculated using Figure 3.3. The CF used for environmental test samples was 4.0.

3.3.5 Current Injection

After testing for their mechanical properties in flexion tests (see Section 3.5.5), the composite coupons were then injected with the following levels of currents for 1 second each in a step function: 5 A, 25 A, 50 A and 100 A. A Lambda EMS Power Supply and Lambda EMS II Power Supply were used for the injections of 5/25A and 50/100A respectively in the Laboratory for Electrical Energy (LEE) at École Polytechnique de Montreal. It was originally planned to inject higher currents, up to 400 A to represent C-component waveforms per SAE ARP 5412 in Section 1.2, but it was dangerous to perform that experiment, therefore lower current values were used.

The reasons are as follow. Current injection was limited by the power of the machines, which could not inject 25 A, 50 A and 100 A in certain samples due to the conductive coating being too thin and resistive. Using more power would have produced fumes and smoke from burning the sample, which the electrical laboratory was not equipped to deal with. This limited the amount of current injected into samples. It was expected that if any damage occurs to the composite underneath the LSP coating, the reduction of mechanical properties would be noticeable in the flexion tests. Hence, for this thesis the electrical and mechanical (flexural strength and flexion modulus) values were tested before and after the current injection. It was hypothesized that the coatings with less volume resistivity will have less damage than with more volume resistivity. One study showed that more conductive layers were able to better resist the lightning strikes, resulting in smaller damaged area during tests than those with less conductivity [2].

3.4 Thermogravimetric Analysis

Thermogravimetric analysis (TGA) was performed on the synthesized silver inks used for the fabrication of samples with silver nanoparticles in matrix to estimate its percentage of silver weight determining which silver nanoparticles fabricating process resulted in a more conductive coating. A TGA machine (Q500, TA Instruments) was used with the following test procedure: The platinum pan's weight was measured during the whole test. The first step was to increase the temperature inside the sealed chamber, which starts at room temperature, increasing by a rate of 10°C/min until a temperature of 600°C was reached. During this phase, the sample flow was 60 mL/min using nitrogen gas to prevent oxidation. Then the rate of increase was changed to 50°C/min using airflow instead of nitrogen until a temperature of 850°C was reached. That temperature was maintained for five minutes as an isothermal period, and then the temperature was decreased by 50°C/min down to 35°C where the pan can then be removed. The weight loss indicated how much mass was left, and thus how much of that weight was silver. A thermocouple was used to measure temperature inside the gas flow.

3.5 Mechanical Characterization

This section details the various test methods used to measure the mechanical properties of LSP coatings and the composite substrate. The scratch test is to determine the adhesion of coating and the adhesion tape test is to compare the adhesion relative to each coating. The indentation test

was to determine the coating's hardness and Young's modulus. Finally, the three-point flexion tests were done to determine if the previous current injections, see Section 3.3.5, caused any damage to the underlying composite substrate by measuring the loss of its mechanical properties such as flexural strength and the modulus of elasticity in bending, or flexion modulus.

3.5.1 Adhesion Tape Test

Adhesion of the conductive coating to composite substrates was assessed using the standard ASTM D3359 – 09 Method B, the Gardco Model P-A-T Paint Adhesion Test Kit, and the multi-tooth cutters. A cross-scratch pattern was made using the cutting tool. For coatings up to 50 microns in thickness, the 11 cutting teeth were spaced 1 mm apart. For coatings between 50 and 125 µm thick, the 6 cutting teeth were spaced 2 mm apart. Scratch lengths were approximately 2 cm long for both cross hatches and cut down to the substrate's surface all the way through the coating as illustrated in Figure 3.6. A light brush was used to sweep away debris from the surface and the cross-scratch region. A pressure-sensitive tape was applied over the cross-scratch area, and a pencil eraser was pressed down on the tape to ensure good adhesion between tape and film. The tape was removed by manually peeling it off at an ~180° angle with a constant pull. The adhesion of the coating film was graded on a scale of 0 to 5, with 0B indicating 65% removal or more of the coating film, which indicates poor adhesion, and 5B having 0% removal, which indicates good adhesion, see Figure 3.7.

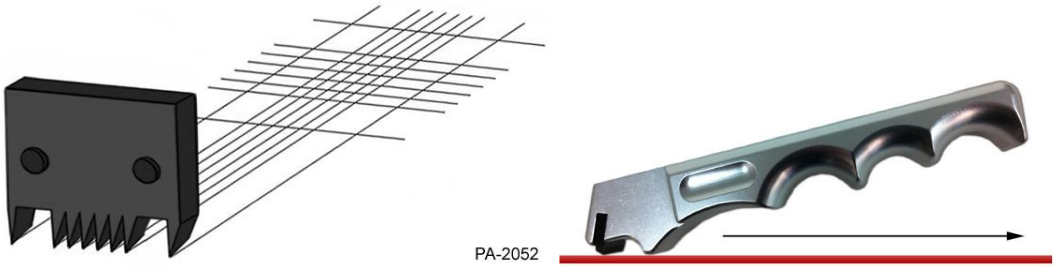

Figure 3.6: Cross-scratch results and cutting handheld tool [90].

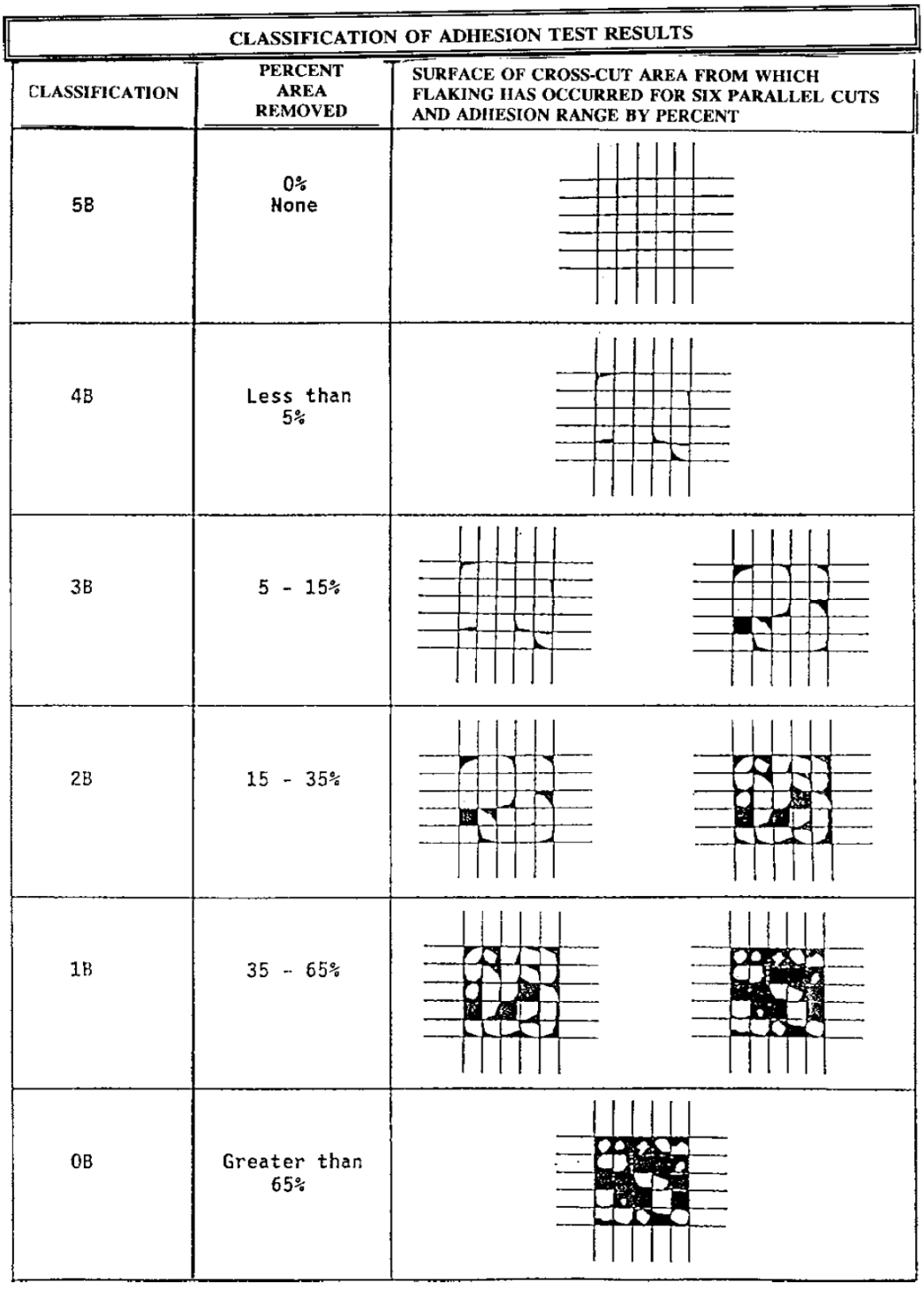

Figure 3.7: Classification of adhesion test results from standard ASTM D3359 – 09 Method B [90].

3.5.2 Scratch Test

Scratch tests using the standard G171 - 03 were used to determine adhesion of the coating to the CFRP substrate in addition to the coating's resistance to scratch. It was also used to determine the coefficient of friction for conductive coatings. The scratch resistance of the conductive coatings was evaluated by a test CSM instrument using a Rockwell diamond indenter (radius of 200 µm), as shown in Figure 3.8. The linearly increasing applied load was 0 to 10 N with a loading rate of 10 N/min and removal speed of 10 N/s. The distance scratched was 10 mm, and the indenter speed was 10 mm/min. The sample surface was pre and post scanned using a contact force of 30 mN in order to get penetration depth and residual depth for each sample. In the case of the composite carbon/epoxy (CFRP) and the surfacing film (ECF/SF), the indenter had a radius of 50 µm, a linearly increasing applied load of 0 to 30 N with same distance scratched (10 mm) and an indenter speed of 2 mm/min.

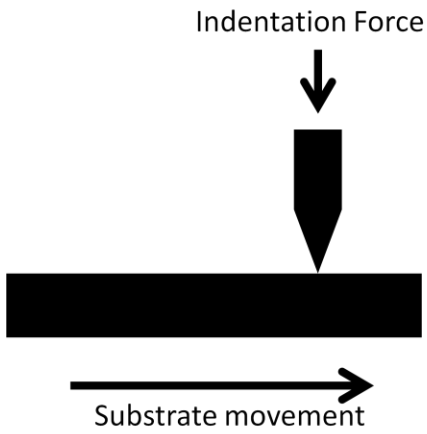

Figure 3.8: Scratch test diagram of substrate and application of progressively increasing load F_N from indenter.

3.5.3 Indentation Test

The mechanical properties of the coating films such as hardness and Young's modulus were evaluated with micro-indentation using a CSM micro-indentation tester according to ASTM E2546. In this technique, a micro-indenter was pressed into the sample that results in both elastic and plastic deformation. A diamond indenter Vickers shape (V-H-46), four sided pyramid at angle 68°, was used. Contact force was increased linearly at rate of 2000 mN/min up to the maximum contact force of 1000 mN. This was held for 10 seconds and then decreased at a rate of 2000 mN/min. The same process was repeated for each indentation at 25 different locations in a

5×5 matrix with 0.5 mm distance between each point. The indentations were done far enough from each other to avoid encountering plastic deformation from a previous indentation. The values of the hardness and Young's modulus were directly obtained from the software using the Oliver & Pharr technique [91] with the unloading curve in Figure 3.9, with P_{max} as the maximum load, h_r the residual depth, h_e the displacement associated with the elastic recovery during unloading, h_c the depth of the contact pyramid/square, and S=dP/dh the slope of the elastic unloading. Both of these values, S and h_c allowed the calculation of the hardness H_{IT} and Young's modulus $E_{IT.}$

A Hysitron TriboIndenter® from the FCSEL at École Polytechnique was used for nanoindentation of the EP Ag and MS Al conductive coatings because their thickness was too small for microindentation. The nanoindenter used a Berkovich diamond tip with load ranging from 100 µN to 5000 µN with 25 indentations. The load and unloading time were 5 seconds long and the maximum load was held for 2 seconds. The Oliver & Pharr technique was used here.

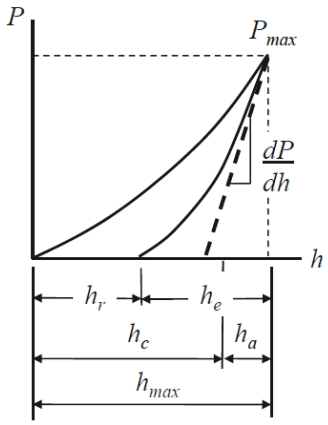

Figure 3.9: Load/displacement curve [92].

3.5.4 Sample Preparations for Flexion Test

The following procedures were respected for all samples. All samples were cut parallel to the alignment of carbon fibers on sample surface. The thickness and width of sample and coating were measured at three points as seen in Figure 3.1. The sample width and thickness were measured with a hand micrometer.

3.5.5 Three-Point Flexion

The flexion tests followed ASTM D790 standards, procedure A was used. A span-to-depth ratio of 32:1 was used. The support span length was changed according to each sample's thickness/depth such that the ratio remains 32:1. The crosshead motion used during the test was calculated by using $R = \frac{ZL^2}{6d}$ where R is the rate of crosshead motion, mm/min, L is the support span, mm, d is the depth/thickness of the beam, mm, and Z is the rate of straining of the outer fibers, mm/mm min. Z shall equal 0.01. The loading nose and supports were aligned with the cylindrical faces such that they were parallel to each other using the test machine guides. The sample was centered and aligned perpendicular to the supports and loading nose using a carton rectangular guide, with its conductive coating facing downward as seen in Figure 3.10. Electrical measurements described in Section 3.3.3 started before the displacement of the loading nose and continue through the duration of flexion test until after the sample broke. Force, displacement and strain were measured at regular intervals, at 5 Hz, during the test.

The machine (MTS insight Electromechanical 50 kN Extended Length, with 50 kN load cell Model 569332-01 Serial 381063, capacity 50 kN and Sensitivity 2.356 mV/V, with a more precise load cell added, MTS Load Cell Model 569327-02 Serial 381063 Capacity 1000 N and sensitivity 2.036 mV/V, with crosshead/load measurements taken into the Testwork 4 software from MTS) applies a constant displacement rate and forces the sample beam to bend downwards until there is a break. The machine automatically stops if the break causes a change in force greater than 75%. Example experiment setup is shown in Figure 3.5.

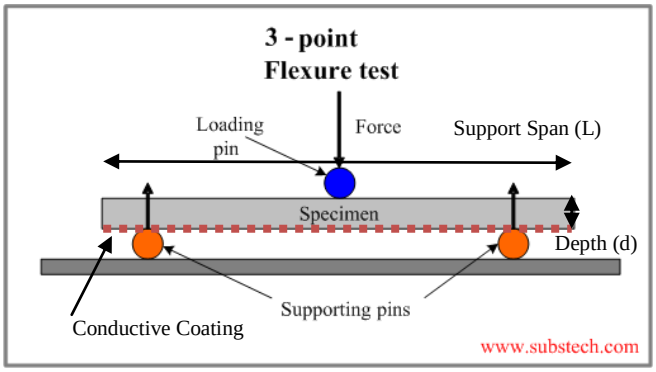

Figure 3.10: 3-point flexion test. The film coating is at the bottom of the specimen and therefore in tension during testing.

3.5.6 Tribology

This test method followed ASTM standard G99 − 05: Standard Test Method for Wear Testing with a Pin-on-Disk Apparatus as seen in Figure 3.11. An aluminum oxide ball, Al_2O_3, with a radius of 4.75 mm, was pressed with 5 N force on a rotating sample such that the relative ball speed was 5 cm/s at radius of 3 mm. It was rotated such that the ball travels an equivalent distance of 25, 50, 100, 200, 400 and 800 meters over the coating. The test was stopped after traveling such a distance. If the underlying composite was exposed during a test, further tests were not completed as the data would no longer be valid for the coating only but would instead be a mix of data for the coating and the underlying substrate. The tests were performed at room temperature (~21°C). The coefficients of friction of the conductive films were obtained.

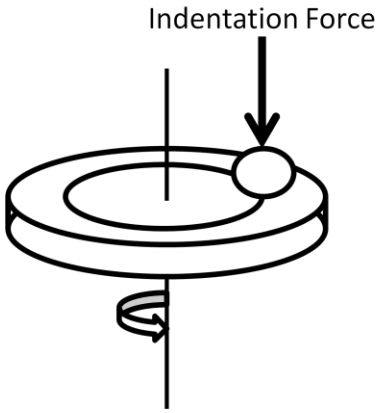

Figure 3.11: Picture/diagram of pin on disk setup.

3.6 Environmental Characterization

Two test procedures are detailed for environmental characterization: thermal cycling and salt spray exposure. Before and after each cycle, the samples were also measured electrically following the method in Section 3.3.4. The mass was measured before and after each cycle. The surface of each coating was also observed via optical microscope and various magnifications. These tests were done at Bell Helicopter in Mirabel

3.6.1 Thermal (Temperature) Cycling

This procedure was first proposed by Bombardier Aerospace. The test procedures, done at the Bell Helicopter facility with a Thermotron chamber (SE-600-3-3), were as follows: Figure 3.12 shows the typical conditioning cycle. For this test, the samples are cut into 12.7x7.62 cm

rectangles. All edges were well polished (grain size 220) before they were placed in the oven. The environmental chamber was preconditioned for a minimum of 12 hours at 50 ± 5°C and 95 ± 5 % RH. The temperature was decreased to -55± 5°C at a rate of approximately 3.5°C per minute (30 minutes) and held for a minimum of 15 minutes. Humidity was kept at 95% RH. The temperature was then increased to 121± 5°C at a rate of approximately 8°C per minute (22 minutes), the temperature was held constant for a minimum of 3 minutes. The temperature was decreased back to –55± 5°C (~51 minutes) and held for minimum 3 minutes. It was later noted that the first two cycles did not reach this temperature, reaching closer to -50°C. The last two cycles reached this temperature by increasing the hold from 3 to 15 minutes). Humidity was no longer controlled as temperature reaches below 0°C. This thermal cycling was continued for 400 cycles (29200 minutes = 20.3 days ~ 21 days) and the chamber temperature was returned to 24± 5°C. The specimens were removed from the chamber and examined visually at magnifications of 20X, 50X, 100X and 200X. This was repeated for four cycling blocks (a block of 400 cycles). The electrical specific resistivity of each sample was measured after each cycle block using method in Section 3.3.4.

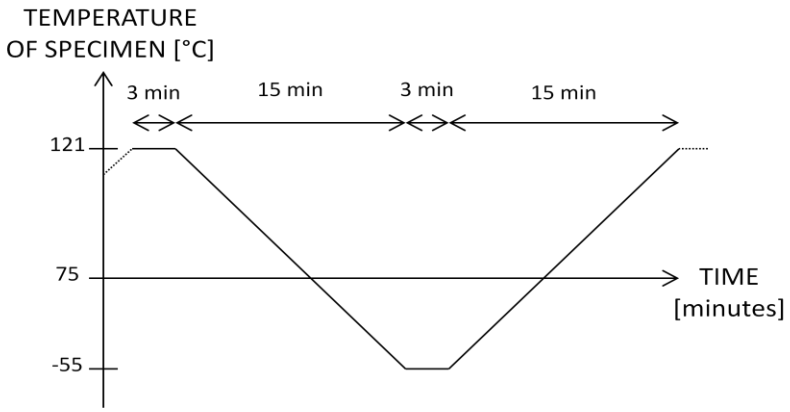

Figure 3.12: Thermal cycling between -55°C (-67°F) and +121°C (248°F).

3.6.2 Salt Spray (Fog) Exposure

The procedure for salt spray exposure followed the ASTM B117 standard (Standard Practice for Operating Salt Spray Fog Apparatus) done at the Bell Helicopter facility with their salt spray chamber (Cyclic Corrosion Tester: Q-Fog Model: SSP600). The carbon and epoxy composite with no conductive coating, the expanded copper foil/surfacing film, and the other LSP coatings were cut into 12.70x7.62 cm dimensions. Some samples provided were smaller than 12.70x7.62 cm; in those cases, the surface area uncovered by primer was still 7.62x2.54in but it did not have

a border and the X scribe line was smaller. Using sandpaper, the resin epoxy of the ECF surfacing film was removed in the 7.62x2.54 cm region to allow current injection and tension measurements in between cycles. These cut edges were then coated with primer paint (mil-PRF 23377 Class C2, cured at 130F for one hour) with a brush. The sample's weight was measured before and after a paint coating. A 7.62x2.54 cm area was left exposed while an X, 6.35 by 5.08 cm was scribed on the surface through the paint and conductive coating down to the composite substrate's first carbon fiber layer as seen in Figure 3.13.

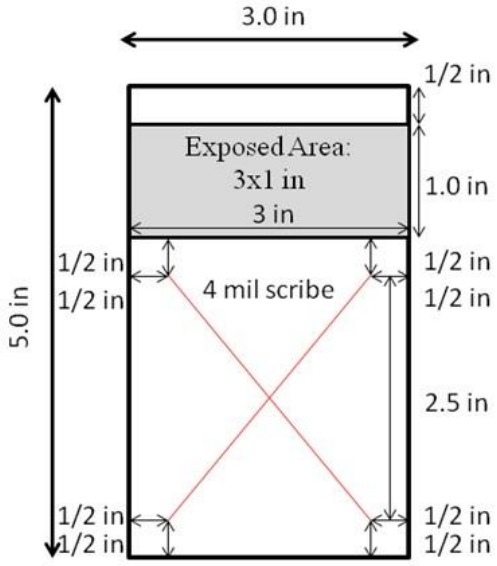

Figure 3.13: Location of exposed area 7.62 x 2.54 cm (3x1 in) and X scribe 4 mils wide (0.1 mm) on panel size 12.7 x 7.62 cm (5x3 in).

This area allowed corrosion effects but did not block current for electrical measurements. The specimens were angled at 15-30 degrees from vertical and parallel with fog flow, where the coated surface faced upwards. They were not in contact with one another and prevented from dripping on one another and were exposed to 5 ± 1% salt with 95% water vapor in spray chamber for 4 periods of 500 hours. The specimens were carefully removed and gently washed with warm water no hotter than 38°C to remove salt deposits. They were immediately dried with a stream of clean compressed air. Periodic inspections were done, including a microscopic observation of 20 X, 50 X, 100 X and 200 X for each surface, at every 500 hours interval/cycle. The weight was measured at each interval. The electrical test according to Section 3.3.4 was performed. The surface was visually inspected for pits, blisters, or other features as described in standard ASTM Method D1654.

CHAPTER 4 EXPERIMENTAL RESULTS AND ANALYSIS

The conductive coatings' volumetric mass density and thickness were used to define certain test parameters and to calculate other properties of the coatings. The electrical properties were compared between the various conductive coatings with their different fabrication parameters and conditions. The mechanical properties were listed including the adhesion, scratch resistance, indentation, three point flexion, and tribology results. Lastly, the environmental test results of thermal cycling and salt spray cycles are analyzed and discussed. The changes in mass and specific resistivity to the samples were compared and interesting results from these tests are explained.

4.1 Coating Densities and Thicknesses

The conductive coating densities and thicknesses are needed in order to calculate specific resistivity. Some of the densities cannot be measured and their theoretical values are used instead. Thickness values were also used to set indentation loads and scratch test parameters.

The densities shown in Table 4.1 were determined by either measuring the weight before and after depositing the film and dividing by the coating volume (thickness multiplied by area) or by using a reference value of the material volumetric mass density. This reference value was used because the purely metallic conductive coatings could not be measured for a variety of reasons. The expanded copper foil is embedded in resin. The cold sprayed tin can damage and remove underlying composite substrate matrix during deposition, and thus change the original weight. The electroless plated silver is coated on the sides and sometimes the back of the sample, which are not considered when making electrical measurements. Magnetron sputtered aluminum conductive coatings are non-uniform in thickness with an unknown profile.

Table 4.1: Volumetric mass density of LSP coatings.

Sample	Volumetric mass density (g/cm^3)
CFRP	No coating
ECF (with no SF)	8.96 [64]
Nano Ag	~1.7
Ag CNF	~2.4
CS Sn	7.31 [64]
GO AgNW	~0.5
EP Ag	10.49 [64]
MS Al	2.7 [64]

The thickness of all sample types was measured using optical microscope or SEM cross section. Thickness of the coating is approximated from this image and its scale, as coating thickness can vary based on location. The thickness of the CFRP is not considered since it has no LSP coating. ECF/SF samples have an expanded copper foil that is 80 μm thick, and it was taken into account that it is a mesh with ~70% open area. Table 4.2 lists the thickness of the coatings.

Table 4.2: Thickness of LSP coatings.

Sample	Thickness (μm)
CFRP	No coating
ECF (SF)	ECF: 80 (Surfacing Film: 200)
Nano Ag	10-20
Ag CNF (SF)	Ag CNF: 8-40 (Surfacing Film: 200)
CS Sn	125-350
GO AgNW	5-120
EP Ag	~5
MS Al	5-15

4.2 Electrical Properties of Different LSP Coatings

The figures below summarize the electrical specific resistivity of most of the samples fabricated for this project. The carbon fibers of the carbon/epoxy composite substrate are conductive and are measured using the method in Section 3.3.2 but this value is mostly an approximation. It is also not conductive enough for LSP purposes as it should be close to value of pure metal like copper and aluminum. The expanded copper foil was measured electrically during the environmental tests Section 3.3.4 and its value is close to the theoretical value for pure copper. The TGA results are included in the silver nanoparticles in matrix section. The values for silver-coated carbon nanofibers are provided by Xavier Cauchy using the same instruments of the GCM lab with 4-point probe method in Section 3.3.1.

4.2.1 Silver Nanoparticles in Matrix

Figure 4.1 shows the results of TGA, the weight percentage of silver, for Ag1 and Ag2 inks. They show that the remaining weight percentage of silver content. Most of the chemical compounds such as the reducing agents monoethaloamine (Ag-1) and diethanolamine (Ag-2) used to fabricate the ink evaporate within the first 200°C range. Ag1-has 82% silver in weight and Ag2-ink has 73% silver in weight.

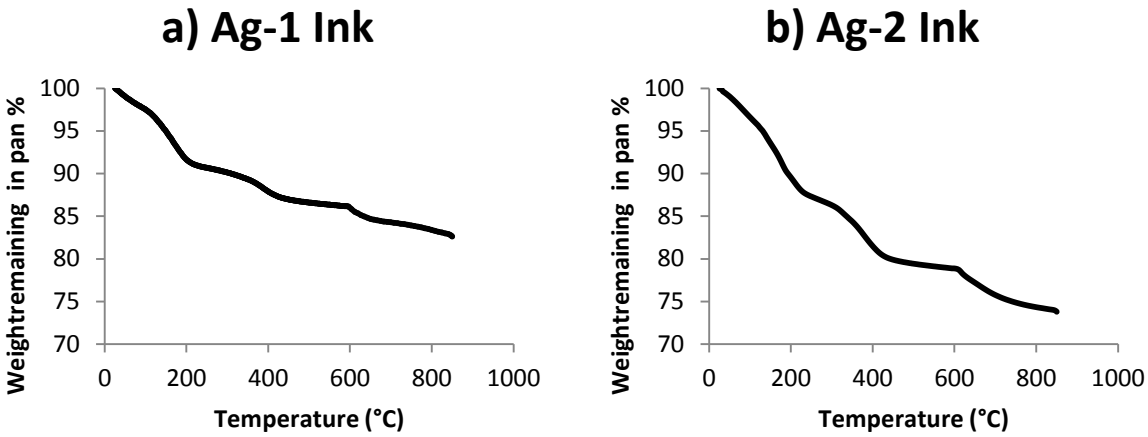

Figure 4.1: TGA results a) Ag1 b) Ag2.

Figure 4.2 shows the electrical specific resistivity of the samples that include silver nanoparticles (see Section 3.1.3). The first sample (P/Ag2/Cast No A) was cast and not annealed, but this method was abandoned due to poor adhesion, likely due to the water evaporated during drying. The next set of samples contains different types of silver inks (Ag1 vs. Ag2), matrix binder (P: PEDOT:PSS vs. E: Epoxy/PEDOT:PSS), and different annealing (A) temperatures (140°C, 180°C, and 200°C) for 1 hour. Annealing generally lowers the specific resistivity of a sample, but the type of ink and matrix used have mixed results, although it is the sample with Ag1 ink, and thus the greater concentration of silver material, that has the lowest specific resistivity. The formation of a network of conductive particles and achieving the electrical percolation threshold (EPT, see Section 2.9 and Figure 2.6) are crucial and play a greater role in determining the specific resistivity of the conductive coatings, which can account for the large standard deviations and variance of the results.

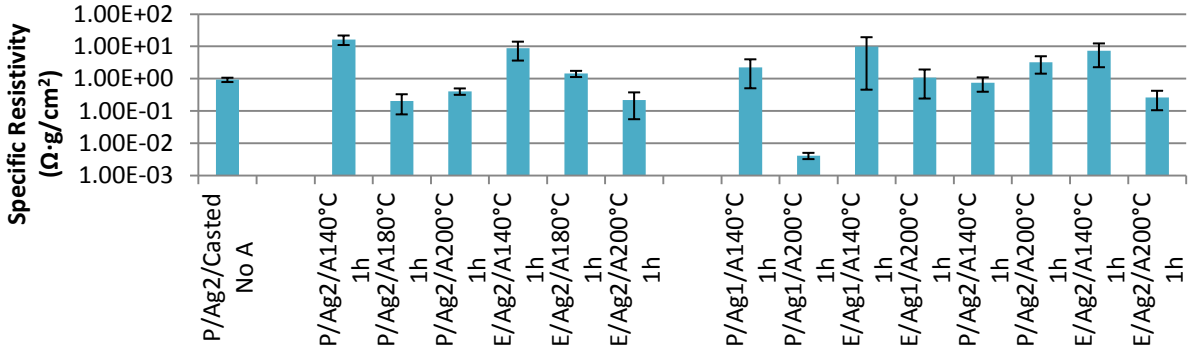

Figure 4.2: Specific resistivity of silver nanoparticles in matrix. First sample was cast, other coatings sprayed onto substrate. Annealing temperatures (A140°C, A180°C and A200°C) for one hour. P = PEDOT:PSS matrix, E = Epoxy and PEDOT:PSS mixture.

4.2.2 Cold Sprayed Tin

Various fabrication parameters were tested for cold sprayed samples (see Section 3.1.5) which are divided into four different sets. The temperature and time were chosen in order to study the effects of annealing on specific resistivity. The temperature was limited by the low melting point of tin. The first set is cold sprayed tin deposited with 300°C gas temperature and 60 psi (assigned as 300°C/60 psi). The individual samples are then annealed at 80 °C for 1, 3, 6, 12, 24, 48 and 72 hours (assigned as 300°C/60 psi A80°C 1-72h). This annealing has little effect on the results.

The second set is a sample where copper powder was mixed with tin powder during spraying of 10%, 30% and 50% copper mixture with the rest being tin powder. They were each annealed for 1, 7 and 12 hours at 200°C in air and room pressure (assigned as 10-50Cu 300°C/60psi A200°C 1-12h). Annealing has reduced the specific resistivity of all samples but not significantly as most samples are within the same order of magnitude. The longer annealing periods increased the specific resistivity of these samples possibly due to oxidation of tin due to high annealing temperature and time. The presence of copper powder also increases the specific resistivity, defeating the purpose of adding copper powder to make the coating more conductive. A pure copper coating would be ideal, but deposition of copper on our composite substrate has failed so far.

The third set looked at various fabrication parameters with gas temperature of 280°C, 300°C or 350°C, and pressure of 60 psi or 80 psi, and also includes 10%, 30% and 50% copper powder mix (assigned as 10-50Cu 280-350°C/60-80psi). The conductive coatings with 30% and 50% copper powder showed the larger specific resistivity. It is possible both the combination of particle mixture and high gas temperature can lead to a higher volume resistivity but annealing would likely return the specific resistivity in line with the other samples.

The fourth set looks at the mixture of 10% zinc powder with temperature of 280°C and 300°C, and pressure of 80 psi or 100 psi. There is no noticeable effect on specific resistivity. It is unlikely that zinc would improve the specific resistivity of samples due to its slightly higher specific resistivity than tin- about twice that of tin.

The results are summarized in Figure 4.3. The gas temperature, pressure, and even the introduction of different metal powders do not significantly affect most of the results. The longer annealing periods do not show significant change in specific resistivity results. It shows most

samples have a specific resistivity within the same order of magnitude, close to the theoretical value of bulk tin. The two main factors for samples not reaching the theoretical value are that the tin powder is partially oxidized and the coating is formed from metallic powders agglomerating together rather than a crystalline bulk material. The use of different powders together creates a problem as the contact resistance between the different types of metals leads to an increase in specific resistivity of the overall sample.

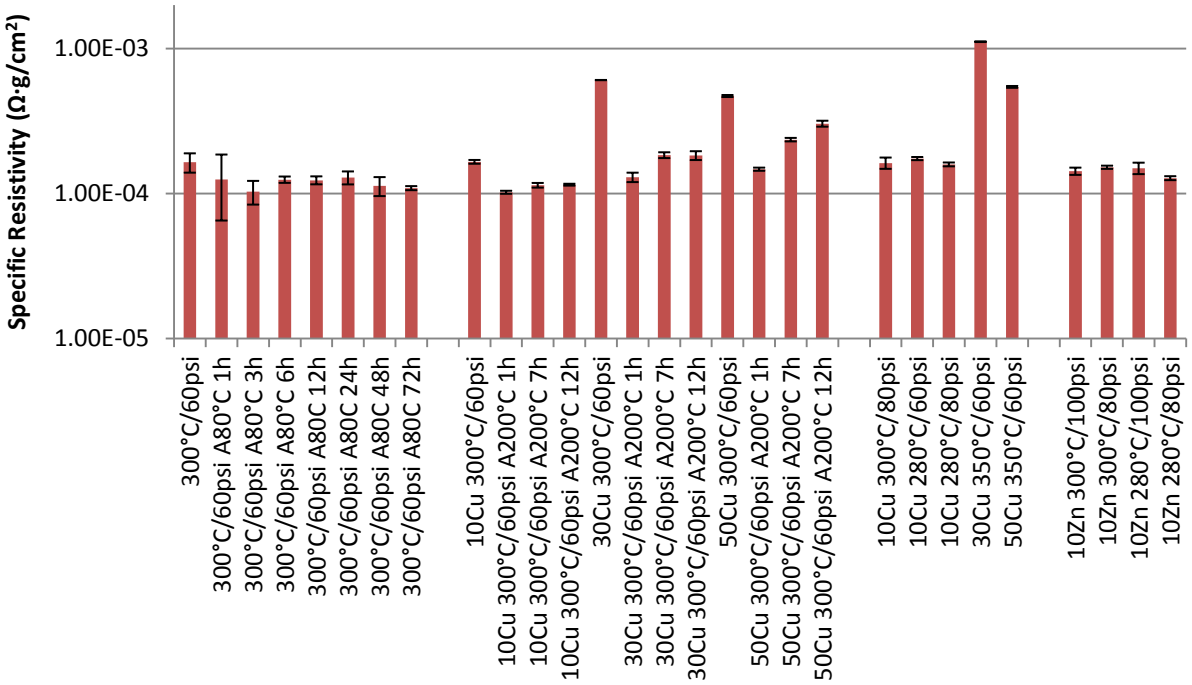

Figure 4.3: Specific resistivity of cold sprayed tin conductive coatings. Pressure and temperature parameters during cold spray. Samples of 10, 30 or 50% copper (Cu) powder or 10% zinc (Zn) powder, the remainder being tin (Sn) powder. Annealed (A) samples from 1, 3, 6, 12, 24, 48 and 72 hours, or for 1, 7 and 12 hours.

4.2.3 Graphene Oxide Functionalized with Silver Nanowires

Figure 4.4 shows the specific resistivity of graphene oxide functionalized with silver Nanowires (see Section 3.1.6). GO AgNW #1 and GO AgNW #3 are more conductive. GO AgNW #103 and GO AgNW #104 have different sheet resistances measured at different locations of the sample, sometimes as much by one or two orders of magnitude. The high specific resistivity values and standard deviations of the conductive coatings indicate that there is a problem with the distribution (location of particles in a volume) and dispersion (distance between each particle) of graphene oxide functionalized with silver nanowires forming an electrical network (see Section 2.9).

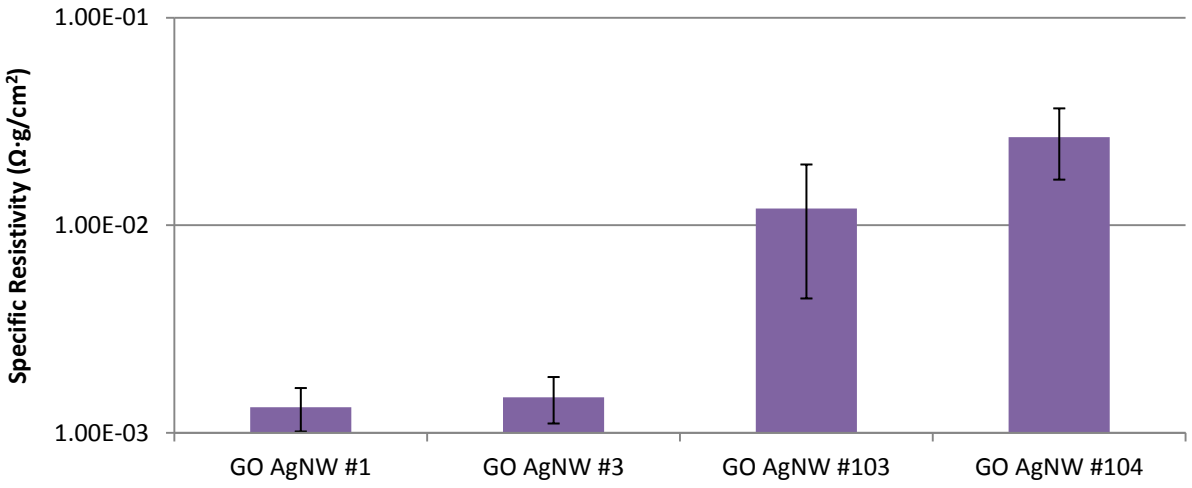

Figure 4.4: Specific resistivity of graphene oxide functionalized with silver nanowires.

4.2.4 Electroless Plated Silver

The results of chemically bonded silver on CFRP (see Section 3.1.7) can be seen in Figure 4.5. The specific resistivity of the samples are in the same order of magnitude but some individual samples can be as much as one order of magnitude more resistive than the others which leads to large standard deviations results for some of the samples. Annealing generally decreases specific resistivity of samples. The specific resistivity values are not the same as the theoretical value, possibly due to some oxidation of the silver during/after the chemical process.

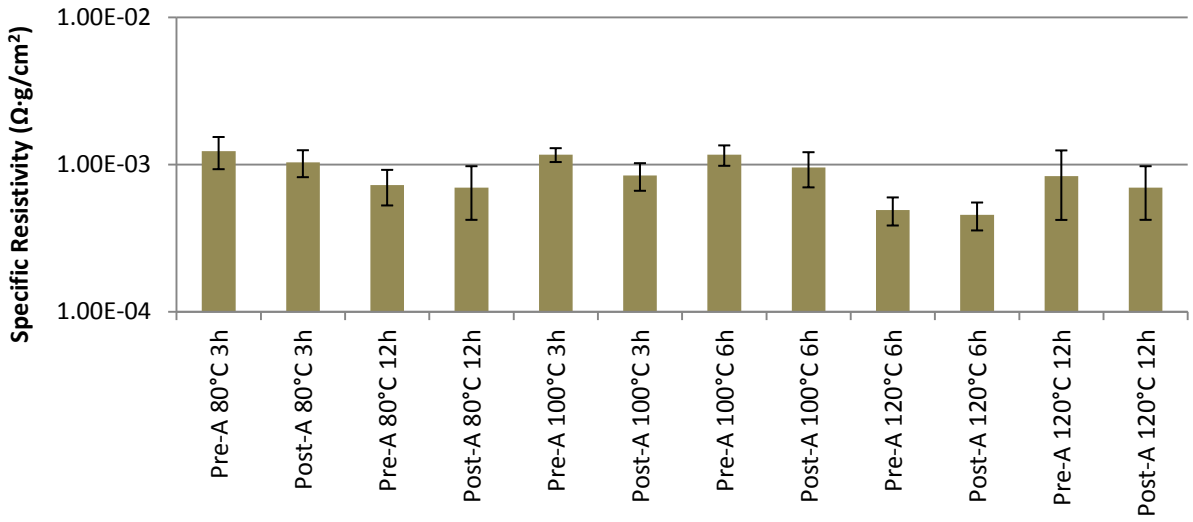

Figure 4.5: Specific resistivity of electroless plated silver on substrate. Includes fabrication parameters and pre/post annealing (A) differences at various durations (3, 6 and 12 hours) and temperatures.

4.2.5 Magnetron Sputtered Aluminum

Results of magnetron sputtered aluminum (see Section 3.1.8) specific resistivity can be seen in Figure 4.6. The longer deposition time (3 hours vs. six times 30 minutes with 30 minutes pauses in between each) can heat up and degrade the sample substrate, leading to oxidation of the aluminum coating and its evaporation. The specific resistivity of sputtered aluminum is close to within an order of magnitude to the theoretical value of aluminum but the uneven thickness around the edges of the sample make it more resistive than its more uniform center.

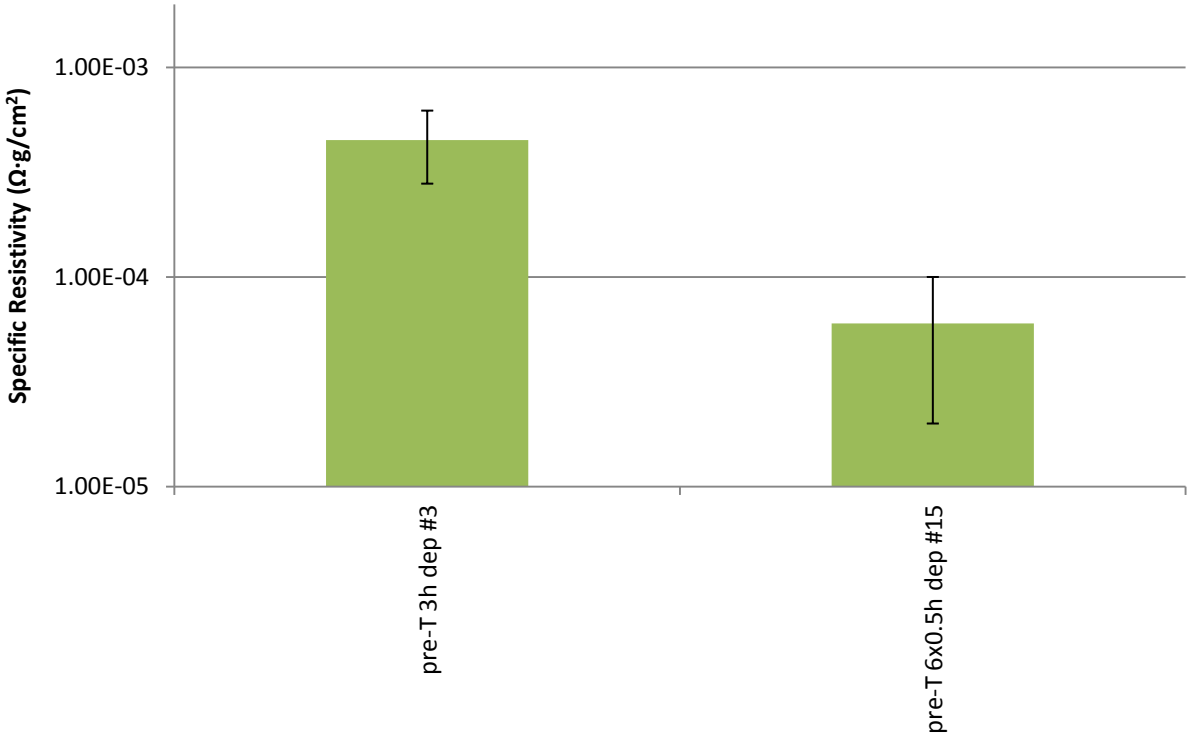

Figure 4.6: Specific resistivity of sputtered aluminum. Pretreatment (pre-T) with Argon ions. The long deposition time (3h dep) of 3 hours and the short deposition time (6x0.5h dep) of six deposition periods of 30 minutes with a 30 minutes pause in between.

4.2.6 Comparisons of Electrical Values

For comparison, the values of specific resistivity of pure crystalline metals from which the samples were fabricated are listed here and the measured values are in Table 4.3:

- Copper: 1.68×10^{-8} Ohms x m x 100 cm/m x 8.96 g/cm^3 = 1.5×10^{-5} ohms g/cm^2.
- Silver: 1.59×10^{-8} Ohms x m x 100 cm/m x 10.49 g/cm^3 = 1.7×10^{-5} ohms g/cm^2.
- Aluminum: 2.65×10^{-8} Ohms x m x 100 cm/m x 2.70 g/cm^3 = 0.7×10^{-5} ohms g/cm^2.
- Tin: 11.0×10^{-8} Ohms x m x 100 cm/m x 7.35 g/cm^3 = 8.1×10^{-5} ohms g/cm^2.

Three conclusions can be derived from these results. First, annealing lowers the electrical specific resistivity of the samples and higher annealing temperatures lower it more effectively than smaller annealing temperature. Second, the more metallic content in the conductive coating, the lower the specific resistivity. Third, purely metallic coatings might not always give the best results due to oxidation and other factors, such as a badly fabricated percolation networks, the mixing of metal powders, or the fabrication parameters like casting vs. spraying.

Table 4.3: Lowest electrical specific resistivity values for LSP coatings.

Sample	Volumetric Mass Density (g/cm^3)	Thickness (µm)	Sample Sheet Resistance (Ω/□)	Sample Specific Resistivity (10^{-5} Ω·g/cm^2)	Reference Specific Resistivity (10^{-5} Ω·g/cm^2)
CFRP	No coating	No coating	N/A	~$1.10 \times 10^{+6}$	N/A
ECF	8.96	80	$4.8 \pm 0.7 \times 10^{-4}$	3.3 ± 0.1	Cu: 1.5
Nano Ag	1.7	10-20	1.9 ± 0.4	420 ± 90	Ag: 1.7
Ag CNF	2.4	8-10	$1 \pm 0.5 \times 10^{-1}$	30 ± 10	Ag: 1.7
CS Sn	7.31	125-350	$1.0 \pm 0.2 \times 10^{-3}$	10 ± 2	Sn: 8.1
GO AgNW	0.5	5-20	$4.6 \pm 1.1 \times 10^{+1}$	130 ± 30	Ag: 1.7
EP Ag	10.49	~5	$6 \pm 1 \times 10^{-2}$	34 ± 5	Ag: 1.7
MS Al	2.7	5-15	$2 \pm 1 \times 10^{-2}$	6 ± 4	Al: 0.7

4.2.7 Change in Specific Resistivity Before and After Current Injections During Flexion Tests

Currents of 5, 25, 50 and 100 A were injected in the LSP Coatings as shown in Table 4.4. Table 4.5 shows a summary of the average changes in specific resistivity that occurs during the flexion test. During flexion of the samples with expanded copper foil and surfacing film, the change in specific resistivity is far too small and within the standard deviation. This is likely due to the almost pure metallic mesh being deformed only minimally such that specific resistivity is not affected. Silver-coated carbon fiber conductive coatings show a small increase in specific resistivity as the conductive fibers are near the surface and subject to greater deformation. The largest increase came from the cold sprayed tin conductive coating, which is thicker than the others by one order of magnitude. Its top layers are non-uniform clumps of tin power that increase the measured resistance as they are separated by tension at the surface from the flexion test. The large standard deviations and lack of pattern from different current injections means that the change in electrical specific resistivity are largely caused by the flexion itself and not affected by previous large current injections in a measurable way. The high standard deviation for the tin conductive coatings also prevented any conclusive pattern in the change in specific resistivity over different injected currents. Electroless plated silver and magnetron sputtered aluminum conductive coatings show a small increase in specific resistivity. Examples are shown in Figure 4.7a for cold sprayed tin and Figure 4.7b for expanded copper foil.

Table 4.4: Currents injected in the sample or its conductive coating.

LSP coating	Currents injected in the sample's conductive coating
CFRP	5, 25 A
ECF/SF	5, 25, 50, 100 A
Ag CNF	5 A
CS Sn	5, 25, 50, 100 A
EP Ag	5 A
MS Al	5, 25 A

Table 4.5: Average increase for specific resistivity of each sample groups, with and without current injections, and the standard deviation of each sample group.

Sample Type	Current Injected into Conductive Coating	Average Specific Resistivity Increase
ECF	No current	0.5 ± 0.1%
ECF	5 A	0.2 ± 0.1%
ECF	25 A	0.3 ± 0.1%
ECF	50 A	0.7 ± 0.6%
ECF	100 A	0.5 ± 0.6%
CS Sn	No current	7%*
CS Sn	5 A	11 ± 4%
CS Sn	25 A	18 ± 10%
CS Sn	50 A	18 ± 5%
CS Sn	100 A	14 ± 6%
Ag CNF	No current	3.8 ± 1%
Ag CNF	5A	3.3 ± 0.5%
EP Ag	No current	N/A
EP Ag	5 A	1.07 ± 0.25%

*: Only one sample was available for testing

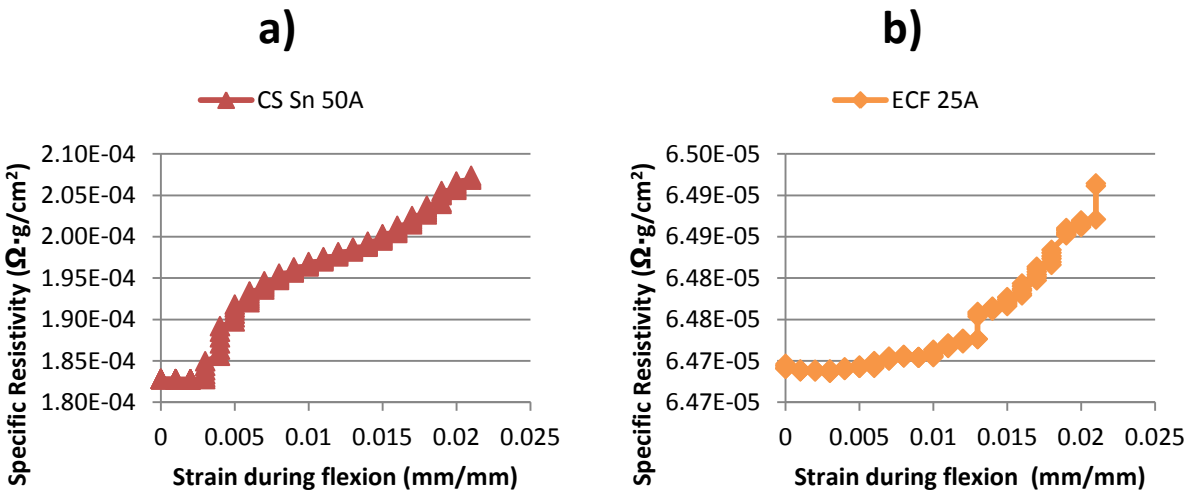

Figure 4.7: Increases of the specific resistivity of LSP coatings after current injections as strain increases from 3-point flexion test for a) cold sprayed tin (CS Sn) injected with 50 A and b) expanded copper foil (ECF) injected with 25 A.

4.3 Mechanical Properties

The important mechanical properties of the conductive coating are mainly adhesion and scratch results. Indentation and tribology tests were performed as required for the project and to learn their properties for potential use in other non-LSP applications. The three point flexion test was completed as a way to measure the loss of mechanical properties after current injections (5, 25, 50 and 100 A) but not as severe as lightning strikes (50-200 kA).

4.3.1 Adhesion Tape Test Results

The composite substrate (CFRP) and the baseline expanded copper foil and surfacing film (ECF/SF) are not applicable for this test. The first has no conductive coating and the second is too thick for this test. The scratch test was used to determine their adhesion (see Section 0). Silver-coated carbon nanofibers are imbedded in a surfacing film of epoxy and could not be tested using this method.

The summary of all adhesion results for all conductive coatings is found in Table 4.6. The percent of removed crosscut area is a semi-quantitative result. The different fabrication methods and compositions of silver ink and matrix binder and the annealing temperatures have an effect on adhesion of Nano Ag samples. The casting method showed poor adhesion results that were evident even without testing as flaking of the conductive coating occurred before any testing was performed. Annealing increased coating adhesion results for all Nano Ag samples. Without annealing, adhesions results are 0B. The test results of adhesion tests on silver nanoparticles annealed at different temperatures show that annealing at higher temperatures increases adhesion for these samples. The type of matrix binder and silver concentration can have an effect on adhesion of conductive coating. With higher annealing temperatures, better adhesion results are found but the matrix binder and silver ink used can affect adhesion. There are too few tests and samples to confirm conclusively whether the different silver inks or the different matrices used have a detrimental or positive effect on adhesion. The CS Sn samples were tested and found to have 5B adhesion. This test method might not be appropriate for some of the thicker samples. It is possible the cutting metal tool did not reach the substrate for those cases. The GO AgNW samples do not have good adhesion, likely due to the fabrication method used. The water evaporation during the casting or spin coating process causes shear stress on the flat graphene

flakes and thus delamination, even without a tape test or crosshatch, which explains why parts of the sample were already flaky and delaminated before the test started. The EP Ag sample was tested and found to have 5B adhesion. Due to the poor adhesion of aluminum sputtered on the composite (1B), the process of deposition was changed such that the surface was pre-treated with argon bombardment before magnetron sputtering of aluminum. This increased adhesion from 1B to 5B.

Table 4.6: Adhesion grade for LSP coatings based ASTM D3359 Procedure B. Epoxy and PEDOT:PSS (E+P), P=PEDOT:PSS (P). Qualitative description: very poor (0B), very bad (1B), bad (2B), good (3B), very good (4B) excellent (5B).

Sample: Fabrication Parameters	Grade	LSP coating on CFRP peel test results: Picture of crosscut area of coating. The more material remains on the substrate, the higher the grade.	LSP coating on CFRP peel test results: Picture of peeled off area of coating on tape. The more material is peeled off, the lower the grade.
CFRP: N/A	N/A	N/A	N/A
ECF/SF: N/A	N/A	N/A	N/A
Nano Ag: Cast P/Ag1/A140°C 1h	0B Very poor	N/A	N/A
Nano Ag: Sprayed P/Ag1/A140°C 1h	0B Very poor	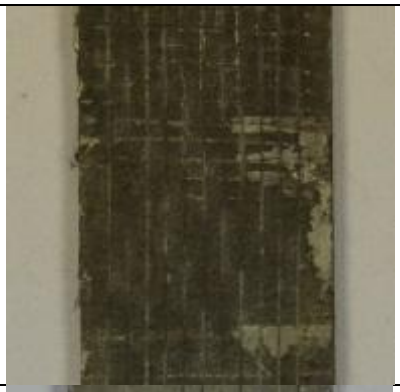	
Nano Ag: Sprayed P/Ag1/A150°C 1h	4B Very Good		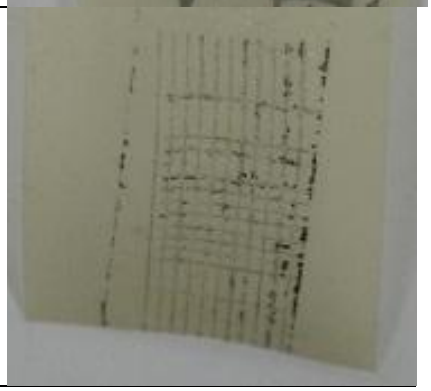

Nano Ag: Sprayed E+P/Ag2/A140°C 1h	0B Very poor	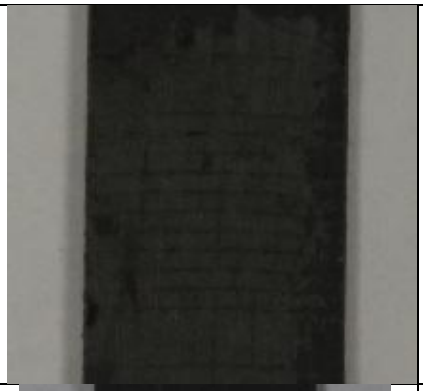	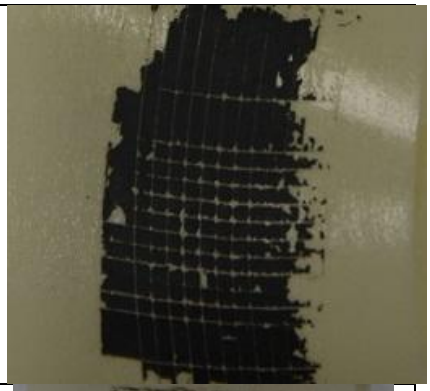
Nano Ag: Sprayed E+P/Ag2/A180°C 1h	5B Excellent	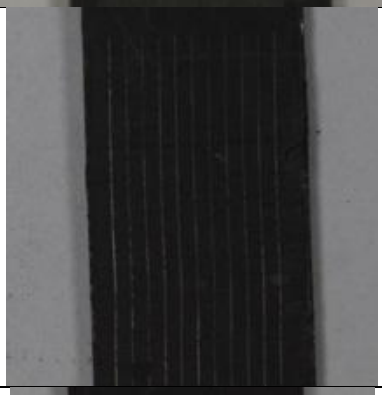	
Nano Ag: Sprayed E+P/Ag2/A200°C 1h	4B Very Good	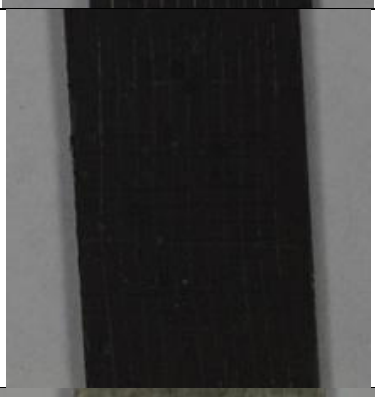	
Nano Ag: Sprayed P/Ag2/A140°C 1h	0B Very poor	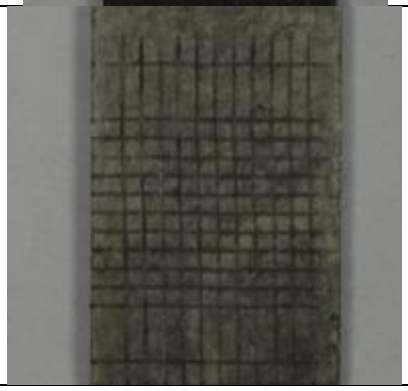	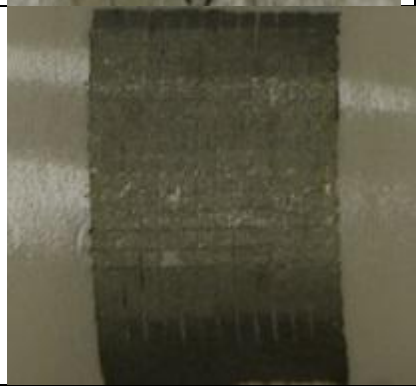

Nano Ag: Sprayed P/Ag2/A180°C 1h	5B Excellent	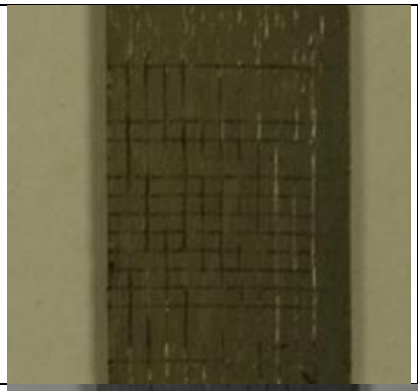	
Nano Ag: Sprayed P/Ag2/A200°C 1h	5B Excellent		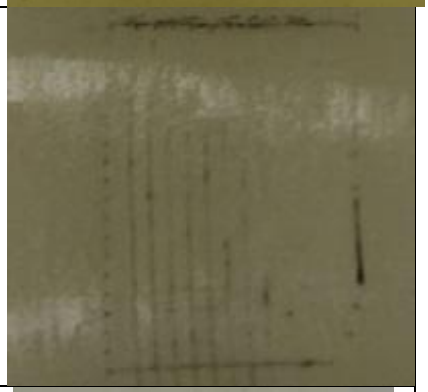
Nano Ag: Sprayed E+P/Ag1/A200°C 1h	4B Very Good		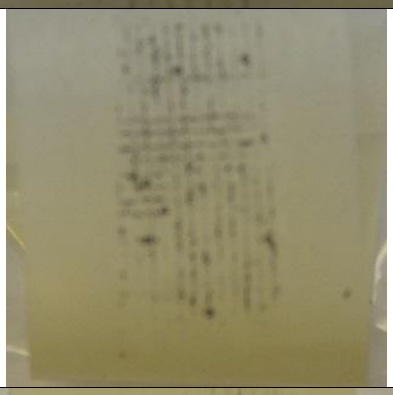
Nano Ag: Sprayed 200°C P/Ag1/A200°C 1h	5B Excellent	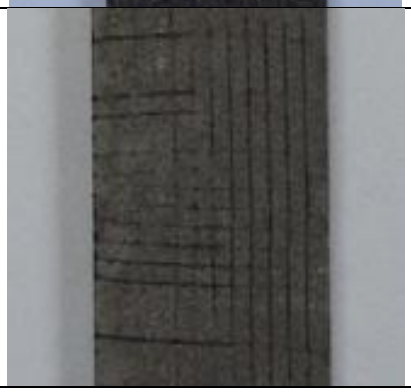	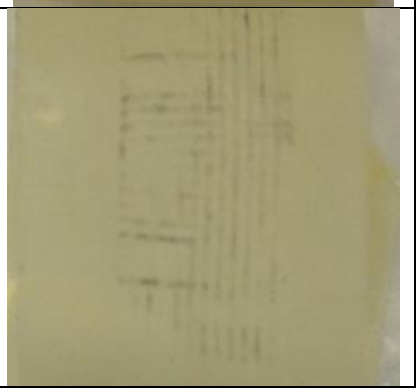

Nano Ag: Sprayed E+P/Ag2/A200°C 1h	2B Bad		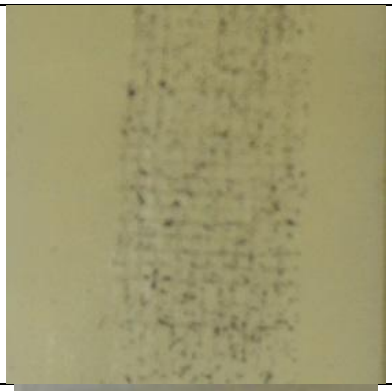
Nano Ag: Sprayed P/Ag2/A200°C 1h	4B Very Good		
Ag CNF: N/A	N/A	N/A	
CS Sn: 300°C/60psi No annealing	5B Excellent	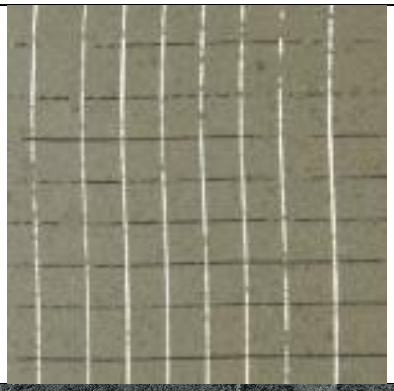	
GO AgNW: N/A	0B Very poor	 50X magnification/scale 1.27 mm	 50X magnification/scale 1.27 mm

EP Ag: No annealing	5B Excellent	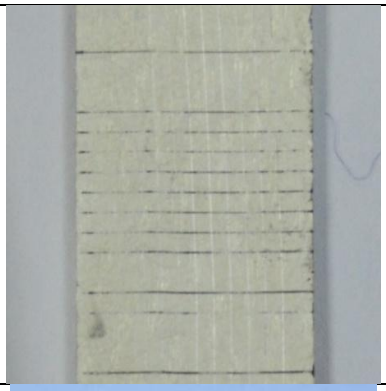	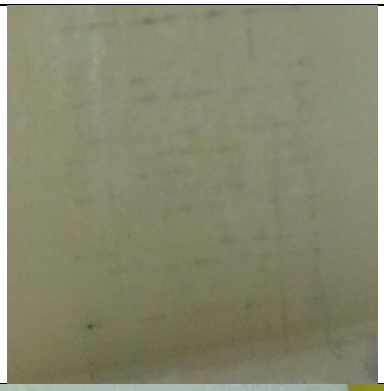
MS Al: No argon ion pre-treatment	1B Very bad		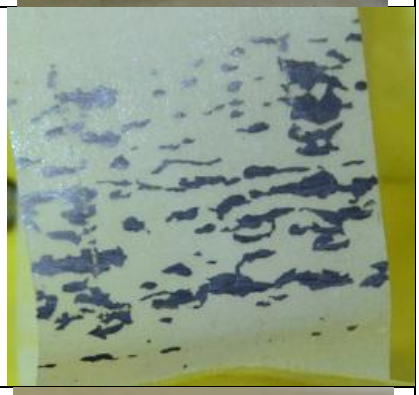
MS Al: Argon ion pre-treatment	5B Excellent		

4.3.2 Scratch Test Results

CFRP and ECF/SF samples were scratch tested and are the baseline samples. Presented in Figure 4.8, the results show good adhesion and no debris that can be seen by the optical microscope at 5 X magnification. Figure 4.9 shows the penetration depth and the residual depth of the carbon/epoxy composite substrate (CFRP) and the surfacing film with expanded copper foil (ECF/SF). As the surfacing film of the ECF/SF is softer, the indenter goes deeper, whereas the CFRP sample is harder due to the proximity (a few microns) of the carbon fibers to the surface.

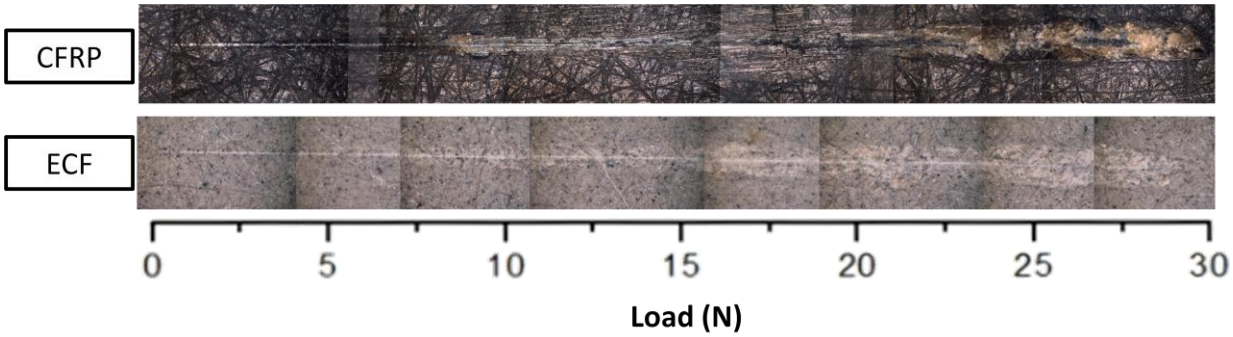

Figure 4.8: Scratch results for samples CFRP and ECF/SF. No debris found on the surface.

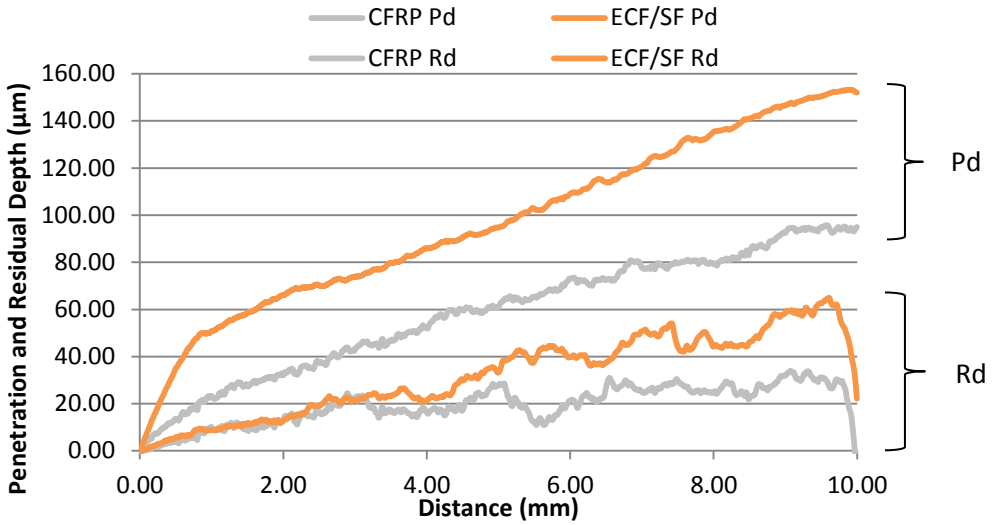

Figure 4.9: Penetration (Pd) and residual (Rd) depth for CFRP and ECF/SF samples.

In Figure 4.10 below, the SEM images show the scratch test results at 100 X magnification after annealing of Nano Ag conductive coatings for one hour. The annealing results show that the lower annealing temperatures lead to more debris and residue after the scratch test. At 140°C, the matrix is granular and delaminates more easily than when higher annealing temperatures of 180°C and 200°C are reached. The Epoxy and PEDOT:PSS (E+P) matrix shows more resistance to scratch than PEDOT:PSS (P) alone does. This shows that annealing and adding epoxy to the matrix improve adhesion. The penetration depth and residual depth of the silver nanoparticles in matrix samples is shown in Figure 4.11 and Figure 4.12. As the hardness value is similar between samples, there is not any significant difference in the graph profiles. Epoxy and PEDOT:PSS samples have less plastic deformation than conductive coatings with only PEDOT:PSS.

Moreover, the samples annealed at higher temperatures (180°C and 200°C) shows higher elastic recovery.

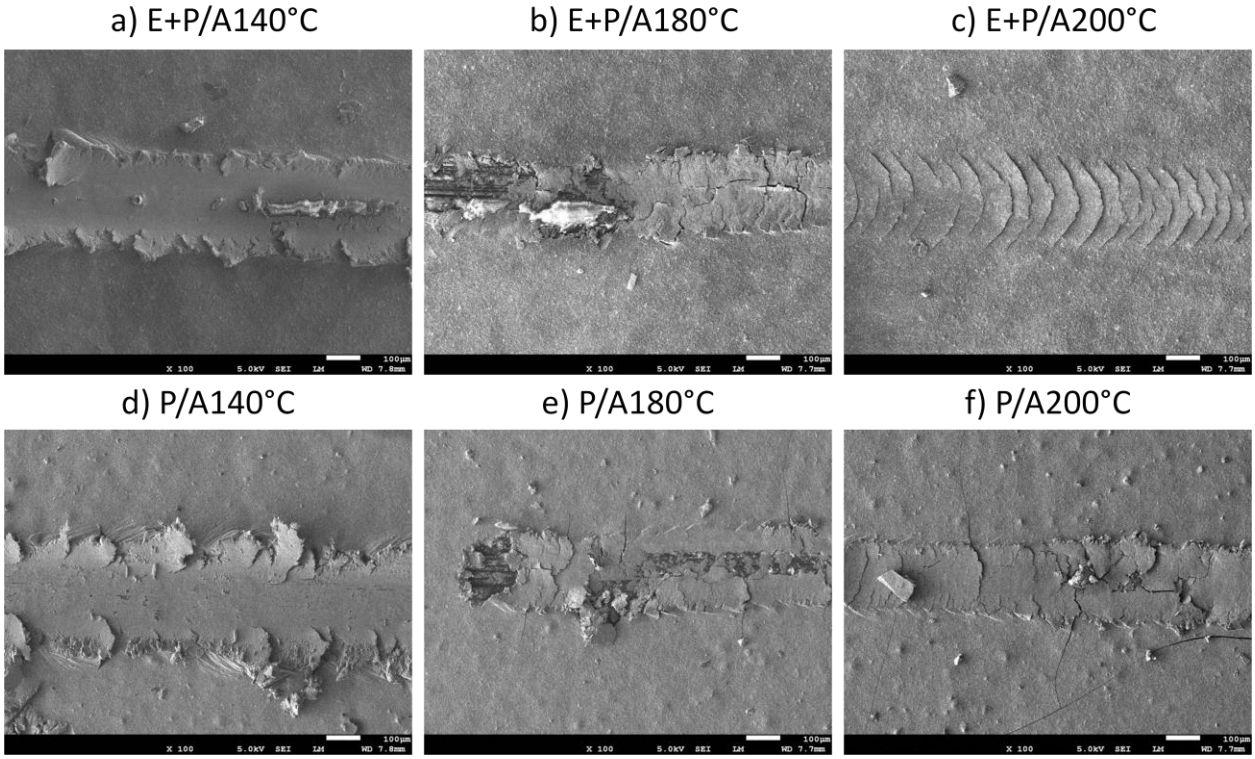

Figure 4.10: Scratch results at 10 N for Nano Ag samples with Ag-2 ink. Annealed for one hour, with Epoxy and PEDOT:PSS (E+P) at a) 140°C, b) 180°C, c) 200°C, and PEDOT:PSS only (P) at d) 140°C, e) 180°C, f) 200°C.

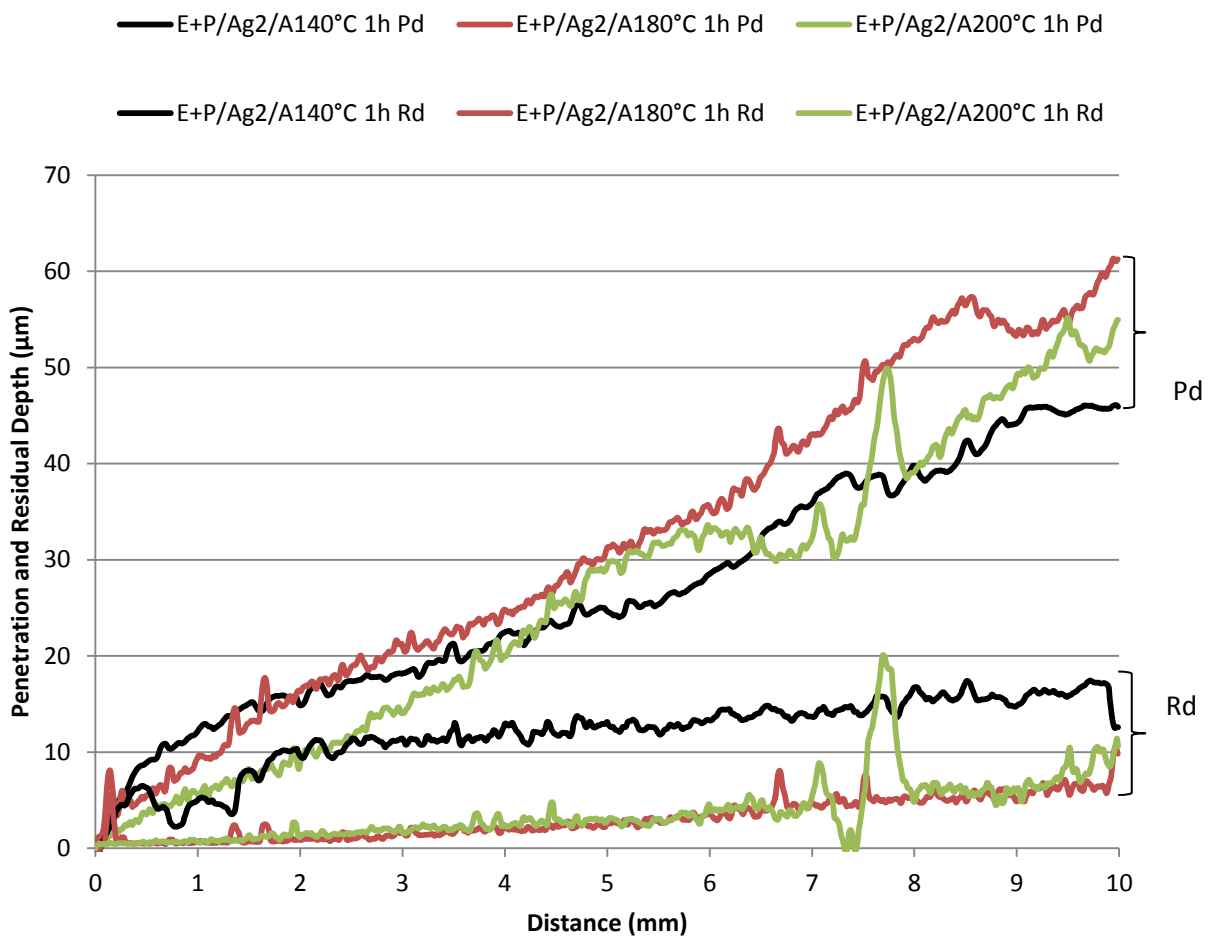

Figure 4.11: Penetration (Pd) and residual (Rd) depths for samples with silver nanoparticles (Nano Ag), Epoxy and PEDOT:PSS (E+P) and Pedot:PSS (P) matrix, with Ag2-Ink (Ag2) and Annealing (A) at 140°C, 180°C, and 200°C for 1 hour. Note: Colors do not represent the different conductive coatings from Table 3.1: List of all LSP conductive coatings..

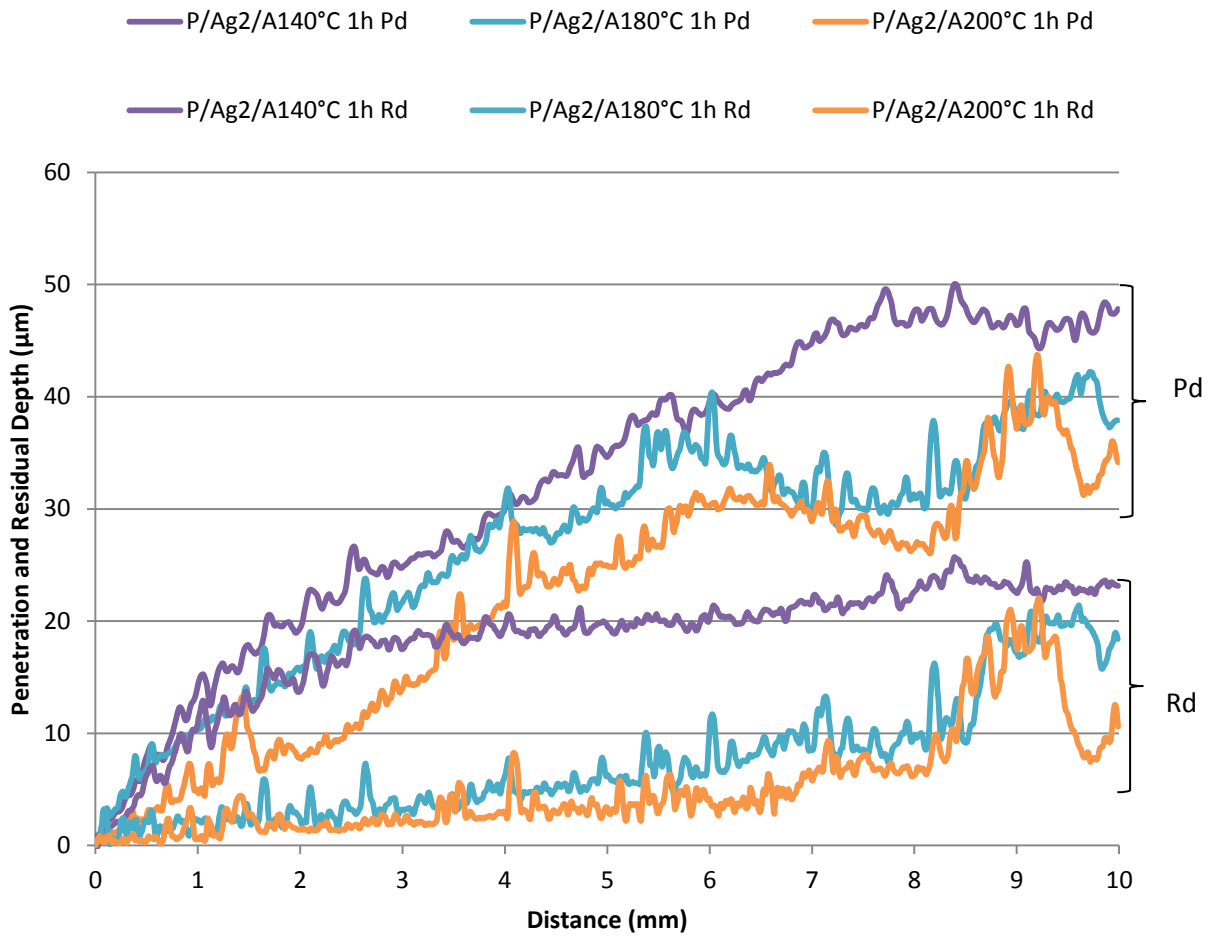

Figure 4.12: Penetration (Pd) and residual (Rd) depths for samples with silver nanoparticles (Nano Ag), Pedot:PSS (P) matrix, with Ag2-Ink (Ag2) and Annealing (A) at 140°C, 180°C, and 200°C for 1 hour. Note: Colors do not represent the different conductive coatings from Table 3.1: List of all LSP conductive coatings.

The CS Sn, GO AgNW, EP Ag and MS Al conductive coating SEM images at 100X magnification can be seen in Figure 4.13 where the indenter load is 10 N. Since the cold sprayed tin sample is soft but thick, the indenter goes more deeply than the other samples as shown in Figure 4.13a but the CFRP substrate is not reached. The graphene functionalized with silver nanowires has significant delamination and the CFRP substrate can be seen as shown in Figure 4.13b, confirming the poor adhesion results from observations of delamination. The electroless plated silver conductive coating is thin and hard with only a little delamination near the end of the scratch as the CFRP substrate is uncovered as shown in Figure 4.13c. Magnetron sputtered aluminum is thin but significantly harder than the other samples, and there is no delamination as

shown in Figure 4.13d and the CFRP substrate is not reached. Except for the GO AgNW sample, the adhesion of the samples is very good, confirming the tape test results. The penetration and residual depths are seen in Figure 4.14. The elastoplastic deformation of tin, shown with its high residual depth, explains why the scratch width is wider than the other coatings. Since the GO AgNW coating delaminates as shown Figure 4.13b the penetration and residual depth are not shown.

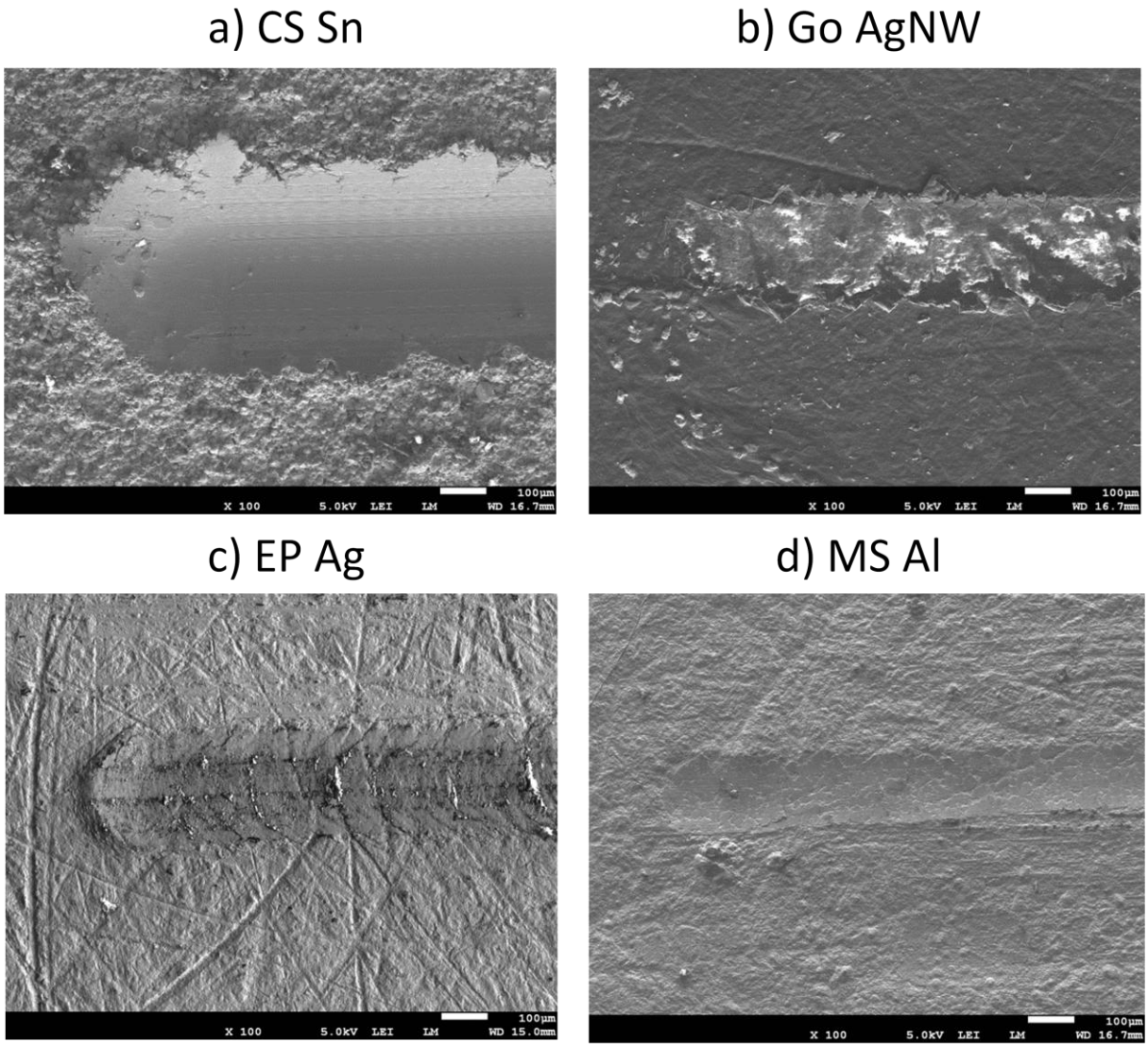

Figure 4.13: Scratch results at 10 N of LSP conductive coatings a) CS Sn, b) GO AgNW, c) EP Ag, d) MS Al.

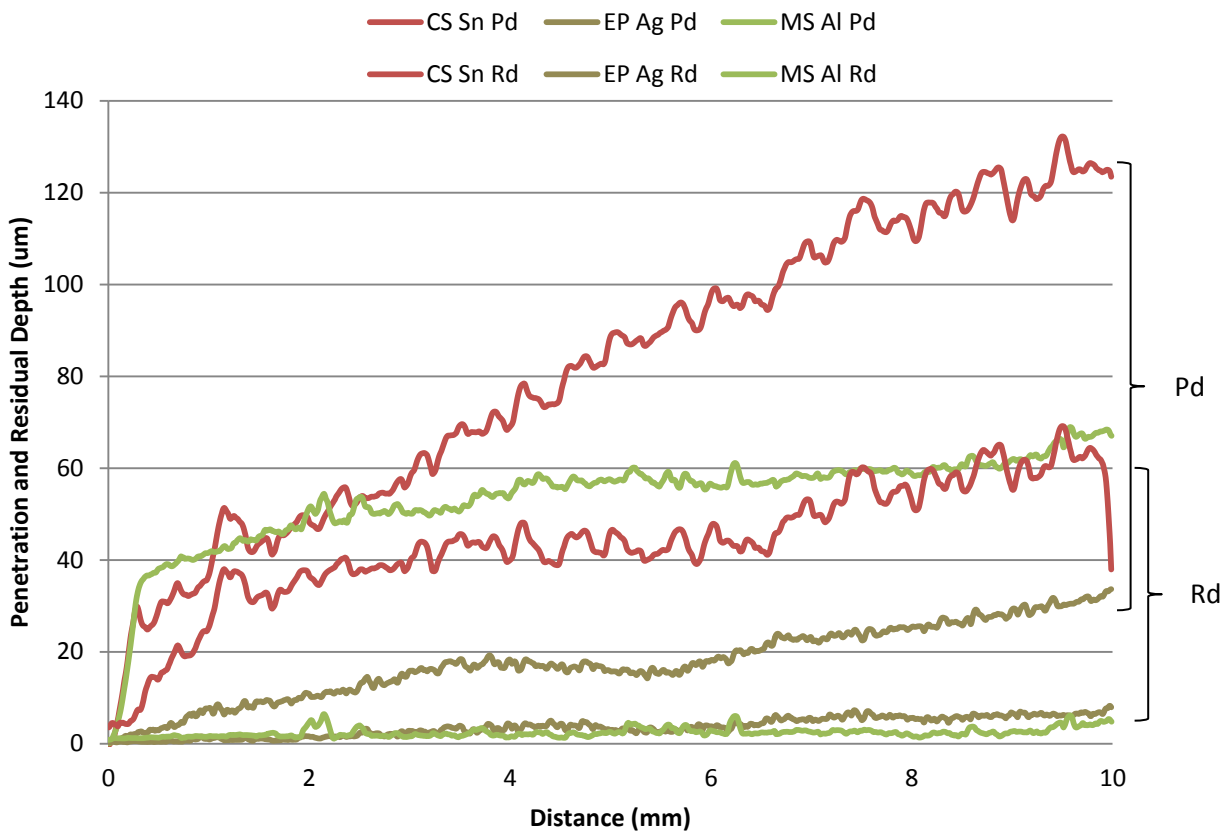

Figure 4.14: Penetration (Pd) and residual (Rd) depths for CS Sn, GO AgNW, EP Ag and MS Al samples.

These results relate with the indentation results in Section 4.3.3. The harder a coating is, the smaller the residual depth will be. Purely metallic coatings have shown good resistance to scratch testing while resin materials such as PEDOT:PSS and Epoxy have shown poor scratch resistance, although annealing partially mitigates these poor results.

4.3.3 Indentation Test Results

A summary of the mechanical properties such as hardness and Young's modulus of the LSP coatings and the composite substrate can be found in Table 4.7. It is not unusual that the hardness value varies greatly for the coatings with resin (Nano Ag, Ag CNF and GO AgNW) as the surface is not uniform and the distribution of polymer particles varies as well. The large variance of results prevents measuring small changes in hardness after annealing and other treatment processes. Typical results of load-displacement curves for some coatings can be seen in Figure

4.15. Due to the smaller thicknesses of EP Ag and MS Al conductive coatings (5-15 µm), nano-indentation was used in order to avoid the influence of the substrate. The micro-indentation technique could not be used due to the substrate influence on the results. The standard deviation is still large as the surface and CFRP substrate are rough.

Table 4.7: Hardness and Young's Modulus for LSP coatings.

LSP Coatings	Hardness (GPa)	Young's Modulus (GPa)
CFRP	0.9±0.2	11.0±0.9
ECF/SF	0.30±0.05	6.9±0.6
Nano Ag	0.23±0.03	8±2
Ag CNF	0.30±0.08	6±1
CS Sn	0.14±0.05	14±2
GO AgNW	0.4±0.2	7±2
EP Ag*	0.6±0.3	10±4
MS Al*	2±1	71±18

*Nano-indentation

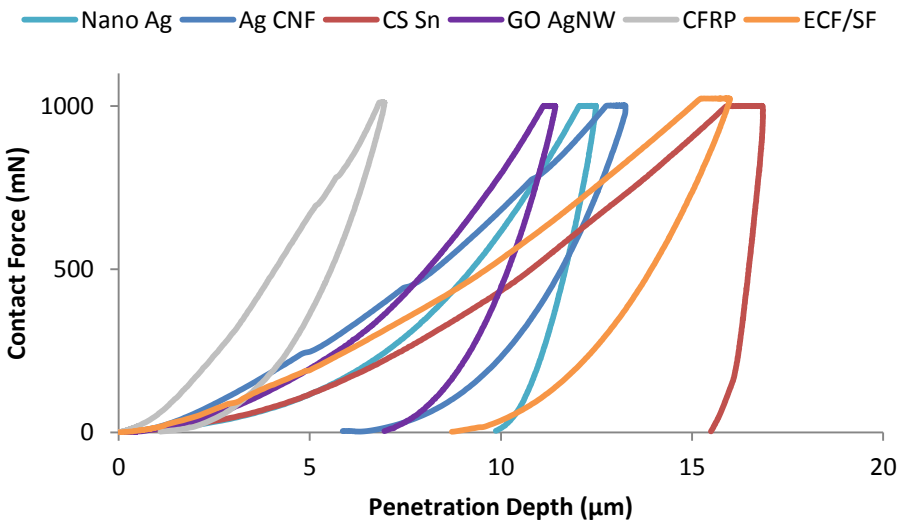

Figure 4.15: Load/displacement curves. Representative curves show the harder materials (on the left) compared to softer ones (on the right).

4.3.4 Three Point Flexion Test Results

Flexion tests were performed on the following samples: CFRP, ECF/SF, CS Sn, Ag CNF and MS Al. Other samples could not be prepared in time or in the right size. The current (5, 25, 50 and 100 A) that is injected in the sample LSP coatings is shown in Table 4.4. The currents are injected from one end of the sample to the other in a step function that lasts one second. In general, it is hypothesized that there is a decrease of the flexion modulus and flexural strength

with increasing current injection into the sample conductive coating. For CFRP and MS Al samples only 5 and 25 A currents could be injected and for Ag CNF and EP Ag samples, only 5 A could be safely injected. The reason for this is that the CFRP samples are too resistive and the Ag CNF, EP Ag and MS Al samples are thinner than 10 µm and could not accept larger currents. Attempts to inject higher currents in CFRP samples led to samples burning and releasing smoke. In the case of the ECF/SF samples, the surfacing film was sanded away at certain points to allow current injections and measurement.

Figure 4.16 shows the values of flexural strength without current injection and at each current injection value. In the case of the flexural strength, the small increase or decrease in strength is smaller than the standard deviation between samples. The injection of currents does not noticeably affect the mechanical strength of these samples.

Figure 4.17 shows the change in flexion elastic modulus of all samples after each current injection. A loss of the modulus is expected for all samples at all current injection values. This is observed for the composite substrate and cold sprayed tin-coated samples but only for some of the expanded copper foil samples at 5 A and 25 A current injections. It was also expected that the higher the current injected into the sample, the more damage would be done and thus a greater reduction of the flexural modulus would be observed. The current injections of 50 A and 100 A instead show an increase in the modulus. This could be due to the difference between one sample and another. When testing multiple samples of the same type, for example CFRP samples with no conductive coatings, a variance of 1000-3000 MPa or higher is not out of the ordinary. This large variance is not unprecedented, as can be seen in Figure 4.16.

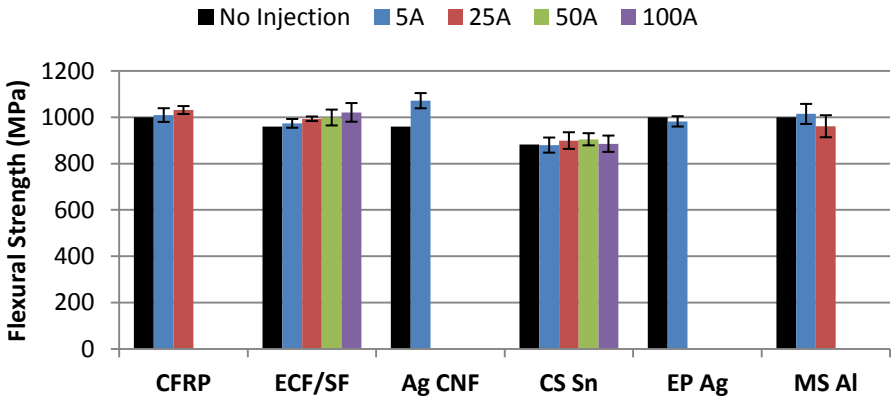

Figure 4.16: Flexural strength for all samples after: no injection, 5A, 25A, 50A, 100A current injected.

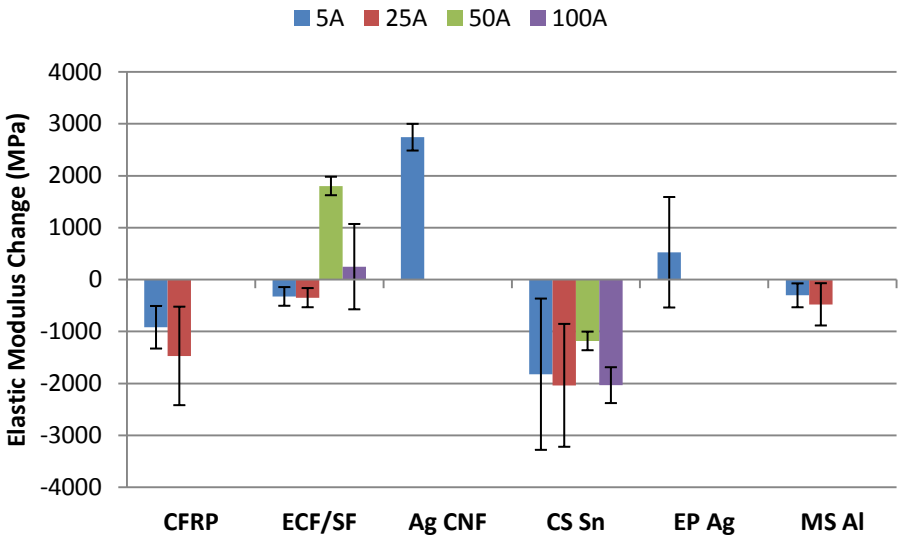

Figure 4.17: Flexion elastic modulus for all samples after 5A, 25A, 50A, 100A current injected.

4.3.5 Tribology Results

The coefficients of friction measured using a load of 5 N, speed of 5 cm/s, radius 3 mm, and distance of 25, 50, 100, 200, 400 and 800 m are similardue to the following factors: the surface of most coatings where the coefficient of friction is measured is composed of epoxy and/or PEDOT:PSS which are mainly soft materials on thin coatings. The composite substrate would also have more friction due to the hard carbon fibers that are reached during the test. The tests were not performed on the GO AgNW coatings due to the GO AgNW having very weak adhesion to the substrate. Ag CNF samples have no results either because the conductive coating is embedded in the surfacing film, which would give the same value as for ECF/SF. Figure 4.18, Figure 4.19 and Figure 4.20 show the coefficient of friction graphs where the coefficient of friction was averaged and Table 4.8 the coefficients of friction for the coatings. Scratch tests give similar results for coefficient of friction as those listed in Table 4.8. Figure 4.20 shows more variation in the coefficient of friction due to the granular nature of the coating from cold sprayed powder. EP Ag and MS Al samples are too thin for this test and their values were found with the scratch test results for coefficient of friction, but the coefficients of friction for all samples under scratch test match with those of the pin on disk tests. Ag CNF particles are embedded into a surfacing film (SF) and would thus have the same value as that of sample ECF/SF.

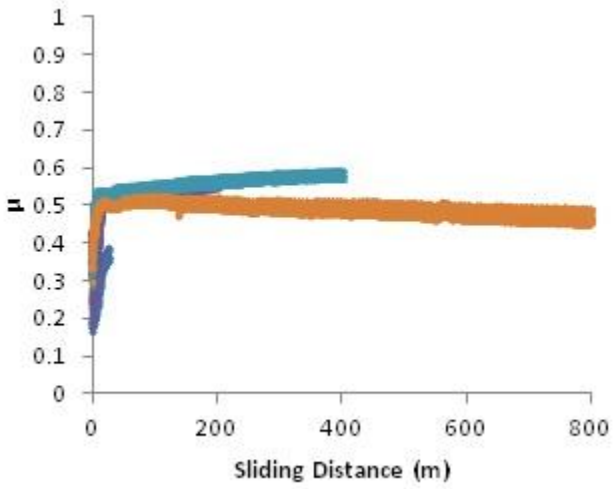

Figure 4.18: Coefficient of friction for CFRP for distances 25, 50, 100, 200, 400, and 800 m.

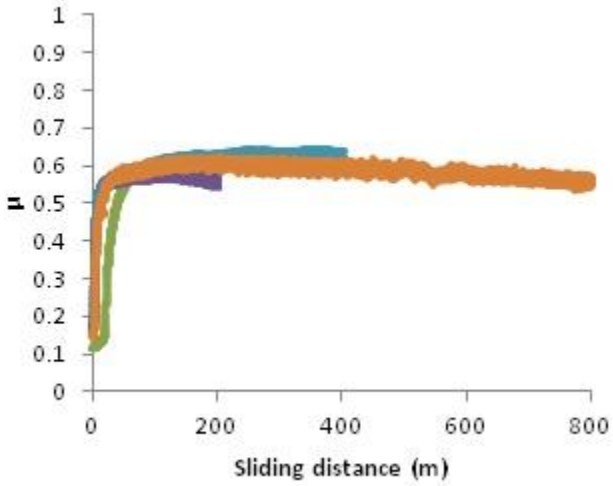

Figure 4.19: Coefficient of friction for ECF/SF for distances 25, 50, 100, 200, 400, and 800 m.

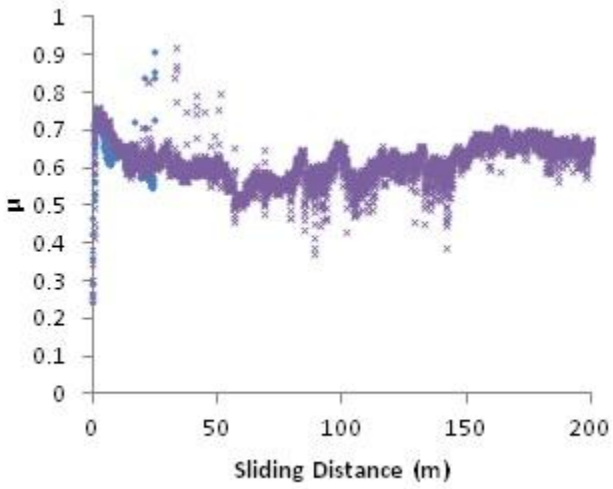

Figure 4.20: Coefficient of friction for CS Sn for distances 25, 50, 100 and 200 m.

Table 4.8: Coefficient of friction for LSP coatings.

Sample	Coefficient of friction
CFRP	0.60
ECF/SF	0.50
Nano Ag	0.50
Ag CNF	N/A
CS Sn	0.70
GO AgNW	N/A
EP Ag	0.20*
MS Al	0.20*

*Results from scratch test

4.4 Environmental Test Results

The environmental tests consist of thermal and salt spray cycling, detailed in Section 3.6. CFRP were used as a baseline comparison with the other samples. The ECF/SF sample had part of its surfacing film sanded away in order to expose the copper to the testing chamber for visual inspections and for electrical measurements. EP Ag and GO AgNW samples were fabricated later and were only tested for the last three cycles. Note that only one sample of MS Al was available, used for salt spray cycling and not thermal cycling, and was fabricated in time only for the last two cycles.

The weight of the samples was measured before and after each cycle. The samples exposed to thermal cycling decrease in weight likely due to water from the composite evaporating. The samples exposed to salt spray increase in weight is likely due to salt deposits during the cycle. The changes in mass are less than 0.5% in all cases and not significant.

A common occurrence across all samples was that the conductive coatings were darker in hue after each cycle, whether thermal or salt spray test. This is likely due to the corrosion and/or oxidation of the metal. The surfacing films of samples ECF/SF and Ag CNF were also darker after each cycle. As the Ag CNF samples had most of the conductive particles inside the surfacing film, it is likely that the surfacing film protected most of the conductive particles from corrosion. See Appendix A for close-up images of all samples at various stages of thermal and salt spray cycling. The specific resistivity was measured before and after each cycle at the same three locations. There are large variations in the three measurements. It is clear however, that there is an overall increase in specific resistivity in all the samples after each cycling.

4.4.1 Thermal (Temperature) Cycling

The test method is described in Section 3.6.1. There are no significant visual changes after each thermal cycle. The CFRP sample has no changes while, the ECF/SF sample has a slight darkening of the copper metal and yellowing of its surfacing film. The Ag CNF surface film turns slightly yellow, the CS Sn sample darkens slightly, and the GO AgNW sample has no visual changes. The EP Ag sample has a slight darkening of the silver coating (In the last cycle, that sample was placed upside down on the metal grid holding the sample, hence the five 'bars' across

the sample.). See Appendix A for close up images of all samples at various stages of thermal cycling.

Figure 4.21 summarizes specific resistivity values for thermal cycling. The specific resistivity mainly increased after each cycle with a small increase for most samples. Most changes are within the range of a standard deviation of the results. The CS Sn sample has the clearer increase in specific resistivity after the first cycle, likely due to the oxidation of the surface.

Table 4.9 shows percentage change in specific resistivity after each cycle. These changes are minor, as they do not show an increase or decrease of an order of magnitude. The CS Sn sample had a noticeable increase in specific resistivity after each cycle but these increases are within one or two standard deviations and the overall increase is not up to an order of magnitude even after the four cycles. The negative values can represent one of two phenomena. The first is that the variation is still minor due to the low specific resistivity values where a small change is magnified (example: 1 to 2 is 100% increase while 10 to 11 is a 10% increase). The second is that it was not possible to measure the exact same place every time and the change represents a more conductive location than normal. The next cycle returns shows a return to the normal value with an increase in specific resistivity of the same order of magnitude.

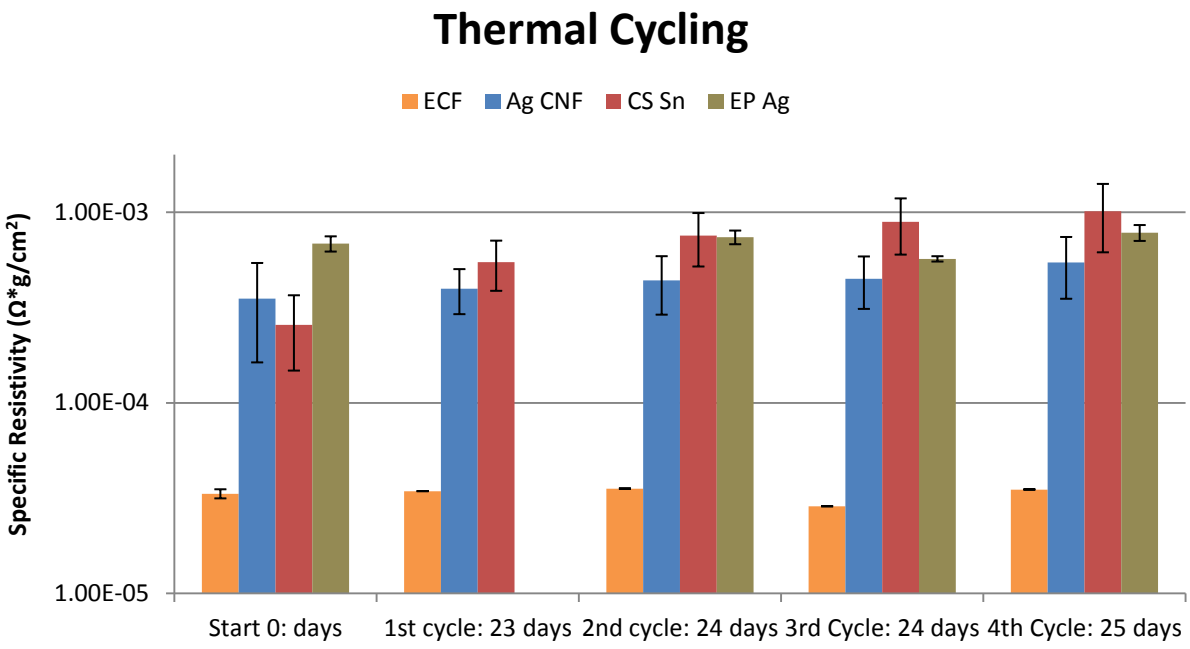

Figure 4.21: Specific resistivity of samples at the start and after each thermal cycle.

Table 4.9: Change in specific resistivity of samples after each thermal cycle.

Thermal Cycle Sample	1st cycle: 23 days	2nd cycle: 23 days	3rd cycle: 23 days	4th cycle: 25 days
CFRP	N/A	N/A	N/A	N/A
ECF	3.1%	3.2%	-19.2%	22.5%
Ag CNF	12.8%	10.5%	2.2%	21.8%
CS Sn	113.1%	37.7%	18.0%	13.6%
GO AgNW	N/A	N/A	N/A	N/A
EP Ag	Not started	8.1%	-23.1%	37.3%

4.4.2 Salt Spray (Fog) Cycling

The test method is described in Section 3.6.2. A certain level of corrosion and oxidation occurred on all samples in the exposed area from Figure 3.13 with the most pronounced effects visible after the first cycle in the salt fog chamber. Further cycles did not show visually pronounced changes. The CFRP has no changes after each cycle while the ECF is corroded by the salt spray exposure. The Ag CNF has little change in appearance after each cycle, likely due to the surfacing film protecting the conductive particles. The CS Sn sample has corrosion after the first cycle and further corrosion is not noticeable on the surface although the area of corrosion on the X scribed lines has about 50% area corrosion which darkens after each cycle but doesn't spread any further. The GO AgNW sample could not be tested due to poor adhesion of the coating, which peeled off after application of the primer paint. The EP Ag conductive coating was removed by the salt spray water droplets as shown in Appendix A with more removed after every cycle increasing its specific resistivity. The entire surface of the MS Al sample is corroded and oxidized after the first cycle. The primer paint delaminates after its second cycle, exposing the substrate, as the adhesion of the coating to the paint was greater than to the substrate. Except for the ECF/SF, Ag CNF and CS Sn samples, the changes cannot be seen in the X-scribed lines of the other samples mainly due to the thinness of the conductive coating. See Appendix A for close up images of the samples at magnifications 20, 50, 100 and 200X.

The CFRP sample was not measured electrically. In the case of the expanded copper foil after the first cycle, it is no longer conductive and no measurements of specific resistivity could be made after each cycle. It is hypothesized that the copper is still conductive underneath the corrosion.

The GO AgNW specific resistivity could not be measured using the 4-point probe method in Section 3.3.4. Sections of the electroless plated silver remained electrically conductive; however, the exposed area is partially removed. The apparatus for electrical measurement in Section 3.3.1 was used rather than the one in Section 3.3.4. The MS Al sample also lost conductivity after its first cycle in the salt spray chamber. Like the ECF sample, it is likely that the surface has been oxidized and that some part of the coating underneath the oxide layer is still conductive. Figure 4.22 summarizes specific resistivity values for salt spray before and after each cycle. Table 4.10 summarizes the changes in specific resistivity of salt sprayed samples.

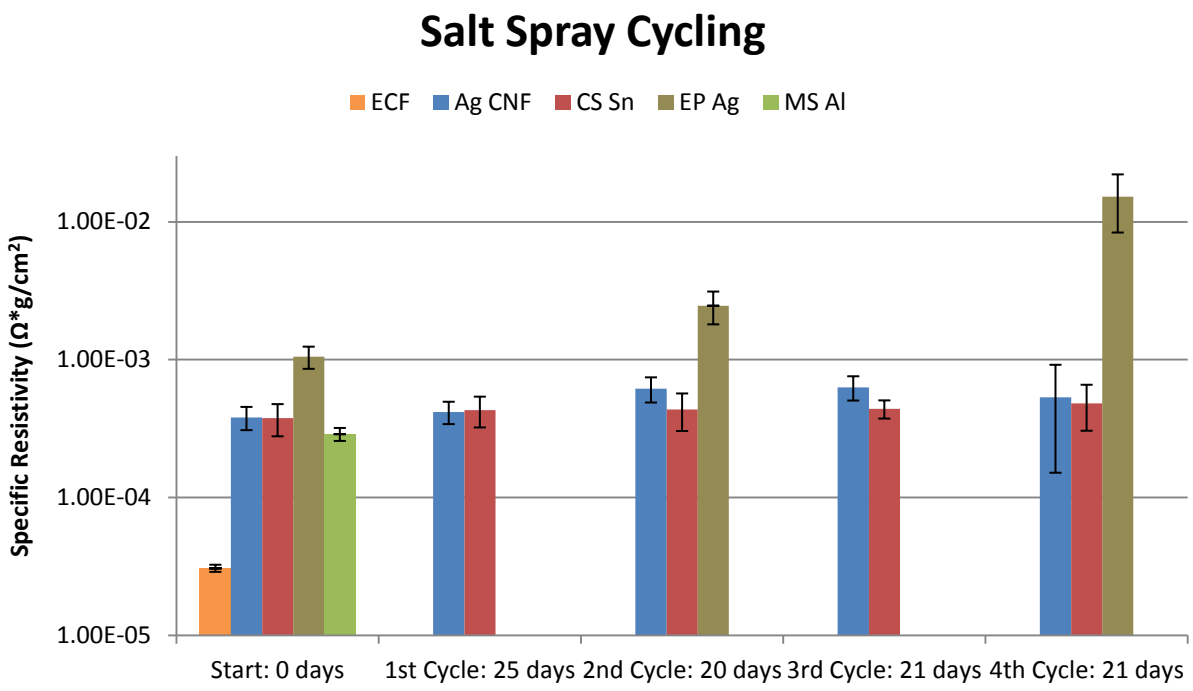

Figure 4.22: Specific resistivity of samples at the start and after each salt spray cycle.

Table 4.10: Change in specific resistivity of samples after each salt spray cycle.

Salt Spray Sample	**1st cycle: 25 days**	**2nd cycle: 20 days**	**3rd cycle: 21 days**	**4th cycle: 21 days**
CFRP	N/A	N/A	N/A	N/A
ECF	Not measurable	Not measurable	Not measurable	Not measurable
Ag CNF	9.7%	47.5%	2.4%	-15.3%
CS Sn	14.3%	1.3%	0.9%	9.3%
GO AgNW	N/A	N/A	N/A	N/A
EP Ag	Not started	134.4%	N/A	518.8%
MS Al	Not started	Not started	Not measurable	Not measurable

The samples retain their specific resistivity within the same order of magnitude with the exceptions being the ECF and MS Al samples that lost their surface conductivity, which might still be conductive under the oxidation layer. The EP Ag sample had significant increases in specific resistivity, more than one order of magnitude, due to corrosion and the coating being washed out during the salt spray exposure.

CHAPTER 5 CONCLUSIONS AND RECOMMENDATIONS

Lightning strike protection of aircraft is critical to the aerospace industry's continued safety record. New LSP conductive coatings have the potential to safeguard aircraft while reducing their overall weight for more fuel-efficient aircraft. The conductive coatings discussed in the thesis are much easier to install than current surfacing film with expanded copper foil.

5.1 Summary and General Discussion

The lowest specific resistivity of the conductive coatings is shown in Figure 5.1. These results are from 4-point probe measurements (see Section 3.3.1), except for CFRP, whose specific resistivity is measured using four-terminal sensing (see Section 3.3.2). The magnetron sputtered aluminum conductive coating has the lowest specific resistivity of all the coatings investigated in this study. It has great promise for LSP but has the following problems: the possibility of galvanic corrosion between carbon fibers and aluminum would require an interlayer film, increasing weight of final coating architecture.

However, the interlayer could be a metallic and conductive coating such as tin or copper, and emulated lightning strike tests could be conducted to verify if this additional layer helps protect the underlying composite substrate from both corrosion and lightning damage. A larger chamber would be required to fabricate these larger samples.

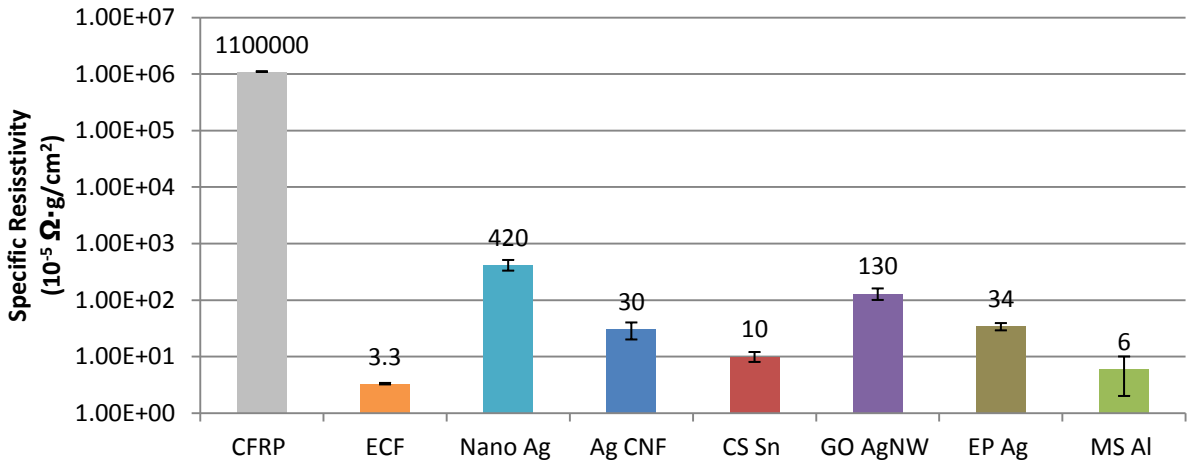

Figure 5.1: Lowest electrical specific resistivity values for baselines CFRP substrate and ECF, and LSP coatings.

The specific resistivity itself does not determine exactly how the lightning strike will damage the conductive coating or the underlying composite substrate. These lightning strike tests are part of the project but not of this thesis. Early results indicate that low resistance helps protect against lightning strikes.

The conductive samples had good adhesion measured by peel and scratch tests, except the GO AgNW sample having the worst adhesion. The scratch results confirmed the adhesion results, and showed the resistance of the LSP coatings to scratch testing. Figure 5.2a shows the hardness results and Figure 5.2b shows the Young's modulus results for the CFRP and all LSP coatings.

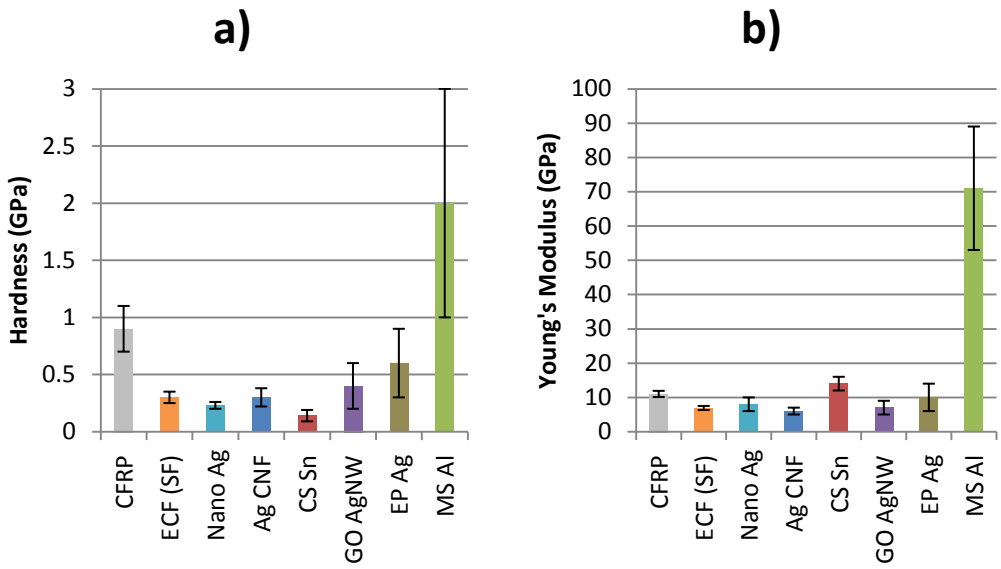

Figure 5.2: Baselines CFRP substrate and ECF/SF, and all LSP coatings values for a) hardness and b) Young's Modulus.

One of the problems with the results of three-point flexion is that the variance and standard deviation are high. This is the case not just for the tests of this thesis but also in the literature, as mentioned in Section 2.11. It is likely that whatever changes occur after a current injection in the LSP coatings, the current is not high enough to damage the composite substrate and affect mechanical properties. The large standard deviations of the results can be caused by numerous effects such as non-consistent thickness and width of samples. In the case of flexion tests, a difference of tens of µm could lead to changes of hundreds of MPa in the modulus results.

Mechanical testing of composites also has a 10-25% variance in mechanical results between samples.

Figure 5.3 summarizes the coefficients of friction for the CFRP baseline and the LSP coatings. Ag CNF was not tested because the particles were imbedded in the same surfacing film used by the ECF/SF; therefore, they have the same values as ECF/SF. The GO AgNW coatings were not adhesive enough to the substrate for this test.

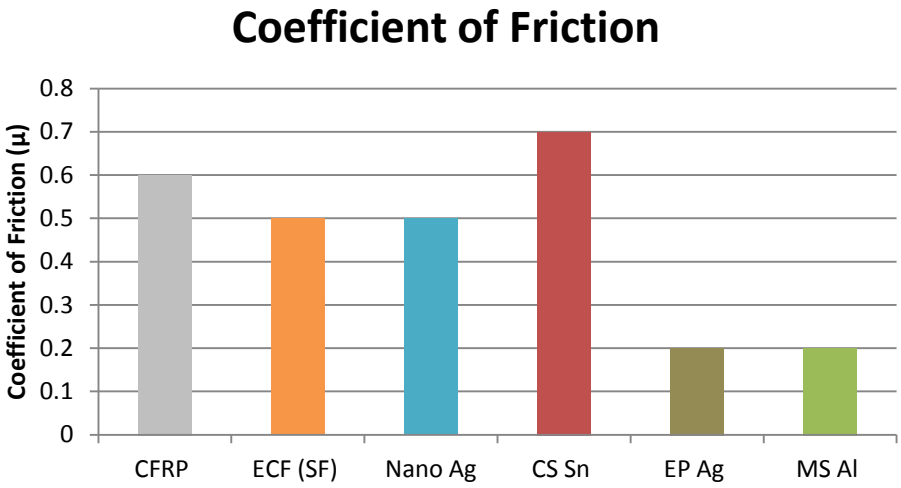

Figure 5.3: Summary of coefficients of friction.

During thermal (temperature) cycling environmental tests, only the cold sprayed tin sample showed a significant increase in specific resistivity. During salt spray (fog) cycling environmental tests, the expanded copper foil, the cold sprayed tin, the electroless plated silver and the magnetron sputtered aluminum suffered the most corrosion and increase in specific resistivity with electroless silver having an increase of an order of magnitude, while copper and aluminum coatings became non-conductive.

5.2 Conclusion

A few general conclusions and can be described for the conductive coatings of this project.

1. Coatings with high metal content possess the lowest specific resistivity; see Figure 5.1 for best results of the CFRP baseline and all conductive coatings.
2. Specific resistivity strongly depends upon the type of metal used. For example, cold sprayed tin (10×10^{-5} $\Omega \cdot g/cm^2$) vs. magnetron sputtered aluminum (6×10^{-5} $\Omega \cdot g/cm^2$) which puts a physical limit on the lowest value that can be obtained for a coating.
3. The conductive coatings developed in this CRIAQ project are very lightweight.
4. The conductive coatings of cold sprayed tin and silver-coated carbon fibers are easy to apply on the carbon/epoxy composites (CFRP) surface by simply spraying it on.
5. These coatings could be used on areas that do not require high level LSP protection while ECF/SF is used for the main protection.
6. Repair patches using certain coatings could be less expensive and easier than to replace expanded copper foil damaged by lightning strikes.

5.3 Perspectives

In order to have electrical results with more certainty and confidence, a few recommendations are suggested. The 4-point probe electrical tests on a single sample should have used five measurements at six locations rather than ten measurements at three locations. This would have kept the precision but it would give a more accurate standard deviation for the results. It is recommended not to expose the samples to air, which could have been a factor for highly oxidizing samples such as cold sprayed tin, electroless plated silver and magnetron sputtered aluminum. Exposure can be reduced in the lab but it is unlikely to be done in an industrial setting unless a surfacing film is installed quickly after fabrication of the coating.

More samples should have been tested at the same time during environmental tests, at least 3-5 samples of each type rather than 1. Samples should have thicker coatings to better observe corrosion progress and prevent the removal of the coating akin to the EP Ag sample. Longer thermal and salt spray cycling tests were also planned but could not be carried out due to time constraints but could be carried out to further investigate conductive coating properties to these

long term effects. Additionally, larger panels could be tested in the environmental chambers after which the sample could be subjected to an emulated lightning strike and compared with results before environmentally tested samples. This would give additional information as to whether or not corrosion and oxidation decrease the ability of a conductive coating to bear a high current lightning strike. The more important test of the effectiveness of the LSP conductive coatings will be determined by simulated lightning strikes on larger panel, which is not part of this thesis but is part of the CRIAQ project and still ongoing.

Finally, although the main purpose of these materials and tests were for LSP, there are other applications where these conductive coatings can be used in other industrial and scientific applications such as EMI shielding. Conductive coatings can be applied on aircraft, satellites or other aerospace craft. The fields of microelectronics and nano-engineering also use conductive wiring and surfaces. Note that for most of these other applications, the parameters and requirements are not as strenuous or high as demanded by LSP design.

BIBLIOGRAPHY

[1] A. Larsson, "The interaction between a lightning flash and an aircraft in flight," *Comptes Rendus Physique,* vol. 3, pp. 1423-1444, 2002.

[2] J. Gou, Y. Tang, F. Liang, Z. Zhao, D. Firsich, and J. Fielding, "Carbon nanofiber paper for lightning strike protection of composite materials," *Composites Part B: Engineering,* vol. 41, pp. 192-198, 2009.

[3] G. Gardiner. (2006, 07/01/2006) Lightning Strike Protection For Composite Structures *High-Performance Composites* Available: http://www.compositesworld.com/articles/lightning-strike-protection-for-composite-structures

[4] P. Feraboli and M. Miller, "Damage resistance and tolerance of carbon/epoxy composite coupons subjected to simulated lightning strike," *Composites Part A: Applied Science and Manufacturing,* vol. 40, pp. 954-967, 2009.

[5] J. A. P. Franklin A. Fisher, *Lightning Protection of Aircraft*. Washington, D.C. 20402: U.S. Government Printing Office, 1977.

[6] L. D. Systems. *Lightning Protection Systems: Lightning Diverter Strips and Lightning Conformal Shield*. Available: http://www.lightningdiversion.com/Products.htm

[7] (03/05/216). *Aircraft Struck by Lightning Strike*. Available: http://i.huffpost.com/gen/1495281/images/o-PLANE-LIGHTNING-facebook.jpg

[8] Y. Hirano, S. Katsumata, Y. Iwahori, and A. Todoroki, "Artificial lightning testing on graphite/epoxy composite laminate," *Composites Part A: Applied Science and Manufacturing,* vol. 41, pp. 1461-1470, 2010.

[9] APCM. *Strike Guard LSP prepreg*. Available: http://www.prepregs.com/products.html

[10] S. Mall, B. L. Ouper, and J. C. Fielding, "Compression Strength Degradation of Nanocomposites after Lightning Strike," *Journal of Composite Materials,* vol. 43, pp. 2987-3001, 2009.

[11] J. B. O'Loughlin and S. R. Skinner, "General Aviation Lightning Strike Report Protection Level Study Report DOT/FAA/AR-04/13," U. S. D. o. T. F. A. Administration, Ed., Final Report ed. Washington, DC, 2004, p. 32 pages.

[12] N/A, "Certification of Transport Airplane Structure," vol. AC 25-21, F. A. A. U.S. Department of Transporation, Ed., Section 25.581 ed. N/A, 1999, p. 187.

[13] J. M. Welch, "Repair Design, Test, and Process Considerations for Lightning Strikes," CACRC/MIL-HDBK-17 Conference07/05/2007 2007.

[14] I. S. Society of Automotive Engineers, "Aerospace Recommended Practice –5414 "Aircraft Lightning Zoning"," ed: SAE International, 1999.

[15] M. C. G. Corporation. (2005). *Strikegrid™ Continuous Expanded Aluminum Foil (CEAF)*. Available: http://www.mcgillcorp.com/alcore/datasheets/paa-core_strikegrid.pdf

[16] S. J. M. Cabler, "Protection of airplane fuel systems against fuel vapor due to lightning," vol. Advisory Circular AC20-53B, U. S. D. o. T. F. A. Administration, Ed., N/A ed: N/A, 2006.

[17] M. Gagné and D. Therriault, "Lightning strike protection of composites," *Progress in Aerospace Sciences*, vol. 64, pp. 1-16, 01// 2014 http://dx.doi.org/10.1016/j.paerosci.2013.07.002.

[18] S. J. Earl, "Some Methods for Modelling CFC for the Effects of Lightning," in *Challenges in the Modelling and Measurement of Electromagnetic Materials, 2006. The Institution of Engineering and technology Seminar on*, 2006, pp. 33-38.

[19] L. M. Gammon and A. Falcone. (2003, 08-01-03) Lightning Strike Damage in Polymer Composites. *ADVANCED MATERIALS & PROCESSES*. 2. Available: http://www.asminternational.org/

[20] Unknown. ASM Handbooks Online [Online]. Available: http://www.asminternational.org/

[21] A. P. M. Corp. *What Is Astrostrike?* Available: http://www.astrosealproducts.com/index.html

[22] F. T. James L. Dye, "alkali metal," in *Encyclopædia Britannica*, Online ed.

[23] Unknown. (08/02/2011). *Magnesium Elektron: Magnesium in Aerospace*. Available: http://www.magnesium-elektron.com/markets-applications.asp?ID=8

[24] H. Corporation. (2005). *Lightning Strike Products: SynSkin® Composite Surfacing Film and Hysol® film Adhesives with Conductive Screens*. Available: http://ableaero.com/tds/Henkel_Lightning_Strike_Products.pdf

[25] Unknown, "Beryllium Copper in the Aircraft Industry," *Aircraft Engineering and Aerospace Technology*, vol. 13, pp. 235-236, 1941.

[26] D. Brisius. (2007, 05/01/2007) Boeing 787 Update. *High_Performance Composites*. Available: http://www.compositesworld.com/articles/boeing-787-update

[27] Unknown. (03/06/2011). *Brochures Dexmet Lightning Strike Protection: Expansion Flattening*. Available: http://www.aero-consultants.ch/page.php?id=716&language=en

[28] Unknown. (03/06/2011). *ANOMET Platinum Clad Impressed: Current Anodes & Materials*. Available: http://www.farwestcorrosion.com/fwst/anodimpr/anomet02.htm

[29] (03/05/2016). *Woven Wire Mesh Anodes*. Available: http://www.anometproducts.com/pca/woven-wire-mesh-anodes

[30] Unknown. (03/06/2011). *Brochures Dexmet Lightning Strike Protection: Dexmet Lightning Strike Brochure*. Available: http://www.aero-consultants.ch/page.php?id=716&language=en

[31] D. Corporation. (04/10/2010). *MicroGrid® Precision-Expanded Foils*. Available: http://www.dexmet.com/

[32] R. Baksht, Y. Yankelevich, I. Ziv, and A. Porkryvailo, "Explosion of thin aluminum foils in air," in *Pulsed Power Conference, 2003. Digest of Technical Papers. PPC-2003. 14th IEEE International*, 2003, pp. 748-751 Vol.2.

[33] I. Integument Technologies. *FluoroGrip® LS-1000*. Available: http://integument.com/lightning.html

[34] A. F. N. D. E. Walpole, "NONWOVEN VEIL TECHNOLOGY FOR LIGHTNING STRIKE PROTECTION," presented at the SAMPE 2006, Long Beach, CA April 30, 2006.

[35] G. Jiang, M. Gilbert, D. J. Hitt, G. D. Wilcox, and K. Balasubramanian, "Preparation of nickel coated mica as a conductive filler," *Composites Part A: Applied Science and Manufacturing,* vol. 33, pp. 745-751, 2002.

[36] C. Hexcel. *Hexcel Products: Thorstrand*. Available: http://www.hexcel.com/Resources/DataSheets/Prepreg-Data-Sheets/Thorstrand_us.pdf

[37] S. P. B. G.D. Liang, S.C. Tjong, "Microstructure and properties of polypropylene composites filled with silver and carbon nanotube nanoparticles prepared by melt-compounding," *Materials Science and Engineering B,* vol. 142, pp. 55-61, 2007.

[38] N/A. (1st May 2011). *Conductive Coating (Decor Engineering)*. Available: http://www.decorengineering.com.au/aeronautics.htm

[39] F. Inam, H. Yan, D. D. Jayaseelan, T. Peijs, and M. J. Reece, "Electrically conductive alumina-carbon nanocomposites prepared by Spark Plasma Sintering," *Journal of the European Ceramic Society,* vol. 30, pp. 153-157, 2010.

[40] Y. Keqin, J. He, P. Puneet, Z. Su, M. J. Skove, J. Gaillard, *et al.*, "Tuning electrical and thermal connectivity in multiwalled carbon nanotube buckypaper," *Journal of Physics: Condensed Matter,* vol. 22, p. 334215, 2010.

[41] K. B. Armstrong, L. G. Bevan, and W. F. Cole, "Care and Repair of Advanced Composites (2nd Edition)," ed: Society of Automotive Engineers, Inc.

[42] D. M. Mattox, "Physical vapor deposition (PVD) processes," *Metal Finishing,* vol. 100, pp. 394-408, 2002.

[43] A. Anders, "Discharge physics of high power impulse magnetron sputtering," *Surface and Coatings Technology,* vol. 205, Supplement 2, pp. S1-S9, 7/25/ 2011.

[44] Unknown. ASM Handbook: Volume 5, Surface Engineering: Plating and Electroplating [Online]. Available: http://products.asminternational.org/hbk/index.jsp

[45] N/A. *MCFDatasheet*. Available: http://www.metalcoatedfibers.com/Site/Home_Page_files/MCFDatasheet.pdf

[46] Unknown. ASM Desk Editions: Engineered Materials Handbook: Processing and Fabrication of Engineering Plastics: Metallizing of Plastics: Metallizing Processes [Online]. Available: http://products.asminternational.org/hbk/index.jsp

[47] D. G. Richard R. Chromik, J. Micheal Shockley, Stephen Yue, Eric Irissou, Jean-Gabriel Legoux, Nicholas X. Randall, "Modified ball bond shear test for determination of adhesion strength of cold spray splats," *Surface & Coatings Technology,* vol. 205, pp. 1409-1414, 2010.

[48] D. G. Yu Zou, Jerzy A. Szpunar, Stephen Yue, "Microstructure and nanohardness of cold-sprayed coatings: Electron backscattered diffraction and nanoindentation studies," *Scripta Materialia,* vol. 62, pp. 395-398, 2010.

[49] W. Q. Yu Zou, Eric Irissou, Jean-Gabriel Legoux, Stephen Yue, Jerzy A. Szpunar, "Dynamic recrystallization in the particle/particle interfacial region of cold-sprayed nickel coating: Electron backscatter diffraction characterization," *Scripta Materialia,* vol. 61, pp. 899-902, 2009.

[50] V. Champagne, Jr., D. Helfritch, P. Leyman, S. Grendahl, and B. Klotz, "Interface material mixing formed by the deposition of copper on aluminum by means of the cold spray process," *Journal of Thermal Spray Technology,* vol. 14, pp. 330-334, 2005/09/01 2005.

[51] J. Affi, H. Okazaki, M. Yamada, and M. Fukumoto, "Fabrication of Aluminum Coating onto CFRP Substrate by Cold Spray," *MATERIALS TRANSACTIONS,* vol. 52, pp. 1759-1763, 2011.

[52] G. A. G. Mohammed H. Al-Saleh, Uttandaraman Sundararaj, "Copper nanowire polystyrene nanocomposites Lower percolation threshold and higher EMI shielding," *Composites Part A: Applied Science and Manufacturing,* vol. 42, pp. 92-97, 2011.

[53] G. A. G. Bin Lin, Joel A. Haber, Petra Po¨tschke, Uttandaraman Sundararaj, "Electrical, Morphological and Rheological Study of Melt Mixed Polystyrene Copper Nanowire Nanocomposites," *Macromolecular Materials and Engineering,* vol. 293, pp. 631-640, 2008.

[54] U. S. Genaro A. Gelves, Joel A. Haber, "Electrostatically Dissipative Polystyrene Nanocomposites containing Copper Nanowires," *Macromolecular Rapid Communications,* vol. 26, pp. 1677-1681, 2005.

[55] K. Locharoenrat, H. Sano, and G. Mizutani, "Field enhancement in arrays of copper nanowires investigated by the finite-difference time-domain method," *Surface and Interface Analysis,* vol. 40, pp. 1635-1637, 2008.

[56] T. M. Kruckenberg, V. A. Hill, A. M. Mazany, E. Young, and S. Chiou, "Film for providing lightning strike protection to composite material for airplanes, comprises polymeric film with low density conductive material containing nanoparticles dispersed on the surface of film in loading level," WO2008048705-A2; EP1996465-A2; WO2008048705-A3; CN101466598-A; US2009227162-A1.

[57] D. Taylor, B. Loeper, and D. Henderson, "Interwoven fabric for aircraft component, has one end within first set of warp ends interwoven with one end of second set of fill ends to join first fabric to second fabric," US2005098224-A1; WO2005047581-A1; EP1682707-A1; AU2004288913-A1; JP2007510821-W; AU2004288913-B2.

[58] C.-C. M. M. Yi-Hsiuan Yu, Siu-Ming Yuen, Chih-Chun Teng, Yuan-Li Huang, Ikai Wang, Ming-Hsiung Wei, "Morphology, Electrical, and Rheological Properties of Silane-Modified Silver Nanowire Polymer Composites," *Macromolecular Materials and Engineering,* vol. 295, pp. 1017-1024, 2010.

[59] Z. T. M. M. Genaro A. Gelves, Matthew J. Krantz, Joel A. Haber, "Multigram synthesis of copper nanowires using ac electrodeposition into porous aluminium oxide templates," *Journal of Materials Chemistry,* vol. 16, pp. 3075-3083, 2006.

[60] L. L. Antoine Lonjon, Philippe Demont, Eric Dantras, Colette Lacabanne, "New Highly Conductive Nickel Nanowire-Filled P(VDF-TrFE) Copolymer Nanocomposites Elaboration and Structural Study," *Journal of Physical Chemistry,* vol. 113, pp. 12002-12006, 2009.

[61] A. Frenot and I. S. Chronakis, "Polymer nanofibers assembled by electrospinning," *Current Opinion in Colloid & Interface Science,* vol. 8, pp. 64-75, 2003.

[62] Y.-D. H. Young-Sik Cho, "Synthesis of ultralong copper nanowires by reduction of copper-amine complexes," *Materials Letters,* vol. 63, pp. 227-229, 2009.

[63] G. A. Gelves, M. H. Al-Saleh, and U. Sundararaj, "Highly electrically conductive and high performance EMI shielding nanowire/polymer nanocomposites by miscible mixing and precipitation," *Journal of Materials Chemistry,* vol. 21, pp. 829-836, 2011.

[64] ASM Handbook Online: Metals Handbook: Structure and Properties of Metals: Properties of Metals: Physical Properties of Metals [Online]. Available: http://products.asminternational.org/hbk/index.jsp

[65] M. Wilms, J. Conrad, K. Vasilev, M. Kreiter, and G. Wegner, "Manipulation and conductivity measurements of gold nanowires," *Applied Surface Science,* vol. 238, pp. 490-494, 2004.

[66] M. T. Byrne and Y. K. Gun'ko, "Recent Advances in Research on Carbon Nanotube–Polymer Composites," *Advanced Materials,* vol. 22, pp. 1672-1688, 2010.

[67] U. S. O. BREUER, "Big Returns From Small Fibers: A Review of Polymer/Carbon Nanotube Composites," *POLYMER COMPOSITES,* vol. 25, pp. 630-645, 2004.

[68] C. M. Schauerman, J. Alvarenga, M. J. Ganter, T. P. Seager, B. J. Landi, and R. P. Raffaelle, "Single wall carbon nanotubes for conductive wiring," in *Sustainable Systems and Technology, 2009. ISSST '09. IEEE International Symposium on*, 2009, pp. 1-5.

[69] S. Stankovich, D. A. Dikin, G. H. B. Dommett, K. M. Kohlhaas, E. J. Zimney, E. A. Stach, *et al.*, "Graphene-based composite materials," *Nature,* vol. 442, pp. 282-286, 2006.

[70] Y. Tang and J. Gou, "Synergistic effect on electrical conductivity of few-layer graphene/multi-walled carbon nanotube paper," *Materials Letters,* 2010.

[71] S.-Y. Yang, W.-N. Lin, Y.-L. Huang, H.-W. Tien, J.-Y. Wang, C.-C. M. Ma, *et al.*, "Synergetic effects of graphene platelets and carbon nanotubes on the mechanical and thermal properties of epoxy composites," *Carbon,* vol. 49, pp. 793-803, 2011.

[72] S. K. N. K. S. Deepa, P. Parameswaran, M. T. Sebastian, J. James, "Effect of conductivity of filler on the percolation threshold of composites," *Applied Physics Letters,* vol. 94, pp. 1-3, 2009.

[73] B. L. G. A. Gelves, U. Sundararaj, J. A. Haber, "Electrical and rheological percolation of polymer nanocomposites prepared with functionalized," *Nanotechnology,* vol. 19, pp. 1-13, 2008.

[74] P. C. M. Jing LI, Chow Wing SZE, To Chi KAI, Ben Zhong TANG, Jang-Kyo KIM, "Percolation Threshold of Polymer Nanocomposites Containing Graphite Nanoplatelets and Carbon Nanotubes," presented at the 16th International Conference on Composite Materials, Kyoto, Japan, 2007.

[75] W. Bauhofer and J. Z. Kovacs, "A review and analysis of electrical percolation in carbon nanotube polymer composites," *Composites Science and Technology*, vol. 69, pp. 1486-1498, 2009.

[76] T.-W. C. Weibang Lu, Erik T. Thostenson, "A three-dimensional model of electrical percolation thresholds in carbon nanotube-based composites," *Applied Physics Letters*, vol. 96, pp. 1-3, 2010.

[77] J. Vavro, M. C. Llaguno, B. C. Satishkumar, D. E. Luzzi, and J. E. Fischer, "Electrical and thermal properties of C60-filled single-wall carbon nanotubes," *Applied Physics Letters*, vol. 80, 2002.

[78] C. Li, E. T. Thostenson, and T.-W. Chou, "Effect of nanotube waviness on the electrical conductivity of carbon nanotube-based composites," *Composites Science and Technology*, vol. 68, pp. 1445-1452, 2008.

[79] M. H. Al-Saleh and U. Sundararaj, "A review of vapor grown carbon nanofiber/polymer conductive composites," *Carbon*, vol. 47, pp. 2-22, 2009.

[80] K. I. Winey, R. A. Vaia, and G. Editors, "Polymer Nanocomposites," *Materials Research Society Bulletin*, vol. 32, 2007.

[81] J. B. a. E. Silverman, "Challenges and Opportunities in Multifunctional Nanocomposite Structures for Aerospace Applications," *Materials Research Society Bulletin*, vol. 32, 2007.

[82] N/A. (May 1st 2011). *graphenesupermarket*. Available: https://graphene-supermarket.com/home.php

[83] L. Tune. (2008, May 2nd, 2011). *Physicists Show Electrons Can Travel More Than 100 Times Faster in Graphene*. Available: https://newsdesk.umd.edu/scitech/release.cfm?ArticleID=1621

[84] D. Heidlebaugh, Avery, W., and Uhrich, S., "Effect of Lightning Currents on Structural Performance of Composite Material," *SAE Technical Paper 2001-01-2885*, 2001.

[85] CM2. *Microscope électronique à balayage à canon à effet de champ*. Available: http://www.cm2.polymtl.ca/MebFeg.php

[86] CM2. *Microscope électronique à balayage*. Available: http://www.cm2.polymtl.ca/Meb.php

[87] *Four Point Probe Resistivity Measurements*. Available: http://www.pveducation.org/pvcdrom/characterisation/four-point-probe-resistivity-measurements

[88] *Correction Factor for 4 Point Probe*. Available: http://www.chm.bris.ac.uk/~gf8856/BScThesis_files/image027.gif

[89] K. K. N. Simon M. Sze, *Physics of Semiconductor Devices*. New York, 2007.

[90] *P-A-T / Paint Adhesion Test Kit*. Available: http://gardco.com/pages/adhesion/PATkit.cfm

[91] A. R. Franco Jr., G. Pintaúde, A. Sinatora, C. E. Pinedo, and A. P. Tschiptschin, "The use of a vickers indenter in depth sensing indentation for measuring elastic modulus and vickers hardness," *Materials Research*, vol. 7, pp. 483-491, 2004.

[92] A. C. Fischer-Cripps, *Nanoindentation*: Springer-Verlag New York, 2011.

APPENDIX A – ENVIRONMENT REPORT FIGURES

All pictures from thermal and salt spray cycling environmental tests. Magnifications, test type, sample type, cycle number and number of days for each cycle labeled on the figure. Note that for some sample after a cycle, the microscope illumination was not the same as the others; it is not the sample that changes but the light intensity/brightness.

The following is a summary of the changes to the samples after thermal cycling:

- CFRP: No changes are visible as shown in Figure A.1.
- ECF: Slight darkening of the copper mesh as shown in Figure A.2.
- Ag CNF: Slight yellowing of the coating as shown in Figure A.3.
- CS Sn: Slight darkening of the tin coating as shown in Figure A.4.
- GO AgNW: No visual changes as shown in Figure A.5.
- EP Ag: Slight darkening of the silver coating as shown in Figure A.6. In the last cycle, the sample was placed upside down, hence the 'bars' across the shorter width of the sample.

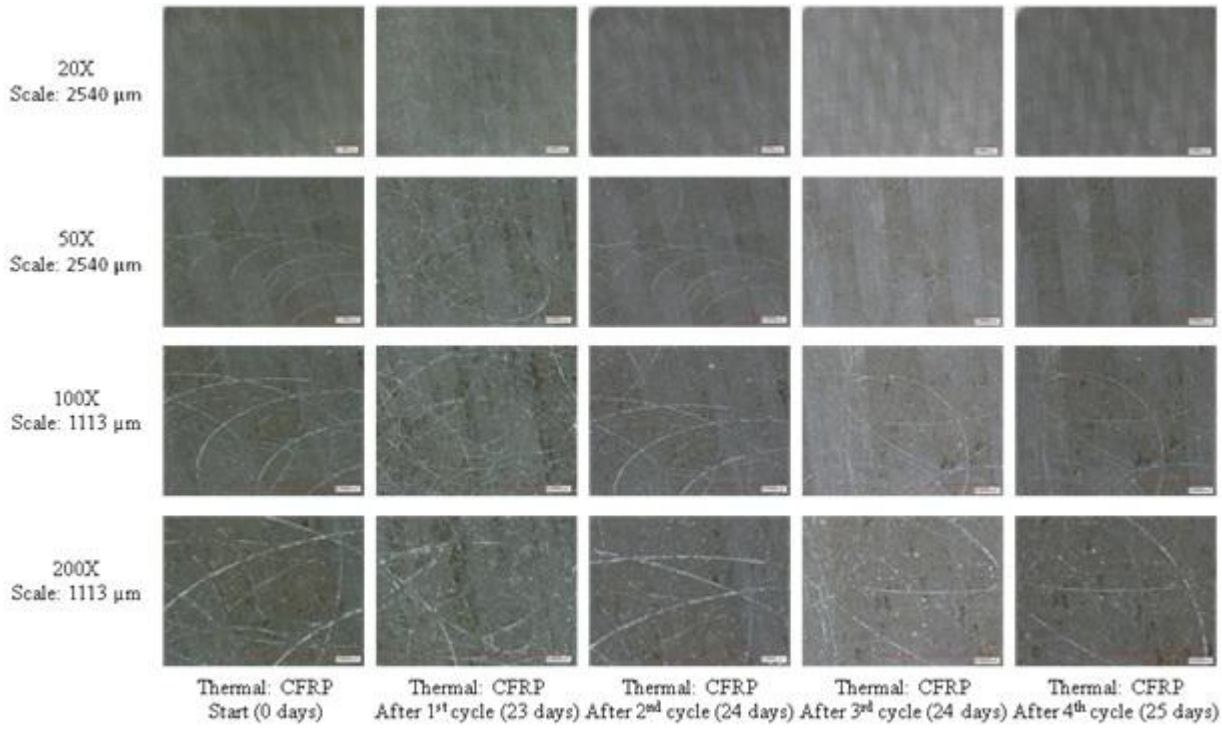

Figure A.1: Thermal Cycling for CFRP at magnifications 20, 50, 100 and 200X.

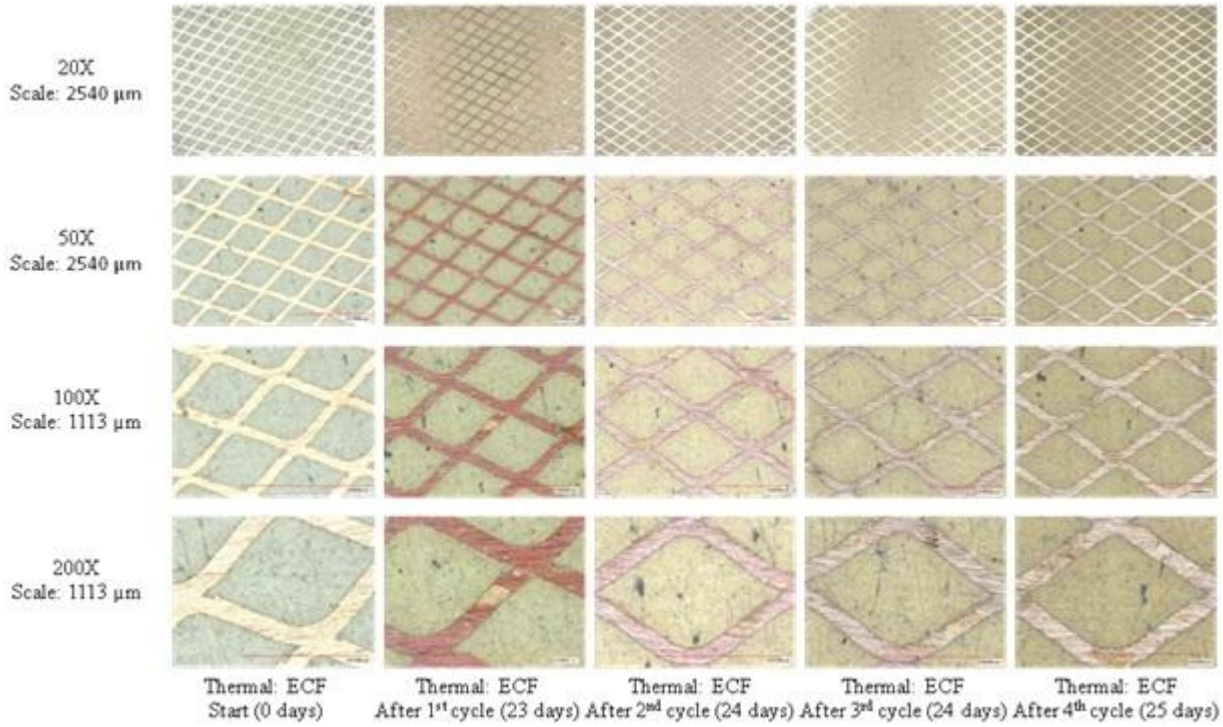

Figure A.2: Thermal Cycling for ECF at magnifications 20, 50, 100 and 200X.

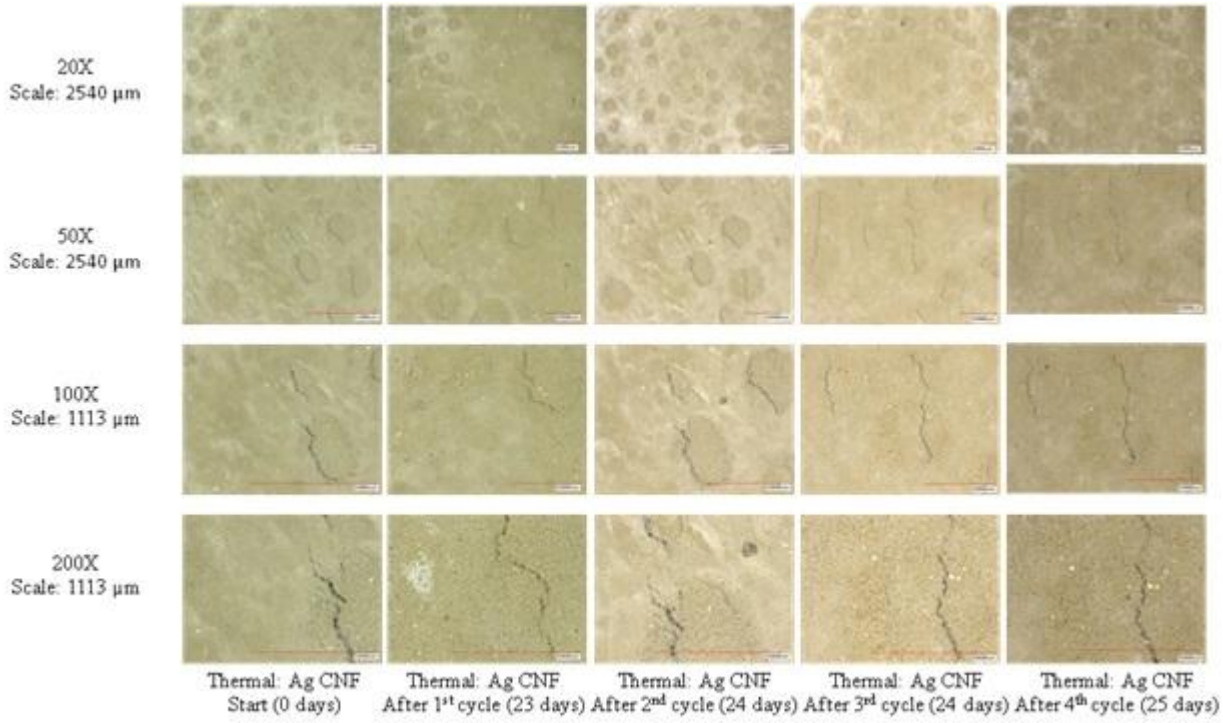

Figure A.3: Thermal Cycling for Ag CNF at magnifications 20, 50, 100 and 200X.

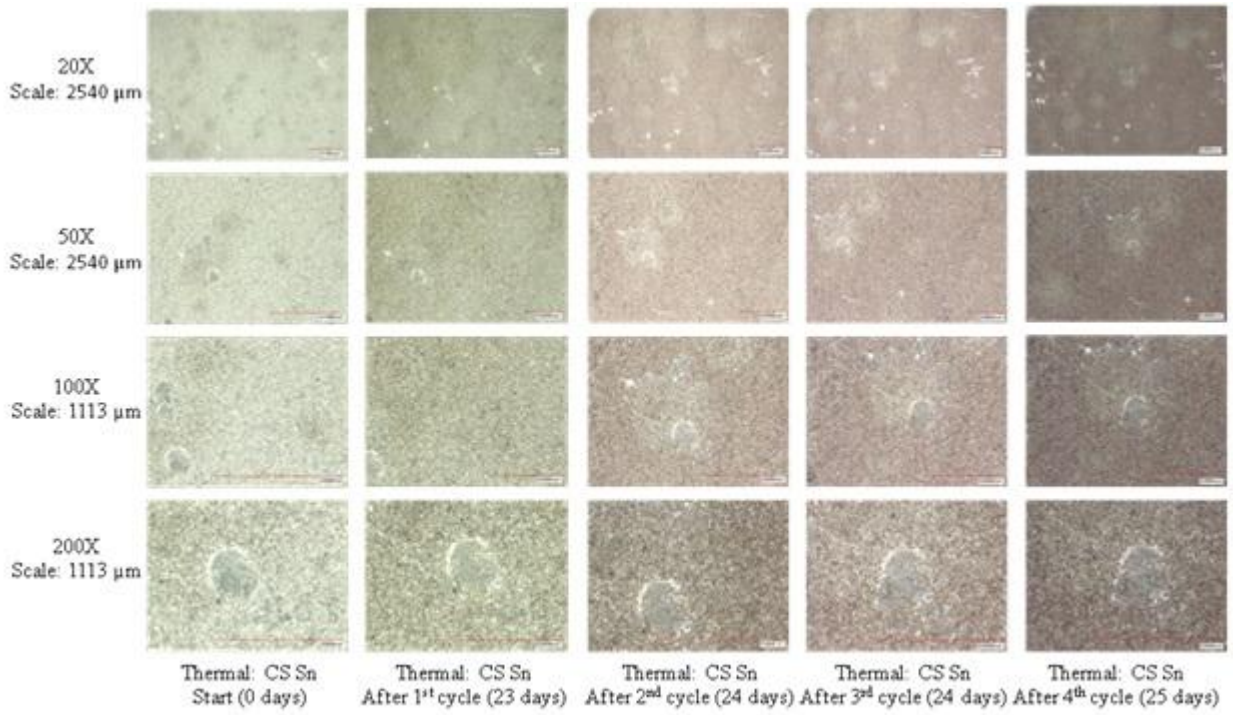

Figure A.4: Thermal Cycling for CS Sn at magnifications 20, 50, 100 and 200X.

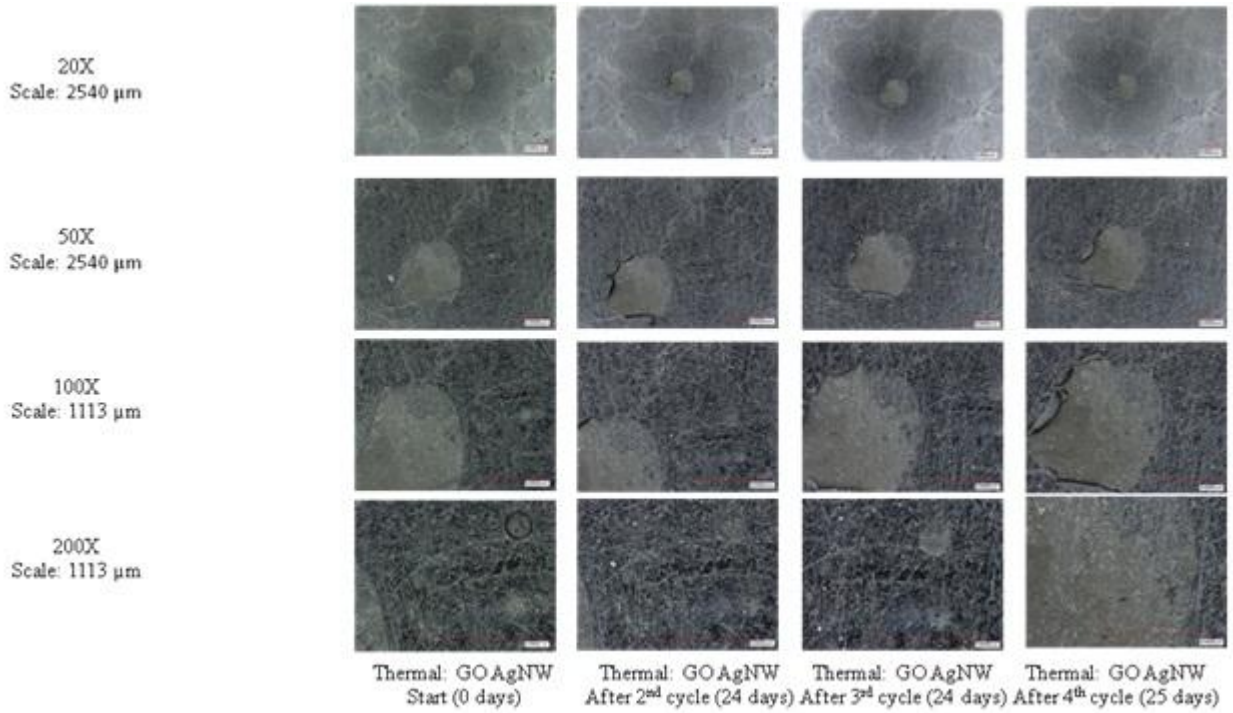

Figure A.5: Thermal Cycling for GO AgNW at magnifications 20, 50, 100 and 200X.

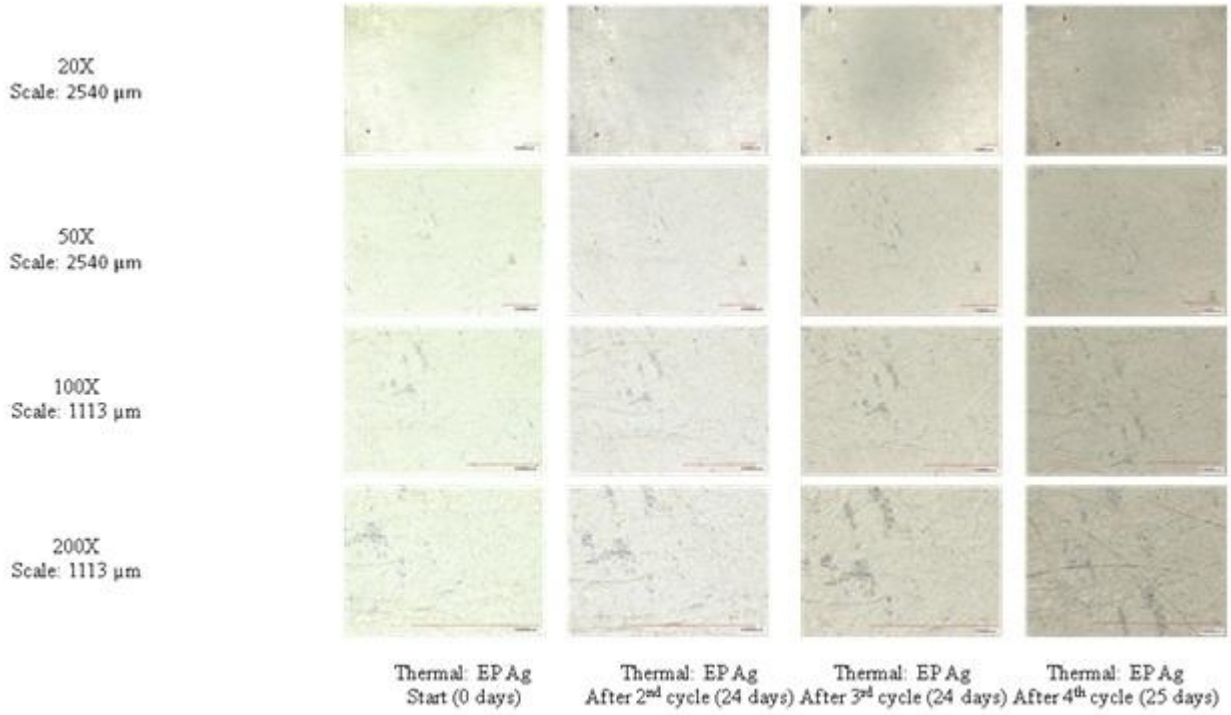

Figure A.6: Thermal Cycling for EP Ag at magnifications 20, 50, 100 and 200X.

A certain level of corrosion and oxidation occurred on all samples that underwent salt spray fog exposure, with the most pronounced effects visible after the first cycle in the chamber. Further cycles did not show pronounced changes visually. The observations of the samples are as follow:

- CFRP: No changes to sample after each cycle as shown in Figure A.7.
- CFRP X: No changes, not shown.
- ECF: Heavy corrosion from salt spray exposure as shown in Figure A.8. It is no longer conductive after first cycle. It is hypothesized that the copper is still conductive under the exposed surface.
- ECF X: Metal mesh is entirely corroded on the surface after the first cycle. This remains throughout the remainder of the cycles as shown in Figure A.9.
- Ag CNF: Surface coating darkens after first cycle but does not appear to change after other cycles as shown in Figure A.10.
- Ag CNF X: Corrosion appears only at the end of the 3rd cycle (about 1-5% surface area), and grows 2-3 times the area size after the end of the 4th cycle as shown in Figure A.11.
- CS Sn: Corrosion on the surface occurs after the first cycle, and stays mostly unchanged after each cycle as shown in Figure A.12.
- CS Sn X: Corrosion occurs after first cycle; about 50% of the X scribe is covered in brown corroded tin as shown in Figure A.13. After the 4th cycle, the area affected is roughly the same, but darker.
- GO AgNW: After primer coat was applied, the tape removed the conductive coating. However, neither salt spray sample nor thermal samples were electrically conductive

across a one-inch distance for the probes, which rendered electrical measurements impossible due to the high resistance. Images of this sample show the underlying substrate and not any conductive coating.

- GO AgNW X: Primer coating delaminated after first cycle, along with the conductive coating. Coating too thin to observe any changes, and coating was not conductive enough to measure electrical resistance.
- EP Ag: Removal of silver coating after each successive cycle as shown in Figure A.14.
- EP Ag X: Since the coating too thin the progress of corrosion cannot be seen through the microscope.
- MS Al: The entire surface is corroded and oxidized after first cycle as shown in Figure A.15.
- MS Al X: The exposed scribe corroded after first cycle. After second cycle, there is the delamination of primer paint and coating on X-scribe, exposing the underlying substrate.

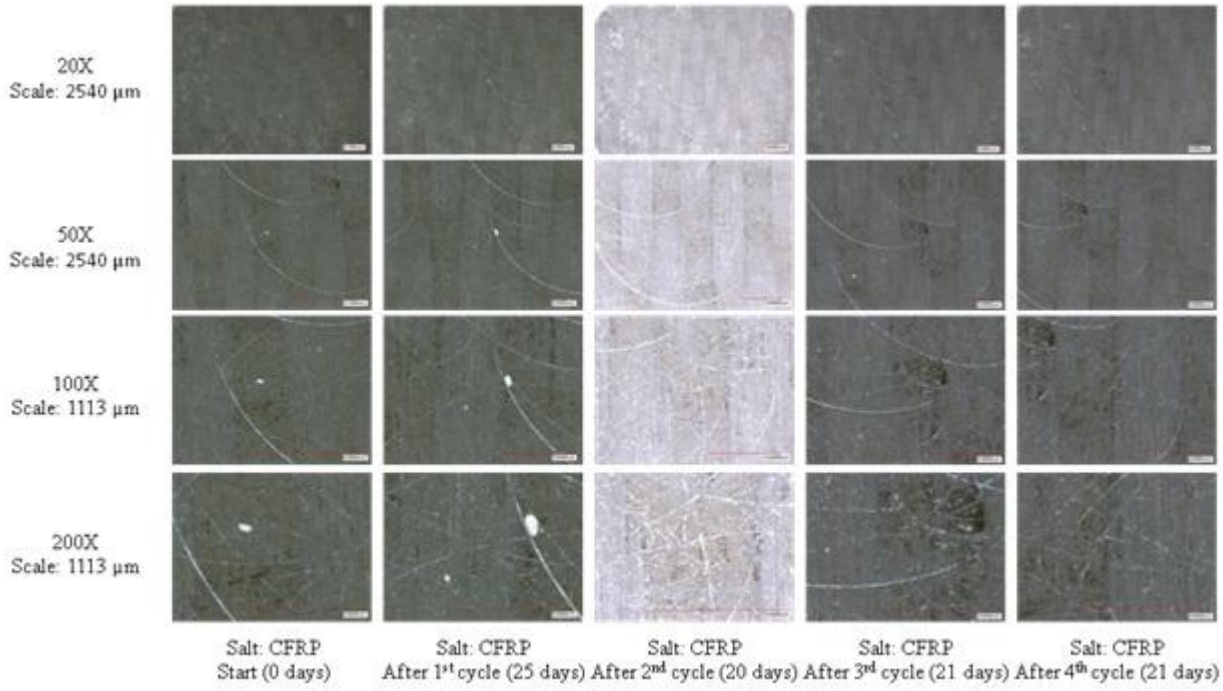

Figure A.7: Salt Spray Cycling for CFRP at magnifications 20, 50, 100 and 200X.

Figure A.8: Salt Spray Cycling for ECF at magnifications 20, 50, 100 and 200X.

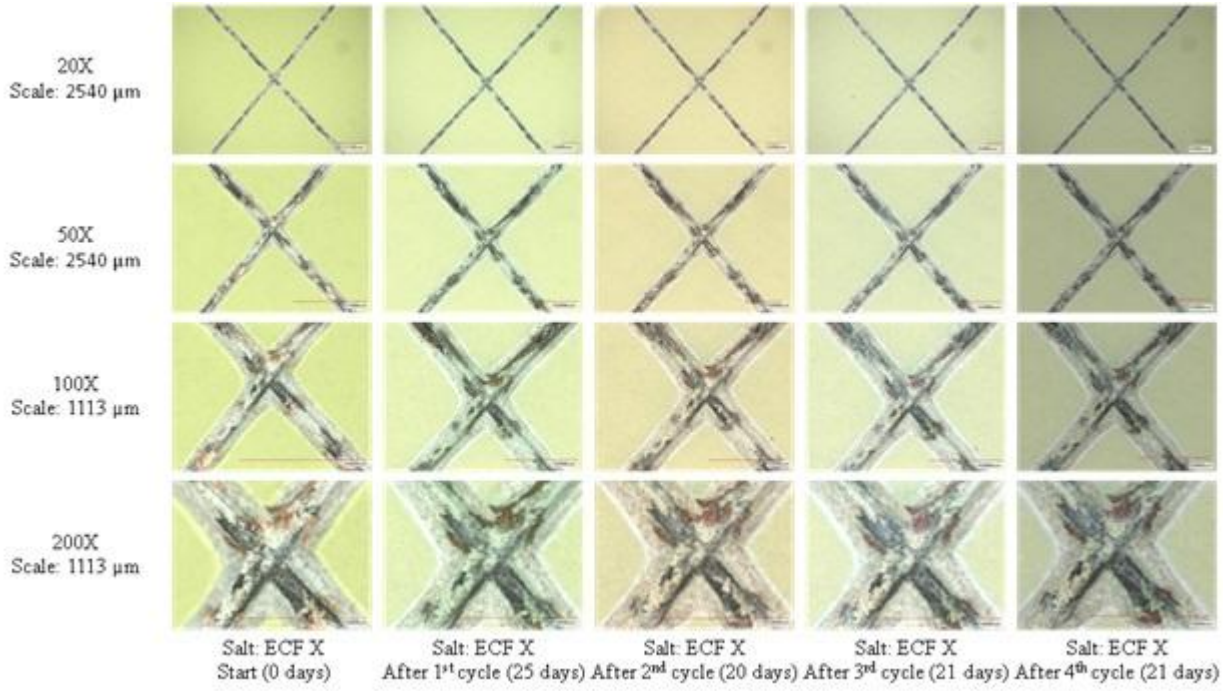

Figure A.9: Salt Spray Cycling for ECF X scribe at magnifications 20, 50, 100 and 200X.

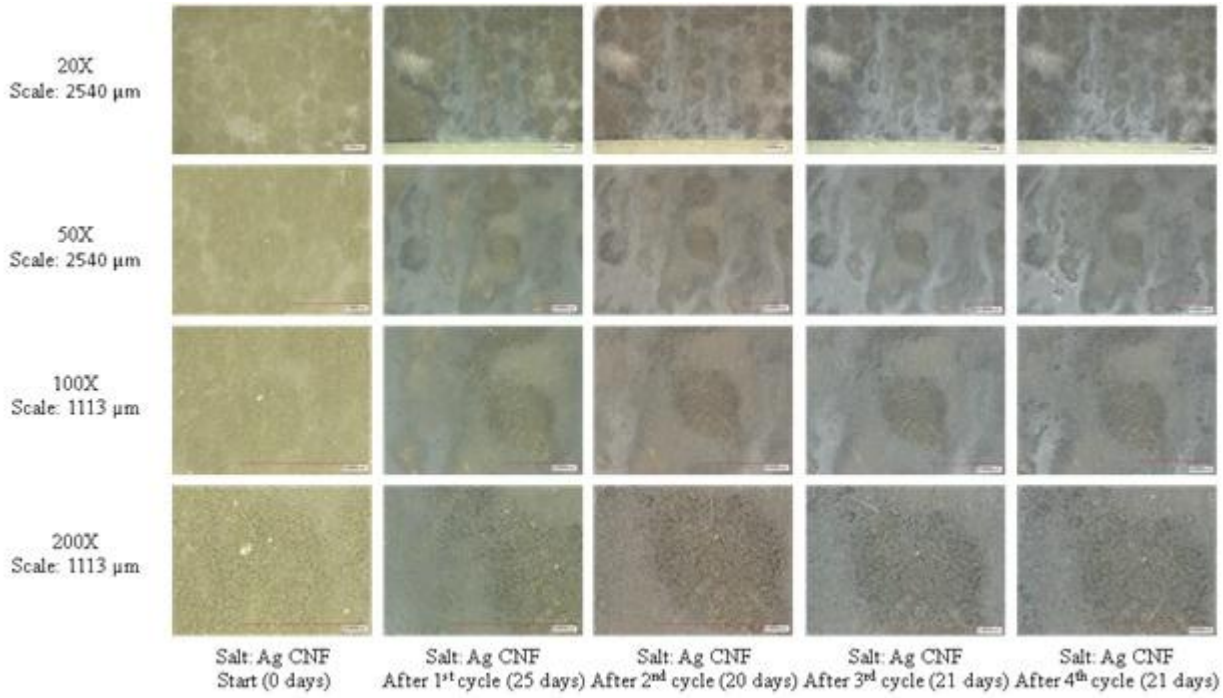

Figure A.10: Salt Spray Cycling for Ag CNF at magnifications 20, 50, 100 and 200X.

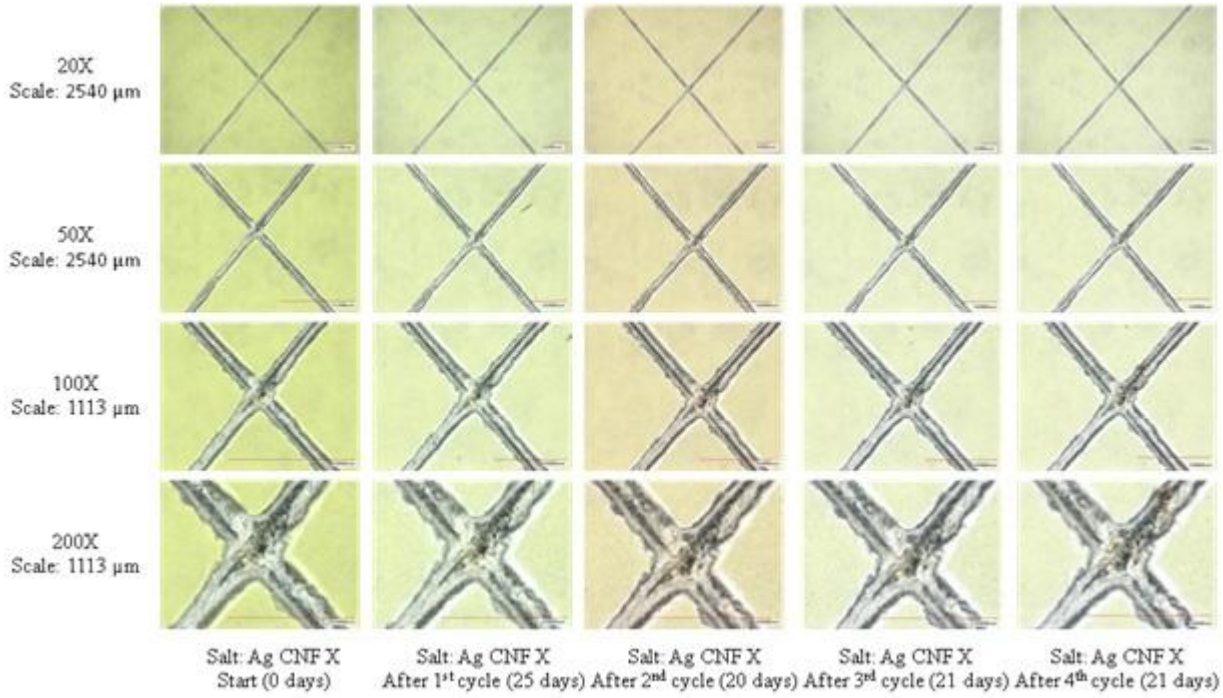

Figure A.11: Salt Spray Cycling for Ag CNF X scribe at magnifications 20, 50, 100 and 200X.

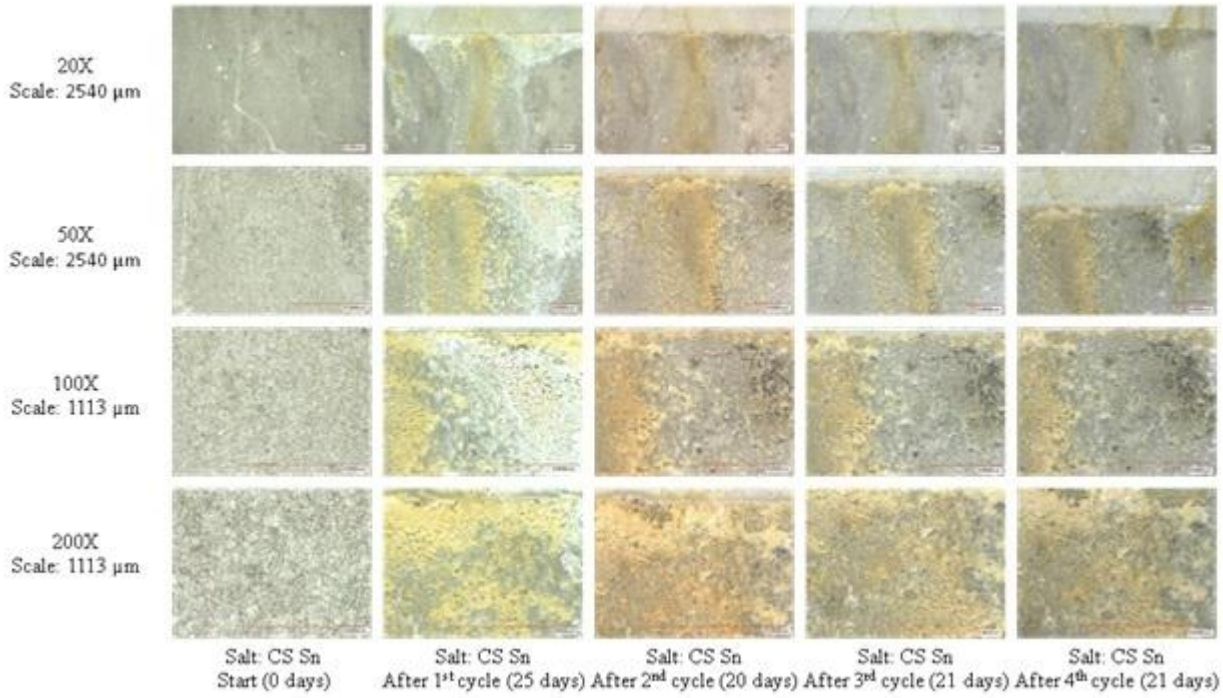

Figure A.12: Salt Spray Cycling for CS Sn at magnifications 20, 50, 100 and 200X.

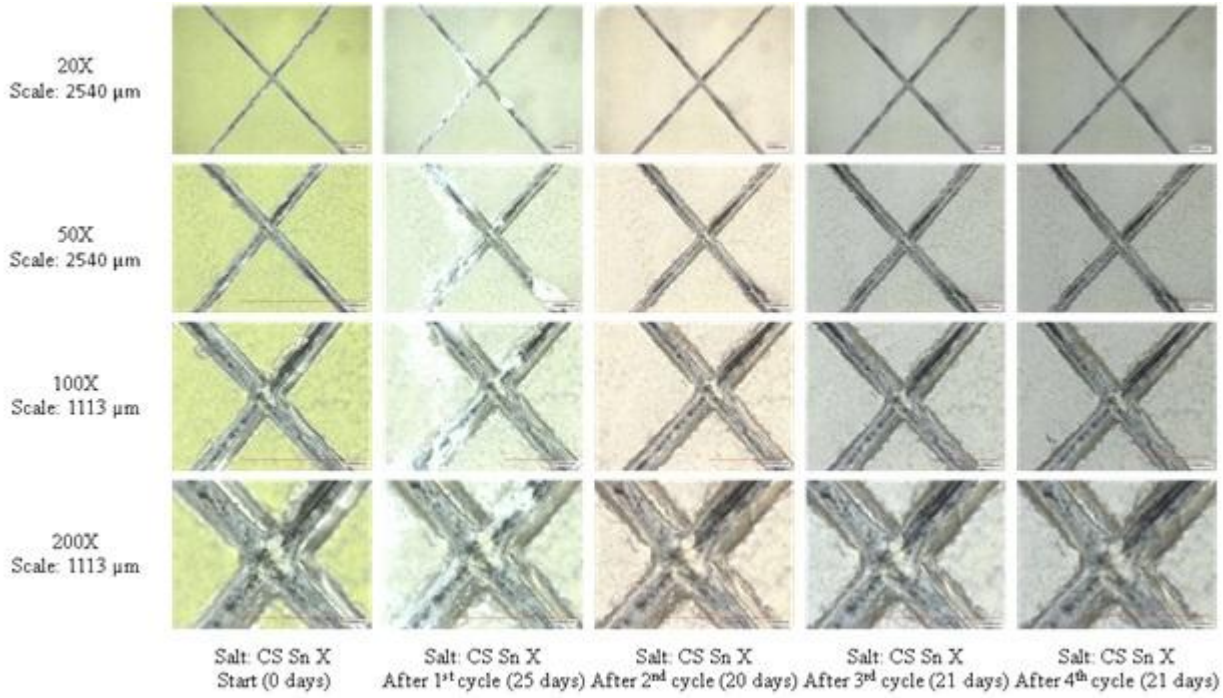

Figure A.13: Salt Spray Cycling for CS Sn X scribe at magnifications 20, 50, 100 and 200X.

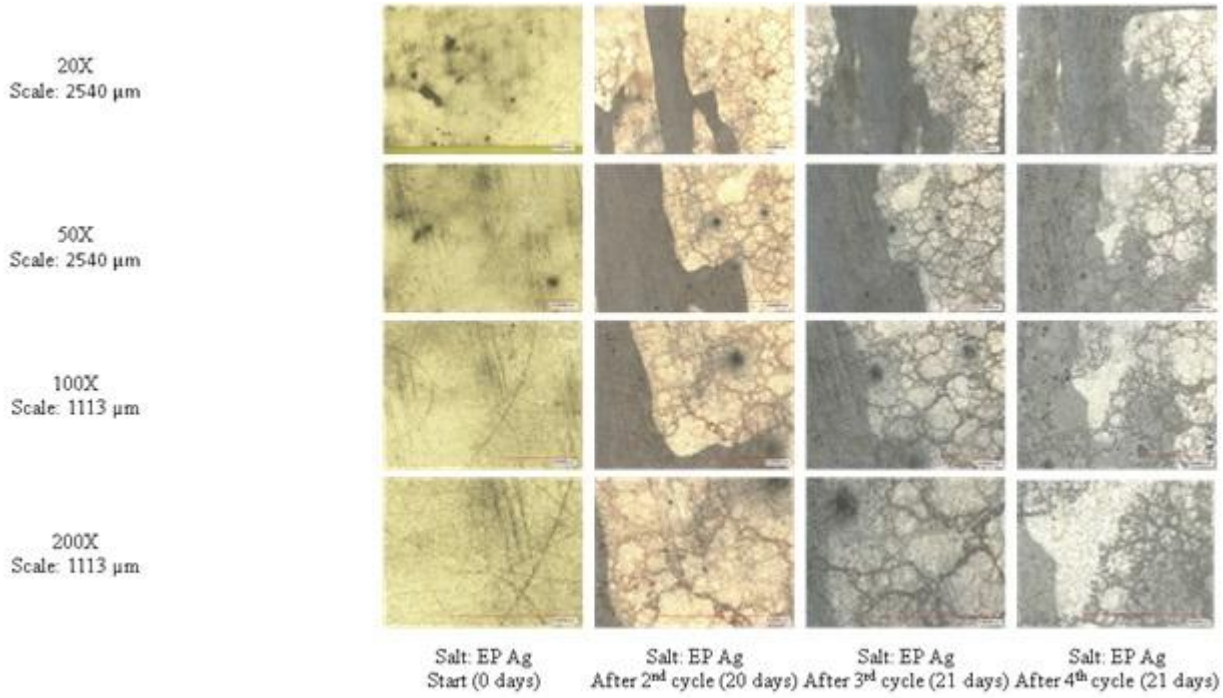

Figure A.14: Salt Spray Cycling for EP Ag at magnifications 20, 50, 100 and 200X.

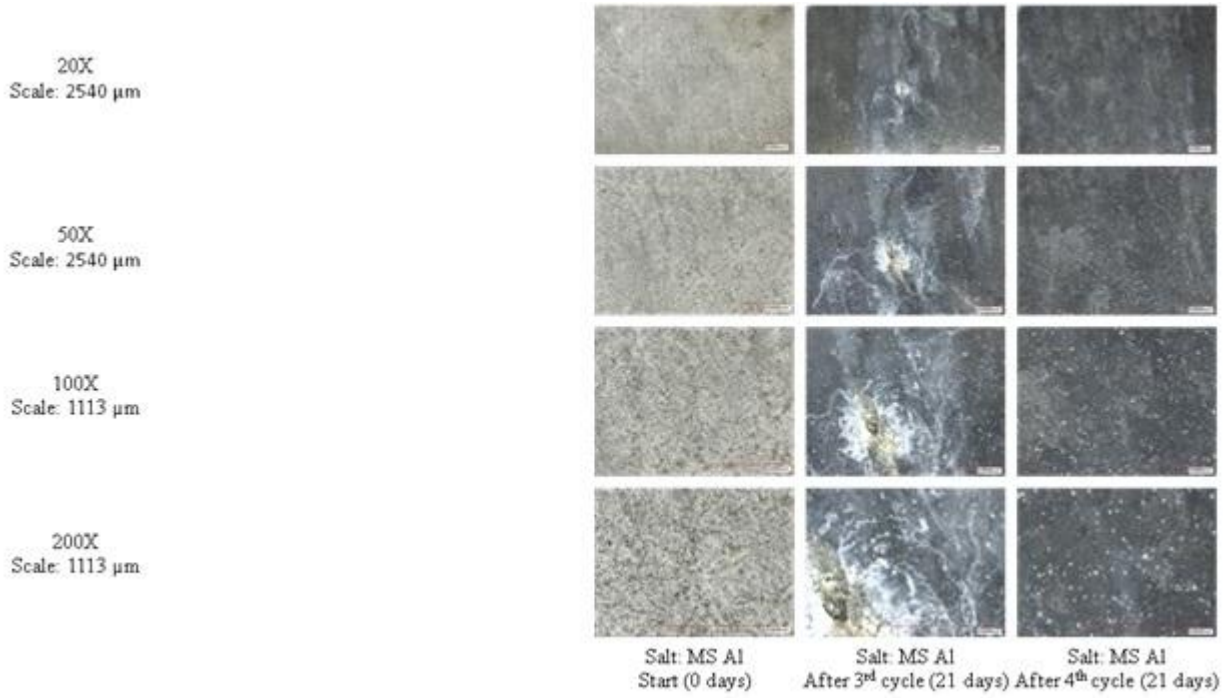

Figure A.15: Salt Spray Cycling for MS Al at magnifications 20, 50, 100 and 200X.

APPENDIX B – LISTS OF PAPERS AS AUTHOR AND CO-AUTHOR

1. Martin Gagné and Daniel Therriault; Lightning strike protection of composites, Progress in Aerospace Sciences, vol. 64, pp. 1-16, 01/2014 http://dx.doi.org/10.1016/j.paerosci.2013.07.002.
2. Rouhollah Dermanaki Farahani, Martin Gagne, Jolanta E. Klemberg-Sapieha, and Daniel Therriault; Electrically Conductive Silver Nanoparticles-filled Nanocomposite Materials as Surface Coatings of Composite Structures, Advanced Engineering Materials, 2016, http://dx.doi.org/10.1002/adem.201500544.
3. P. S. M. Rajesh, Xavier Cauchy, Martin Gagne, Jolanta E. Klemberg-Sapieha, Frederic Sirois, Daniel Therriault; Wet Chemical Metallization of Aerospace Composites as a Lightning Protection Strategy, TMS 2015: 144th Annual Meeting & Exhibition; Orlando, USA; 2015; Engineering Solutions for Sustainability: Materials & Resources II — Innovations in Processing to Meet Emerging Demands; p. 187-192.
4. P. S. M. Rajesh, Martin Gagne, Xavier Cauchy, Jolanta E. Klemberg-Sapieha, Frederic Sirois, Daniel Therriault; Lightning Protection Testing of Wet Metalized Polymer Composites; The 20th International Conference on Composite Material (ICCM20); Copenhagen, Denmark; 2015.